

Final report

# PROCESSES FOR THE PRODUCTION OF TRANSPORTATION FUEL VIA DEOXYGENATED BIO-OIL

May 2022

Lucio Rodrigo Alejo Vargas<sup>1</sup>, Shivani Ramprasad Jambur<sup>1</sup>, Pontus Bokinge<sup>2</sup>,  
Gopi Subramaniam<sup>3</sup>, Elin Svensson<sup>2</sup>, Simon Harvey<sup>3</sup>, Rolf Ljunggren<sup>4</sup>, Klas Engvall<sup>1</sup>,  
Shareq Mohd Nazir<sup>1\*</sup>

<sup>1</sup> KTH Royal Institute of Technology

<sup>2</sup> CIT Industriell Energi AB

<sup>3</sup> Chalmers University of Technology

<sup>4</sup> Cortus Energy AB

\*Corresponding author: Shareq Mohd Nazir, [smnazir@kth.se](mailto:smnazir@kth.se)

A project within

**RENEWABLE TRANSPORTATION FUELS AND SYSTEMS 2018-2021**

A collaborative research program between the Swedish Energy Agency and  
f3 The Swedish Knowledge Centre for Renewable Transportation Fuels



## PREFACE

This project has been carried out within the collaborative research program *Renewable transportation fuels and systems* (Förnybara drivmedel och system), Project no. 50466-1. The project has been financed by the Swedish Energy Agency and f3 – Swedish Knowledge Centre for Renewable Transportation Fuels.

The Swedish Energy Agency is a government agency subordinate to the Ministry of Infrastructure. The Swedish Energy Agency is leading the energy transition into a modern and sustainable, fossil free welfare society and supports research on renewable energy sources, the energy system, and future transportation fuels production and use.

f3 Swedish Knowledge Centre for Renewable Transportation Fuels is a networking organization which focuses on development of environmentally, economically and socially sustainable renewable fuels. The f3 Centre is financed jointly by the centre partners and the region of Västra Götaland. Chalmers Industriteknik functions as the host of the f3 organization (see <https://f3centre.se/en/about-f3/>).

### Acknowledgments

The authors acknowledge the financial support received from Swedish Energy Agency and f3 Swedish Knowledge Centre for Renewable Transportation Fuels for the project.

### This report should be cited as:

Vargas, L.R.A, Jambur, S.R., Bokinge, P., Subramaniam, G., Svensson, E., Harvey, S., Ljunggren, R. Engvall, K. & Nazir, S.M. (2022) *Processes for the Production of Transportation Fuel via Deoxygenated Bio-Oil*. Publ. No FDOS 47:2022. Available at <https://f3centre.se/en/renewable-transportation-fuels-and-systems/>



## SUMMARY

Sweden aims to achieve net-zero greenhouse gas (GHG) emissions by 2045. This will require a reduction of GHG emissions from domestic transport (excluding aviation) by 70% by 2030 with respect to the levels in 2010. An important element for achieving this is Sweden's resources of sustainable biomass in the form of forestry and agricultural residues, which can be used as raw materials for the production of renewable fuels for the transport sector to accelerate the transition to net-zero greenhouse gas emissions. Biofuels currently account for 19.5%, or 16 TWh/year, of the entire Swedish transport sector's energy needs, which is forecasted to increase to 38 TWh/year by 2045. Today, mainly ethanol, FAME (i.e. Fatty Acid Methyl Ester) and hydro-treated vegetable oils (HVO) are used as "drop-in" fuels, where increased use is limited by the compatibility with the vehicle fleet and the availability of raw materials. The production of hydrocarbon-based fuels such as petrol and diesel from bio-based raw materials would provide greater benefits in terms of the possibility of utilizing the existing industrial processes, distribution networks and the compatibility with the existing vehicle fleet. This is also in line with the Swedish Energy Agency's priority to produce "drop-in" fuels from bio-based waste raw materials. Fast pyrolysis at elevated temperature is an attractive process for the production of bio-oils, which can be used directly by today's refinery industry for petrol and diesel production with residual biomass as raw material. Bio-oil from fast pyrolysis, however, contains a larger amount of oxygen (35-40% by weight), which makes the oil unstable and therefore not suitable for primarily storage or longer transport. Therefore, depending on the location of the pyrolysis process, the oxygen must be removed from the bio-oil, which can be done by a reaction with hydrogen in a hydro-deoxygenation (HDO) process. The process requires relatively large amounts of hydrogen of between 40-100 kg of hydrogen per tonne of dry biomass. This means, to achieve the 2045 targets, we will need 0.17-0.42 million tonnes of hydrogen per year for the HDO process. Therefore, hydrogen generation is a key element in producing biooils that can be further converted into drop-in fuels.

The main aim of this study is to increase knowledge in techno-economic performance of integrating hydrogen generation processes with pyrolysis and HDO step to produce deoxygenated bio-oil. This study also presents a first-of-its-kind techno-economic analysis of integrating vapor phase HDO step with pyrolysis to generate hydro-deoxygenated bio-oils. Four process pathways are presented in this study. The first three process pathways include biomass fast pyrolysis and vapor phase HDO step integrated with different hydrogen generation processes (i) natural gas reforming (ii) electrolysis (iii) biomass gasification. The fourth process pathway is the in-situ catalytic hydro-pyrolysis and hydro-conversion process, named as IH2. In-house process models for fast pyrolysis and HDO step have been developed in this project with the aid of thermodynamic, kinetic and experimental data available in literature. The mass and energy balance for the IH2 process is established based on the published data available from the experience of technology provider. The processes have also been analyzed when integrated with CO<sub>2</sub> capture and storage (CCS) for the cases with hydrogen generation from natural gas and biomass gasification. The economic and GHG emission assessment has been carried out for two scenarios, Sustainable Development (SD) and New Policies (NP) scenarios. The main difference in the two scenarios is that the SD scenario assumes biomass to be a limited resource while the NP scenario assumes it to be unlimited.

The IH2 process, which is an in-situ catalytic hydro-pyrolysis and hydro-conversion process, outperforms the other process routes in terms of both process and economic performance. The bio-oil

yield, carbon recovery and system efficiency of the IH<sub>2</sub> process is higher than other process routes. Among the other process routes, integrating electrolysis with pyrolysis and HDO step has a higher carbon recovery while having higher system efficiency than the process route with biomass gasification. However, the process with biomass gasification integrated with HDO step has lower production costs in the NP scenario. In addition, this process route will offer additional cost benefits if integrated with CO<sub>2</sub> capture and Storage when negative emissions are incentivized.

This topic requires further research to demonstrate vapor phase HDO step experimentally while developing suitable high-performance catalysts. The study also shows that more than 55% of the carbon from the process is lost in the form of CO<sub>2</sub> from the process. Therefore, CO<sub>2</sub> utilization through either in-situ recycling or ex-situ downstream synthesis of fuels will enable higher carbon recovery in the form of biofuels and result in efficient sustainable biomass utilization.

## SAMMANFATTNING

Sverige har som mål att uppnå nollutsläpp av växthusgaser fram till 2045. Detta kräver en minskning av växthusgasutsläppen från inrikes transporter (exklusive flyg) med 70 % år 2030 relativt nivåerna 2010. En viktig tillgång för att uppnå detta är Sveriges tillgångar av hållbar biomassa i form av skogs- och jordbruksrester, som kan användas som råvaror för produktion av förnybara drivmedel för transportsektorn, vilket kan påskynda övergången till nollutsläpp av växthusgaser. Biodrivmedel står idag för 19,5 %, eller 16 TWh/år, av hela svenska transportersektorns energibehov, vilket förutspås öka till 38 TWh/år till år 2045. Idag används främst etanol, FAME (dvs. Fatty Acid Methyl Esther) och hydrerade vegetabiliska oljor, s.k. HVO (hydrogeneated vegetable oils), som ”drop-in” bränslen, där en utökad användning begränsas av kompatibiliteten med fordonsflottan och tillgången på råvara. En produktion av kolvätebaserade drivmedel som bensin och diesel från biobaserad råvara skulle ge större fördelar i form av möjligheten att utnyttja de befintliga industriella processerna, distributionsnäten och kompatibiliteten med den befintliga fordonsflottan. Detta är även i linje med Energimyndighetens prioritering att producera ”drop-in” bränslen från biobaserade avfallsråvaror. Snabb pyrolys vid förhöjd temperatur är en attraktiv process för produktion av bioolja, som direkt kan användas av dagens raffinaderiindustri för bensin- och dieselproduktion med restbiomassa som råvara. Bioolja från snabb pyrolys innehåller dock en större mängd syre (35-40 vikt-%), vilket gör oljan instabil och därför inte lämpar sig för främst lagring eller längre transporter. Syret måste därför beroende på placeringen av pyrolysisprocessen avlägsnas från biooljan, vilket kan göras genom en reaktion med vätgas i en HDO-process (HDO-hydrodeoxygenation). Processen kräver förhållandevis stora mängder vätgas på mellan 40 - 100 kg vätgas per ton torr biomassa, vilket innebär att vi behöver mellan 0,17-0,42 miljoner ton vätgas per år för HDO-processen. Vätgasgenerering är därför en nyckelprocess för produktion av bioolja, som kan vidareförädlas till drop-in bränslen.

Huvudsyftet med studien var att öka kunskapen om teknisk-ekonomisk prestanda för produktion av deoxygenerad bioolja i integrerade processer där produktion av vätgas, pyrolys av restbiomassa tillsammans med ett HDO-processsteg för direkt detygenering av pyrolysoljan i ångfas ingår. Fyra processvägar undersöks i studien, där de första tre processvägarna, inkluderar snabb pyrolys av restbiomassa och ett HDO-processsteg, integrerat med olika processer för vätegasproduktion: (i) reformering av naturgas (ii) elektrolys (iii) förgasning av restbiomassa. Den fjärde processvägen är en process, IH<sub>2</sub>-processen, där vätgasen introduceras redan vid den primära omvandlingen av restbiomassa till bioolja i en katalytisk pyrolysisprocess. Vätgasen produceras från restgaser internt i processen. Vi har utvecklat egna modeller för processerna snabb pyrolys och HDO-steget med hjälp av teoretiska och experimentella data tillgängliga i litteraturen. Material- och energibalansen för IH<sub>2</sub>-processen baseras på publicerade data och erfarenheten publicerade av teknikleverantören. En analys av en integrering av CO<sub>2</sub>-infångning och lagring (CCS - CO<sub>2</sub> capture and storage) utfördes även för de fallen med vätegasproduktion från naturgas och biomassaförgasning. Den ekonomiska bedömningen och utsläppen av växthusgaser har utförts för två scenarier, hållbar utveckling och nya riktlinjer. Den största skillnaden mellan de två scenarierna är att scenariot för hållbar utveckling antar att restbiomassa är en begränsad resurs medan scenariot för nya riktlinjer antar att den är obegränsad.

Resultaten visar att IH<sub>2</sub>-processen, där vätgasen introduceras i en katalytisk pyrolysisprocess, överträffar de andra processvägarna både när det gäller process och ekonomisk prestanda. Utbytet av

bioolja, kolomvandlingen och totalprocessens verkningsgrad är högre för IH<sub>2</sub>-processen än för de andra processvägarna. För de övriga tre processvägarna så ger en integrering av elektrolys för vätegasproduktion en högre kolomsättning och en högre processverkningsgrad än för fallet där förgasning restbiomassa används för vätegasproduktion. Processen där förgasning av restbiomassa integreras tillsammans med HDO-steget har dock lägre produktionskostnader i scenariot för nya riktlinjer. Dessutom erbjuder denna processväg ytterligare kostnadsfördelar om den integreras med CO<sub>2</sub>-avskiljning och lagring, vilket möjliggör negativa utsläpp av CO<sub>2</sub>.

HDO-processen för en direkt omvandling pyrolysolja i ångfas för att minska mängden syre i den producerade pyrolysoljan kräver i dagsläget ytterligare FoU för att utveckla lämpliga högpresterande katalysatorer och demonstrera teknologin experimentellt. Studien visar även att mer än 55 % av kolet från processen går förlorat i form av CO<sub>2</sub>. Därför kommer möjligheten att utnyttja CO<sub>2</sub>-aningen internt i processen eller externt i syntesprocesser för produktion av biodrivmedel vara viktigt för att minska kolförlusterna (ökad kolomsättning) och därmed ett effektivare utnyttjande av restbiomassa som råvara.

## CONTENTS

1	INTRODUCTION.....	15
2	PROCESS DESCRIPTION AND PROCESS MODELLING.....	19
2.1	BIOMASS FAST PYROLYSIS AND HDO PROCESS .....	19
2.2	MEA SOLVENT BASED CO2 CAPTURE UNIT.....	31
2.3	BIOMASS GASIFICATION.....	31
2.4	HYDROGEN PRODUCTION FROM NATURAL GAS REFORMING .....	35
2.5	HYDROGEN PRODUCTION FROM ELECTROLYSIS.....	36
2.6	IH2 PROCESS.....	36
2.7	BIOOIL TO TRANSPORTATION FUELS .....	37
3	PROPOSED PROCESS SCENARIOS.....	38
4	METHODOLOGY.....	39
4.1	PROCESS PERFORMANCE .....	39
4.2	ECONOMIC AND GHG ASSESSMENT .....	40
5	RESULTS AND DISCUSSION.....	49
5.1	RESULTS FOR PROCESS PERFORMANCE.....	49
5.2	ECONOMIC AND GHG ASSESSMENT RESULTS.....	52
6	CONCLUSIONS.....	56
	REFERENCES .....	58
	APPENDIX .....	63
	DETAILED PROCESS ANALYSIS OF BIOMASS FAST PYROLYSIS AND HDO .....	63
	EFFECT OF HYDROGEN FLOW TO HDO STEP ON BIO-OIL PRODUCTION.....	66
	EFFECT OF DIFFERENT BIOMASS SPECIES ON BIO-OIL PRODUCTION .....	67
	MODELLING OF BIOMASS GASIFICATION PROCESS IN ASPEN PLUS .....	67
	ANALYSIS OF BIOMASS GASIFICATION PROCESS .....	75
	PROCESS DESCRIPTION FOR SCENARIOS REF3 AND REF4 AS PROPOSED IN TABLE 7.....	76
	ANALYSIS OF REF1 SCENARIO .....	80
	BIOMASS SPECIES AND THEIR COMPOSITION .....	81

COMPONENTS OF BIOMASS CONSIDERED IN MODELLING OF FAST PYROLYSIS  
IN ASPEN PLUS .....82

THERMOPHYSICAL PROPERTIES OF BIOMASS INTRODUCED IN MODELLING OF  
PROCESS USING ASPEN PLUS .....83

KINETIC SCHEMES FOR BIOMASS FAST PYROLYSIS PROCESS REPORTED IN  
LITERATURE .....85

SUMMARY OF REVIEW FOR VAPOR PHASE HDO PROCESS .....88

ASSUMPTIONS FOR YIELD IN MODELLING HDO STEP .....90

PROCESS DETAILS FOR DIFFERENT BIOMASS SPECIES .....91

PROCESS DETAILS FOR REF4, CCS2, CCS3, CCS4 AND CCS5 CASES.....93

## LIST OF FIGURES

Figure 1. C-H-O ternary diagram for biomass conversion (Source for figure: [5]). The figure shows the main products from biomass conversion through different processes. Bio-oil is the key product obtained from fast pyrolysis route (indicated as F in the figure, pointing towards mainly pyrolysis vapors containing biooils and non-condensable gases)..... 16

Figure 2. Different routes for hydrogen and deoxygenated bio-oil production. Blue boundary is for the process that uses hydrogen for HDO from electrolysis. Green boundary is for the process where hydrogen is generated from biomass or char gasification. The grey boundary is for the process route that has NG reforming for hydrogen production for HDO. The red boundary is the IH2 process. NCG is the abbreviation for non-condensable gases. For the cases with biomass gasification and NG reforming, analysis have also been performed for the process integrated with CCS. .... 18

Figure 3. Simplified process flow diagram of biomass fast pyrolysis process. .... 20

Figure 4. Process flow of the biomass fast pyrolysis process in Aspen Plus. The details in the figures are described in the sections below. .... 22

Figure 5. Fast Pyrolysis reactor model in Aspen Plus..... 28

Figure 6. Conversion of the fast pyrolysis stream to conventional components as modelled in Aspen Plus..... 28

Figure 7. HDO unit in Aspen Plus. .... 29

Figure 8. Biomass gasification process diagram flow in the plant of Güssing, Austria. Source: <https://web.archive.org/web/20120324011457/http://www.ficfb.at/>. .... 32

Figure 9. Fast Internally Circulating Fluidized Bed (FCICFB) schematic diagram (Source: [31]). 33

Figure 10. Water gas shift section diagram flow as modelled in Aspen Plus. .... 34

Figure 11. Intercooled syngas compressor train and PSA section as modelled in Aspen Plus. .... 35

Figure 12. Schematic of the SMR plant using FTR for the reforming of Natural gas – Reproduced from Nazir et al. [27]..... 35

Figure 13. Simple process flow schematic of IH2 process as proposed by GTI (Source: [34]). .... 37

Figure 14. Assumed mass balance for refinery processing of the produced deoxygenated bio-oil. 37

Figure 15. System boundaries and inputs/outputs considered for the GHG assessment. PINK: Included in all process routes, ORANGE: Included in all fast pyrolysis routes, BLUE: Pyrolysis/electrolysis route (Ref2), GREY: Pyrolysis/steam reforming route (Ref1, CCS1), GREEN: Pyrolysis/gasification route (Ref3-4, CCS4), RED: Hydro pyrolysis route (IH2). (+) denotes inputs and (-) denotes outputs/products. .... 47

Figure 16. Total fuel production OPEX for the investigated biofuel pathways in the ENPAC (a) SD Scenario and (b) NP Scenario. The resulting investment opportunity (in terms of annualized TCI) is calculated as the fuel sale price (dashed line) minus the OPEX sum (diamonds). If OPEX is lower than the sales price, the investment opportunity can be read as the distance between the OPEX sum and the dashed lines in the figure. The fuel sale price is the average biofuel sale price at gate calculated from diesel and gasoline prices and the diesel/gasoline product split. Ref1: Natural gas, CCS1: Natural gas with CCS applied to fossil CO<sub>2</sub>-emissions, Ref2: Electrolysis, Ref3: Gasification, Ref4: Gasification with char utilization, CCS4: Gasification with char utilization and BECCS applied to all CO<sub>2</sub> emissions. IH2: IH2 process based on work by [35]...... 53

Figure 17. Well-to-gate + combustion emissions for the process routes investigated in this work. (a): emission factors from ENPAC Scenario SD. The dashed line represents the 65% emission reduction limit for transportation fuels in REDII. The comparison to REDII is only relevant for scenario NP. (b): emission factors from ENPAC Scenario NP. Ref1: Natural gas, CCS1: Natural gas with CCS applied to fossil CO<sub>2</sub>-emissions, Ref2: Electrolysis, Ref3: Gasification, Ref4: Gasification with char utilization, CCS4: Gasification with char utilization and BECCS applied to all CO<sub>2</sub> emissions. IH2: IH2 process based on work by [P5]. Note the y-axis breaks in the positive and negative direction, since the values are significantly higher for two points..... 55

Figure 18. Bio-oil produced vs Supplied Hydrogen..... 66

Figure 19. Overall flowsheet of the biomass gasification process in Aspen Plus. .... 69

Figure 20. Effect of gasification temperature on the syngas composition by the model of Doherty et al. [31]. .... 73

Figure 21. Effect of gasification temperature on the syngas composition by our model. .... 73

Figure 22. Effect of steam to biomass ratio on the syngas composition by the model of Doherty et al. [31]. .... 74

Figure 23. Effect of steam to biomass ratio on the syngas composition by our model. .... 74

## LIST OF TABLES

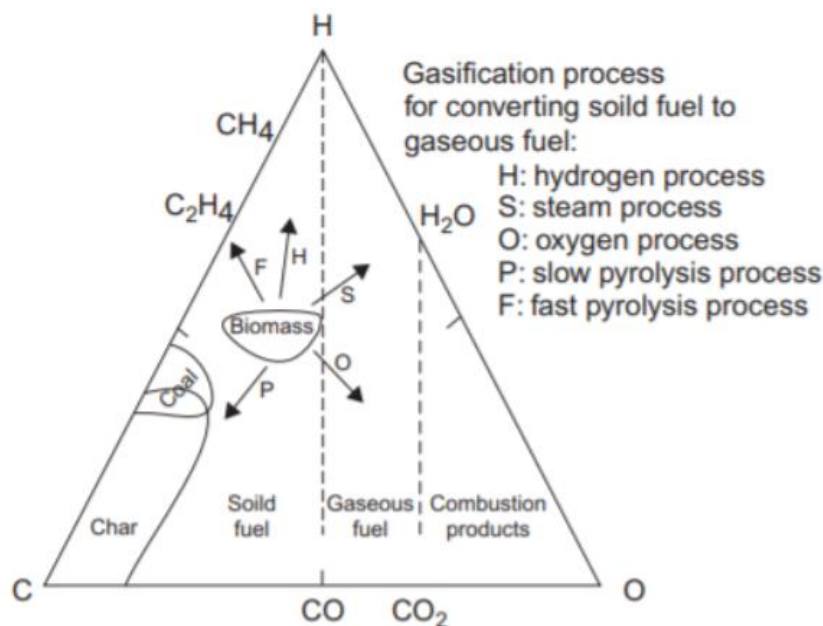
Table 1. Assumed (dried) biomass composition in pyrolysis step in the analysis (Composition is similar to the composition of dried Douglas fir wood belonging to the pine family). (Source [21])	23
Table 2. Different components in biomass, intermediate species and end-products involved in the fast pyrolysis process. Non-biomass components are also listed in the table. ....	24
Table 3. Required estimated properties for the solid and conventional components. ....	25
Table 4. Adapted multistep kinetic scheme of the biomass fast pyrolysis process from the original multistep kinetic scheme of Ranzi et al. [22]. [The kinetic data for *Reaction 14 reported in the table is the modified value to fit the resulting product composition available in literature. Comparison with the value from Ranzi et al. [22] is shown in Table 5]. (A is the pre-exponential factor, x is the power to which temperature is raised in the equation, Ea is the activation energy). Please refer to Table 2 and Table 26 (in Appendix) for definition of components in the reactions.	26
Table 5. Modified reaction from the original multistep kinetic scheme of Ranzi et al. [22]. This table reports the adjustments we made in kinetic data for Reaction 14 with respect to literature ...	27
Table 6. Comparison between the experimental results of Caudle et al. [21] and our model. ....	29
Table 7. Definition of different process scenarios. ....	38
Table 8. Input data used to generate ENPAC scenarios, and the resulting output data used in GHG and economic assessments in this work. ....	42
Table 9. Parameters and data used in the economic assessment. ....	44
Table 10. Summary of Total Capital Investment (TCI) estimates for the investigated process routes. The studies by Jones et. al. and Dutta et.al. considered production of deoxygenated bio-oil with hydrogen supply via steam methane reforming (i.e., Ref1 in the present study). An average of their TCI estimates was used directly for Ref1. For other routes, TCI values were adjusted to account for differences in hydrogen supply and the use of (BE)CCS, where relevant. All monetary values have been escalated to EUR-2019 using the CEPCI composite index and annual average currency exchange rates. IEC: Installed Equipment Cost, PEC: Purchased Equipment Cost. ....	46
Table 11. ENPAC GHG emission factors used in the GHG assessment. ....	48
Table 12. Main results from process analysis. ....	51
Table 13. Analysis of reference case pyrolysis process with HDO (irrespective of the source of hydrogen). ....	63
Table 14. Analysis of reference case pyrolysis process with HDO (irrespective of the source of hydrogen) integrated with CO2 capture for combustion exhaust gases from pyrolysis unit. ....	65
Table 15. Effect of Hydrogen flow to HDO step on bio-oil production. ....	66
Table 16. Results of the fast pyrolysis process for different biomass species. ....	67

Table 17. Biomass Gasification reactions specified in the model – Source: Doherty et al. [31]. ....	68
Table 18. Biomass composition. ....	70
Table 19. Yield Distribution of each component based on the biomass ultimate analysis data.....	70
Table 20. Results for the biomass gasification process with CO <sub>2</sub> capture. ....	75
Table 21. Details of Ref 3 scenario. ....	77
Table 22. Details of the Ref4 scenario. ....	79
Table 23. Details of Ref1 scenario. ....	80
Table 24. Composition of the Douglas fir wood sample and Spruce samples from the work of Caudle et al. [21] and Debiagi et al. [24]. ....	81
Table 25. Composition of the Pine samples from the work of Debiagi et al. [24]. ....	81
Table 26. Biomass components, intermediate species and end products involved in the fast pyrolysis process, reproduced from the work of Gorenssek et al. [25]. ....	82
Table 27. Estimated properties for conventional solid components in pyrolysis process model. Table reproduced from the work of Gorenssek et al. [25]. ....	83
Table 28. Estimated properties for conventional fluid components in pyrolysis process model. Table reproduced from the work of Gorenssek et al. [25]. ....	84
Table 29. Original Multistep kinetic scheme of the biomass fast pyrolysis process. Table reproduced from the work of Ranzi et al. [22]. ....	85
Table 30. Simplified multistep kinetic scheme for biomass fast pyrolysis process, table reproduced from the work of Caudle et al. [21]. ....	87
Table 31. Summary of review on vapor phase hydrodeoxygenation. ....	88
Table 32. Carbon, oxygen and hydrogen wt% for hydro-deoxygenated bio-oil as reported in literature. ....	89
Table 33. Yield used in the HDO process model. ....	90
Table 34. Analysis for Ref1 case when using different biomass types ....	91
Table 35. Analysis for Ref2 case when using different biomass types ....	91
Table 36. Analysis for Ref3 cases for different biomass types ....	92
Table 37. Process details for the Ref4 case ....	93
Table 38. Process details for the CCS2-5 cases ....	93

# 1 INTRODUCTION

Sweden has the long-term goal to achieve net-zero greenhouse gas emissions by 2045. Throughout this path there are different milestones that need to be achieved first, one of them is to have a vehicle fleet independent of fossil fuels by 2030 [1]. According to the *European Biofuels Technology Platform*, and an internal governmental investigation performed in 2013, one of the first steps to achieve mentioned milestone would be by powering up approximately 50% of the passenger cars on biofuels. However, achieving this sole milestone would require approximately 20 TWh of bio-fuel production in Sweden. The feedstock for the production of this amount of biofuel is expected to come from Sweden's forest industries as a sustainable and resource efficient energy system [1]. Another key element that is used in the production of transportation fuels from biogenic feedstocks biofuels and several other industrial processes is hydrogen, which is used in the hydrogenation and hydrocracking processes of vegetable oils for the production of hydrogenated vegetable oil (HVO) [2]. Thus, hydrogen plays an important role in Sweden's bio-economy, since it is used in producing the most common biofuel used in the transport sector, which is HVO, followed by fatty acid methyl ester (FAME), ethanol and biogas [1].

In Sweden, the residues from the forest industries can be used as feedstock and treated via thermochemical conversion, enabling in this manner the production of a variety of energy carriers and chemicals, including transport fuels. One example of this thermochemical conversion processes is the process called Pyrolysis. Pyrolysis is the heating of organic matter (temperatures are around 300-650°C) in an environment with no oxygen present, with the help of a catalyst. There are several modes to run the pyrolysis in, but the two most common one is called fast pyrolysis and slow pyrolysis. The difference between them is that fast pyrolysis takes only a few seconds (0.5-2 sec), by using a higher operating temperature and a higher heating rate. Using fast pyrolysis can increase the yield of pyrolysis oil (higher hydrocarbon fractions obtained after condensing pyrolysis vapors) and lower the bio-char yield compared to the case when using slow pyrolysis [3], also seen in Figure 1. The aim with slow pyrolysis is typically to produce bio-char [4]. In this project, our focus is on fast pyrolysis process, as we would like to optimize the production of bio-oils.



**Figure 1. C-H-O ternary diagram for biomass conversion (Source for figure: [5]). The figure shows the main products from biomass conversion through different processes. Bio-oil is the key product obtained from fast pyrolysis route (indicated as F in the figure, pointing towards mainly pyrolysis vapors containing biooils and non-condensable gases).**

While operating fast pyrolysis, it is the liquid phase that is of interest. The crude bio-oil that is formed in the fast pyrolysis process consists of a wide spectrum of organic oxygenated substances [4]. Wood derived crude bio-oil has a black or red-brown to dark green color. The water content in the bio-oil ranges from 15-50 wt. % depending on production and collection. Bio-oils cannot be dissolved in water but can tolerate some water before a phase separation occurs. It is miscible with polar solvents such as methanol but immiscible with petroleum-derived fuels. It also has a density around 1.2 kg/L, compared to light fuel oil at 0.85 kg/L. The viscosity varies between 25-1000 cSt (measured at 40°C). The oil is chemically unstable and the instability increases with temperature. There is a time-dependent behavior called aging where the viscosity increases, volatility decreases and phases separate with time [6]. In addition, the level of deoxygenation of the oils required for successful co-refining is as yet unclear but initial recommendations state that oxygen content should be reduced to less than 7% to be considered as stabilized and completely miscible with petroleum [7]. An approximation of the composition of the crude bio-oil is presented by the chemical formula  $\text{CH}_{1.34}\text{O}_{0.43}$ . In order to upgrade the oils a hydrodeoxygenation (HDO) step could be implemented. In the hydrogenation step, oxygen is rejected in a catalytic reaction, which makes use of hydrogen, and leaves in the form of water. As a result, the plant requires a hydrogen supply in order to perform the upgrading, either produced on or off site.

There are two different methods for HDO (i) high pressure HDO of liquid bio-oil (ii) atmospheric vapor phase HDO. with high pressure HDO being the conventional process. The high-pressure liquid phase HDO is the conventional process designed at 20 MPa and 400°C [8], and requires 0.073 kg  $\text{H}_2$  per kg of fast pyrolysis oil [9]. However, vapor phase HDO step designed at atmospheric pressure is an interesting route that can be easily integrated with conventional pyrolysis units without the need for condensing of pyrolysis vapors and pressurizing the bio-oil. However, the process to directly apply HDO to pyrolysis vapors is still in experimental phase and has been reported to use 0.1 kg  $\text{H}_2$  per kg of dry biomass feed to pyrolysis step [10]. Attempts to reduce the load on the

HDO process by introduction of in situ catalysts in the pyrolysis process or using hydrogen instead of nitrogen in the pyrolysis process, have been proposed [11, 12]. A recent successful example is the IH2 (integrated hydro-pyrolysis and hydroconversion) process, which mitigates this problem through pyrolysis in a hydrogen-rich environment [13]. The bio-oil produced from these processes is further treated for oxygen removal, cracking of heavy carbon compounds to lighter products and upgrading the product to meet the transportation fuel requirements. However, there is still need for 0.053 kg hydrogen per kg of bio-oil in the IH2 process to upgrade the bio-oil [9]. Therefore, the source of hydrogen affects the techno-economic performance of bio-oil upgrading.

This project increases knowledge in integrating hydrogen generation processes with bio-oil production. Four different process pathways to produce deoxygenated bio-oils are investigated. Three of them are ex-situ hydro-deoxygenation of pyrolysis vapors, with hydrogen generated from (i) natural gas reforming (ii) electrolysis (iii) biomass/char gasification. The fourth pathway is the in-situ hydro-pyrolysis and hydro-conversion process, termed as IH2. These four pathways can be depicted in Figure 2. The investigated processes can be integrated with existing (i) sawmills where there is sawdust available or (ii) bio-refineries where the biooil can be converted into transportation fuels. The first three pathways, have the same pyrolysis and HDO step, and only the H<sub>2</sub> generation process is different. In this study, we analyze the vapor phase HDO process and its integration with bio-oil production. In-house process models for pyrolysis, gasification and HDO step have been developed using ASPEN Plus and validated against experimental results available in literature. We also present scenarios with improved process integration and including CO<sub>2</sub> capture and storage (CCS). Mass and energy balance for the IH2 process is developed based on the publicly available data and literature about the Gas Technology Institute's (GTI) patented technology. Finally, techno-economic analysis and greenhouse gas (GHG) assessment is presented for the different scenarios. These analysis helps us achieve the main objectives of the project to (i) obtain quantitative understanding of the proposed configurations production of transportation fuels based on pyrolysis and hydrodeoxygenation (ii) evaluate environmental (greenhouse gas) and techno-economic performance of the proposed process chains based on the quantitative understanding (iii) assessing future perspectives of integrating the process with biorefineries and potentially sawmills where sawdust is available for biooil production.

Section 2 presents the process description of the process pathways and modelling assumptions. In Section 3, we define the specific process scenarios analyzed in this project. In Section 4, we present and discuss the key results for process performance and techno-economic analysis followed by GHG assessment. Key performance indicators (KPIs) are also defined in Section 4. In Section 5 we summarize our conclusions. The detailed process modelling of different process steps and underlying assumptions is described in the Appendix.

The detailed analysis of the IH2 process was part of a master thesis project [14]. A YouTube video<sup>1</sup> is also available for step-by-step description of developing process model for biomass pyrolysis in ASPEN Plus.

---

<sup>1</sup> Modelling of biomass pyrolysis process in Aspen Plus, available: <https://youtu.be/s56NaOcPVg4>

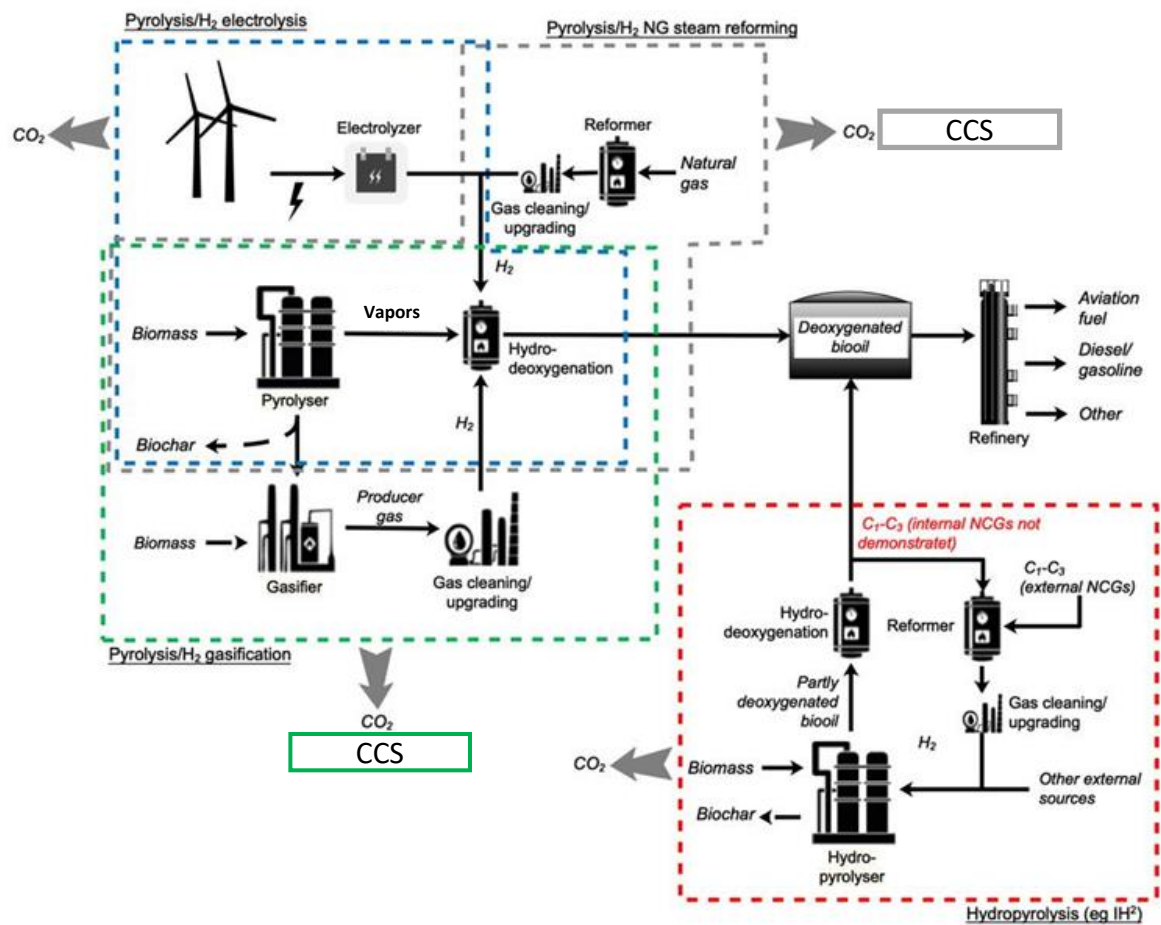


**Figure 2. Different routes for hydrogen and deoxygenated bio-oil production. Blue boundary is for the process that uses hydrogen for HDO from electrolysis. Green boundary is for the process where hydrogen is generated from biomass or char gasification. The grey boundary is for the process route that has NG reforming for hydrogen production for HDO. The red boundary is the IH2 process. NCG is the abbreviation for non-condensable gases. For the cases with biomass gasification and NG reforming, analysis have also been performed for the process integrated with CCS.**

## 2 PROCESS DESCRIPTION AND PROCESS MODELLING

In this section, we describe the different process steps and the modelling methodology used to analyze the process. The key process steps include biomass fast pyrolysis, vapor phase HDO step, hydrogen generation and bio-oil upgrading to diesel and gasoline fractions. The last step of upgrading to diesel/gasoline is same in all the process routes investigated, and therefore discussed only in the results and discussion section. The IH<sub>2</sub> process is also discussed in this section, but the detailed description is available in Subramaniam [14]. We also discuss the CO<sub>2</sub> capture process, which is integrated with pyrolysis and hydrogen generation processes.

### 2.1 BIOMASS FAST PYROLYSIS AND HDO PROCESS

#### 2.1.1 Process description

In this section, a general description of the whole biomass fast pyrolysis process is provided and covering all the steps considered for the production of bio-oil from biomass. Two options exist for production of bio-oils from fast pyrolysis: in situ catalytic fast pyrolysis followed by hydro-conversion and the pyrolysis followed by ex-situ vapor phase catalytic HDO. In this section we discuss the ex-situ process route based on the analysis presented by National Renewable Energy Laboratory (NREL) [15]. The reason why this specific configuration was chosen is because of the advantages this configuration provides. More specifically, the in-situ configuration combines both the fast pyrolysis process and the catalytic upgrading process of the fast pyrolysis vapors within the same reactor. In this manner, mixing the catalyst with biomass, char, and ash, and posing different challenges related to the catalyst performance and a need of continuous maintenance to the reactor. In exchange, the ex-situ configuration performs the fast pyrolysis and upgrading processes in separate reactors. The advantages that the ex situ configuration provides is that the upgrading process of the fast pyrolysis vapors are not exposed to the solid products associated with the pyrolysis process, providing in this manner a more favorable environment for reaction chemistry [15]. In addition, another advantage that the report of NREL highlights regarding the ex-situ configuration is that there is the possibility to attach a hot gas filter in between the reactors in order to remove the fine solid materials present in the vapor stream before entering the upgrading reactor. The overall process flow diagram is shown in Figure 3.

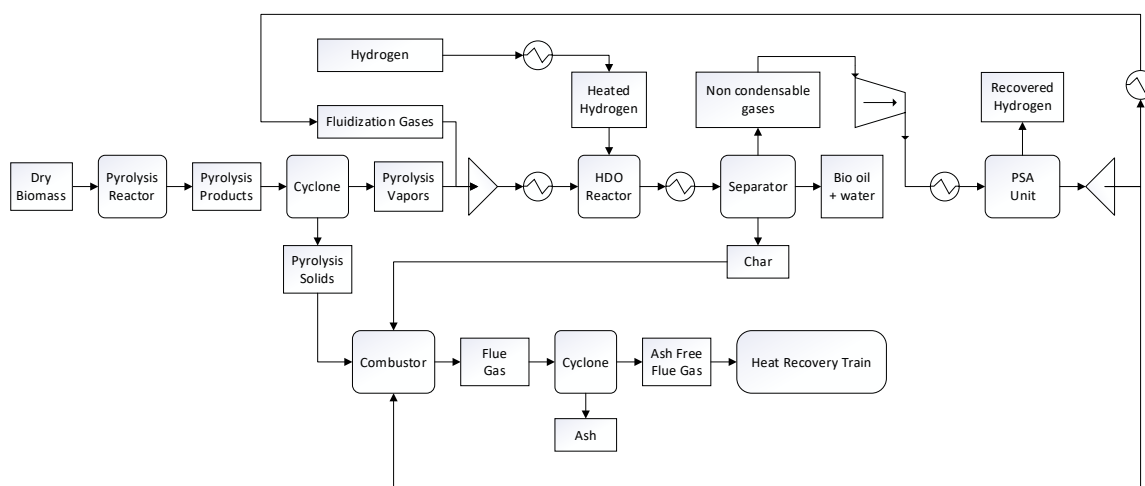


**Figure 3. Simplified process flow diagram of biomass fast pyrolysis process.**

In the fast pyrolysis process, the pyrolysis reactor is designed at a pressure of 2.3 bar, with an operating temperature of 500°C, and a residence time of 1.5 seconds. Dried biomass feedstock is fed to the reactor along with fluidizing gases and recirculating hot sand. This recirculation of hot sand stream provides the necessary heat required by the endothermic reactions of the pyrolysis process. After the dried biomass is pyrolyzed, the products of the process are composed of char, ash, pyrolysis vapor, steam, and non-condensable gases (which has mainly CO and CO<sub>2</sub>). The solid products such as char, sand and ash are separated from the vapor product stream and sent to the combustor, while the vapor product is cooled down in a heat exchanger and sent to the hydrodeoxygenation reactor to produce biooil that can be used in refinery to generate drop-in transportation fuels.

At the combustor, which operates at ambient pressure, the streams of char, sand and ash, and a stream of compressed air are supplied. A specific amount of air is provided to the combustor in order to achieve a complete combustion. The flue gas, besides being composed of CO<sub>2</sub> as the major component, it also contains residual ash and other finer particles, which are separated using a cyclone. Then, the solid-free flue gas stream is sent to a heat recovery train to preheat other streams and processes at the plant, and generate steam which is consequently sent to the turbine section to generate electricity. The recirculating sand stream is heated up during the combustion process and sent to the fast pyrolysis reactor with enough thermal capacity to satisfy the heat requirements by the endothermic reactions of the process.

The pyrolysis vapor stream, after being cooled, is sent to the HDO reactor, where the necessary amount of hydrogen is supplied for the hydrodeoxygenation process. The hydrodeoxygenation upgrading process of biomass pyrolysis oil removes oxygen atoms using hydrogen gas as a reducing agent [16]. The main focus in the project was the ex-situ hydrodeoxygenation of bio-oil under atmospheric pressure in the vapor phase, as it is an energy efficient and promising upgrading method. There are several catalysts that have been studied for vapor phase HDO upgrading at atmospheric pressure, but we have assumed a MoO<sub>3</sub> catalyst. The biomass fast pyrolysis vapors are hydrodeoxygenated with the help of the catalyst MoO<sub>3</sub>, and using hydrogen at a low pressure of 1.8 bar. The product stream consists mostly of linear alkanes (C1-C6) and aromatics [17]. Efficient HDO reactions with the suitable catalyst and design conditions can minimize the total hydrogen consumption of the process and therefore reduce capital and operation costs. The catalyst MoO<sub>3</sub>, [17]

proved to be very effective for the production of hydrocarbons at higher yields than those obtained by other studies using different catalysts and at different process conditions.

Hence, after the HDO process, the main composition of the product stream is bio-oil with water, char and non-condensable gases. The product stream is cooled down to condense the water content. Char is separated and sent for combustion to the combustor block to provide the sufficient energy for the endothermic reactions of the fast pyrolysis process. The bio-oil along with the condensed water leaving the reactor is consequently separated as well. The non-condensable gases stream is sent to a compressor, where it is pressurized to a specific pressure of 8 bar for the hydrogen recovery process. Once the stream of non-condensable gases has been compressed to the desired pressure, it is then sent to the pressure swing adsorption unit (PSA). Recovered hydrogen is ready to be used in the HDO process. Fraction of the resulting off gas from PSA is used as a fluidization gas and the remaining is combusted to generate heat for the endothermic processes.

### 2.1.2 Modelling of biomass fast pyrolysis

In general, the process modeling of biomass fast pyrolysis represents a challenge for most researchers as many variables are involved, which can impact the process results. Humbird et al. [18] presents that approximately more than a thousand species can be produced in fast pyrolysis systems. These differences in product species are caused by different sources such as feedstock composition, feedstock particle size, operating conditions of the reactor, reactor's size and configuration, and ultimately the variations in heat and mass transfer effects due to the previous elements mentioned.

Humbird et al. [18] presents the most common approaches to simulate fast pyrolysis reactors in large processes for techno-economic analysis:

- The first approach is through the yield specification of the representative process products previously obtained from experimental data [18].
- The second approach is the use of predictive models with reaction kinetics. However, the main challenges using a kinetic reaction framework are the scarcity of studies based on this approach, and that the reported kinetic parameters of these few studies often include mass, heat, and momentum transfer effects that are unique for each experiment.
- Finally, the third approach for the simulation of the fast pyrolysis process is the use of 2-dimensional or 3-dimensional Computational Fluid Dynamic (CFD) models, which would be more beneficial for modeling the dynamics inside the reactor from first principles. However, the downside of using a CFD model are the long computation times that can significantly increase with the addition of more reaction kinetics or when a more detailed simulation is required. The few available studies that take the approach of using a CFD model are based on simple reaction kinetics, and lump the fast pyrolysis products in three categories, char, tar, and gas.

In order to balance the fluid dynamics and detailed kinetics, Humbird et al. [18] used a 1-dimensional fast pyrolysis reactor with a reasonably detailed speciation of process products. The latter is important as an adequate speciation of products is necessary for the proper modeling of downstream operations such as the hydrodeoxygenation of fast pyrolysis oil. Finally, another study that uses a CFD modeling approach is the work of Trendewicz et al. [19], in which the issues that arise

from the variations of biomass composition, residence time, and reaction temperature on the pyrolysis process, were addressed by incorporating a flexible pyrolysis reaction mechanism, a 1-dimensional steady state momentum balance for the solids-gas flow, a 1-dimensional steady state energy equation, and the use of a multistep, multicomponent reaction system developed by Ranzi et al. [20]. The model used by Trendewicz et al. [19] provides a reasonable distribution of products for the modeling of the downstream processing section of bio-oil.

The approach taken in our study for the modeling of biomass fast pyrolysis follows the same approach taken by Caudle et al. [21], and using a more recent multistep kinetic scheme of biomass pyrolysis developed by Ranzi et al. [22]. Although, some improvements were made on the multistep kinetic scheme to correct model deficiencies in our work, these improvements will be addressed in detail in the following section. Thus, the process flow for the biomass fast pyrolysis process, represented in Figure 1, was developed using the commercial process modeling software Aspen Plus. An overall process flow diagram of the biomass fast pyrolysis process can be seen in Figure 4.

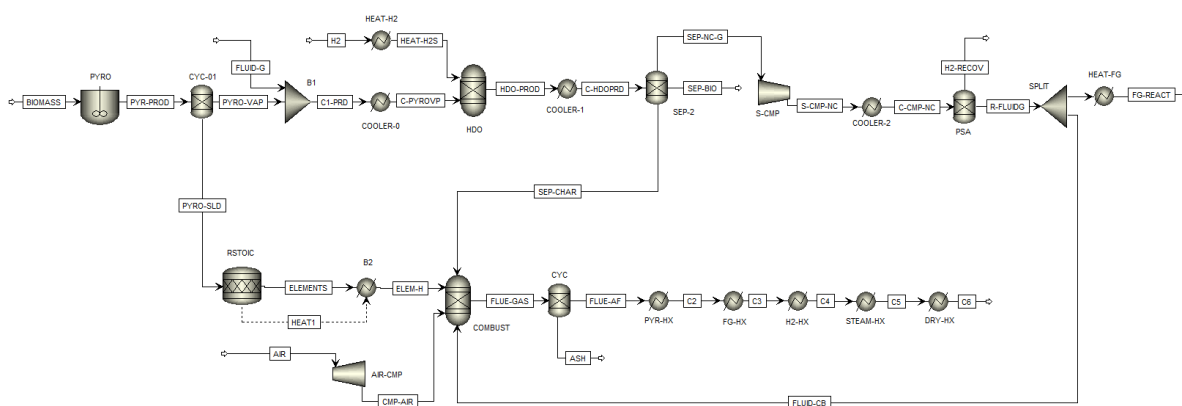


**Figure 4. Process flow of the biomass fast pyrolysis process in Aspen Plus. The details in the figures are described in the sections below.**

#### Simulation environment setup

The following steps were taken for the modeling of the biomass fast pyrolysis in Aspen Plus: (i) specification of biomass components and the composition of the biomass samples used in the study (ii) manually specifying the thermophysical properties of the biomass components (iii) selection of a suitable fluid package (iv) specification of the thermodynamic framework.

#### Biomass composition

The three major building blocks of biomass are cellulose, hemicellulose, and lignin. Other important components are extractives, moisture and ash. The content of each one of these components depends entirely on the sample of biomass taken for the process. The following table, Table 1, summarizes the components in biomass:

**Table 1. Assumed (dried) biomass composition in pyrolysis step in the analysis (Composition is similar to the composition of dried Douglas fir wood belonging to the pine family). (Source [21])**

<i>Biomass Components</i>	<i>Weight fraction (wt%) (dry)</i>
Cellulose	42.93
Hemicellulose: Glucomannan (Softwood)	21.46
Hemicellulose: Xylan (Hardwood)	-
Lignin rich in Carbon	4.56
Lignin rich in Oxygen	10.67
Lignin rich in Hydrogen	11.75
Tannin	1.20
Triglyceride	4.92
Moisture	2.04
Ash	0.48

The composition of biomass is similar to Douglas fir wood (having 30% moisture content before drying), which belongs the pine family. It is important in Sweden’s context, because 70% percent of Sweden’s land area is covered by forest, from which: 42% is spruce, 39% is pine, 12% is birch, and 7% being other deciduous trees [23].

In this project, we also present the results for bio-oil production for different biomass types. We consider 4 different types of spruce and pine. The characteristics of the different samples of Spruce and Pine wood present in different physical forms (such as chips or sawdust) have been assumed from study of Debiagi et al. [24], and are summarized in Table 24 and Table 25 in the Appendix.

*Thermophysical properties of biomass*

The thermophysical properties for the biomass components, biomass pyrolysis intermediate species, and biomass pyrolysis end products were taken from the work of Gorenssek et al. [25]. It includes 49 components, from which 20 are not present in the Aspen plus databank. The reason for which these 20 components are not present in the commercial process simulator databank is because of the complexity of representing biomass on hypothetical “model compounds” that cannot be isolated for their respective measurement of physical properties [25]. Since the accuracy of a process model depends entirely on the fidelity of its component’s properties model, Gorenssek et al. [25] compiles information from different studies of the thermophysical properties for these missing components.

Hence, in the present section a summary of the different components generated during the biomass fast pyrolysis are presented. A complete table of the different components along with their formulas, ID, type, and specification of their availability of the thermophysical properties data in the Aspen plus databank can be found in Table 26 in the Appendix. In the following section, the different thermophysical properties of the missing components, biomass pyrolysis intermediate species, and biomass pyrolysis end products - that were manually introduced into the simulation environment - are addressed.

For biomass fast pyrolysis process, Ranzi et al. [22] assumes that each biomass component behaves independently, giving as a resulting 7 components that form reactive intermediates, which undergo further decomposition. These reactive intermediate components are activated cellulose, two acti-

vated components of hemicellulose, three intermediate components of lignin, and a tannin intermediate. Table 2 summarizes different components involved in the biomass fast pyrolysis process. The overall components are divided into four groups, the first group “Biomass components” presents the un-pyrolyzed biomass components. The second group “Biomass Pyrolysis Intermediate Species” describes the intermediate products of biomass pyrolysis. The third group “Biomass Pyrolysis End-Products” presents the 28 end products of biomass pyrolysis.

**Table 2. Different components in biomass, intermediate species and end-products involved in the fast pyrolysis process. Non-biomass components are also listed in the table.**

<i>Biomass Components</i>		
- Cellulose (CELL)	- O – rich lignin (LIGO)	- Moisture
- Glucomannan	- H – rich lignin (LIGH)	- Ash
- Xylan	- Tannin (TANN)	
- C – rich lignin (LIGC)	- Triglyceride (TGL)	
<i>Biomass Pyrolysis intermediate Species</i>		
- Secondary lignin intermediate (LIG)	- Activated hemicellulose 1 (HCE1)	- Tannin intermediate (ITANN)
- C – rich lignin intermediate (LIGCC)	- Activated hemicellulose 2 (HCE2)	
- H/O – rich lignin intermediate (LIGOH)	- Activated cellulose (CELLA)	
<i>Biomass pyrolysis end products</i>		
- Char	- Acrolein	- Formaldehyde
- Sinapyl aldehyde	- n – propionaldehyde	- Formic acid
- Free fatty acid	- 3 – hydroxypropanal	- Methane
- High–molecular–weight lignin	- Furfural (FURF)	- Methanol
- Glyoxal (GLYOX)	- Xylosan	- Carbon monoxide
- Ethylene	- Levoglucosan (LVG)	- Carbon dioxide
- Acetaldehyde	- Phenol	- Hydrogen
- Acetic acid	- 5–hydroxymethyl–furfural	- Water
- Glycolaldehyde	- Anisole	
- Ethanol	- P – coumaryl alcohol (COUMARYL)	
<i>Non biomass components also included in the simulation environment</i>		
- Argon	- Nitrogen	- Oxygen
- Sand		

More details are available in Table 26 in the Appendix.

#### *Thermodynamic model to estimate properties*

The selection of a proper thermodynamic model in Aspen plus for the simulation of the fast pyrolysis process of biomass is based on the approach taken by Gorenssek et al. [25], where the Peng-Robinson cubic equation of state with the Boston-Mathias alpha function (also known as the PR-BM method) was chosen as the thermodynamic basis for the calculation of the properties for the different streams in the biomass fast pyrolysis process. This fluid package is recommended for gas pro-

cessing, refinery, and petrochemical applications, and it also has been used by other researchers for the modeling of the biomass fast pyrolysis process.

However, Table 3 summarizes the property data required in simulation. These properties have been assumed from the work of Gorenssek et al. [25] and are summarized in Table 27 and Table 28 respectively in the Appendix.

**Table 3. Required estimated properties for the solid and conventional components.**

Required estimated properties	
Solid Components	Conventional components
<ul style="list-style-type: none"> <li>- Molecular weight</li> <li>- Standard solid heat of formation</li> <li>- Solid molar heat capacity</li> <li>- Solid molar volume</li> </ul>	<ul style="list-style-type: none"> <li>- Molecular weight</li> <li>- Ideal gas standard state heat of formation</li> <li>- Critical temperature</li> <li>- Critical Pressure</li> <li>- Acentric factor</li> <li>- Vapor pressure</li> <li>- Ideal gas molar hear capacity</li> </ul>

Once the different properties for the conventional solid and conventional fluid components have been specified in Aspen Plus, we proceed with the definition of the multistep kinetic scheme of biomass fast pyrolysis. The scheme is based on Ranzi et al. [22]. Biomass is characterized as a mixture of reference components, and each one of these components decompose independently through a series of lumped kinetic mechanisms. The original multistep kinetic scheme by Ranzi et al. [22] can be found in Table 29 in the Appendix.

**Table 4. Adapted multistep kinetic scheme of the biomass fast pyrolysis process from the original multistep kinetic scheme of Ranzi et al. [22]. [The kinetic data for \*Reaction 14 reported in the table is the modified value to fit the resulting product composition available in literature. Comparison with the value from Ranzi et al. [22] is shown in Table 5]. (A is the pre-exponential factor, x is the power to which temperature is raised in the equation, Ea is the activation energy). Please refer to Table 2 and Table 26 (in Appendix) for definition of components in the reactions.**

Reaction		$An$ ( $K^{-xn} * s^{-1}$ )	$xn$	$Ea$ [kcal/kmol]
<b>Cellulose</b>				
1)	CELL → CELLA	$1.5 \times 10^{14}$	0	47 000
2)	CELLA → 0.4 HAA + 0.05 GLYOX + 0.15 CH <sub>3</sub> CHO + 0.25 HMFU + 0.35 ALD3 + 0.15 CH <sub>3</sub> OH + 0.3 CH <sub>2</sub> O + 0.61 CO + 0.36 CO <sub>2</sub> + 0.25 H <sub>2</sub> + 0.93 H <sub>2</sub> O + 0.02 HCOOH + 0.05 C <sub>3</sub> H <sub>6</sub> O <sub>2</sub> + 0.05 CH <sub>4</sub> + 0.61 CHAR	$2.5 \times 10^6$	0	19 100
3)	CELLA → LVG	3.3	1	10 000
4)	CELL → 5 H <sub>2</sub> O + 6 CHAR	$6 \times 10^7$	0	31 000
<b>Hemicellulose</b>				
5)	GMSW → 0.7 HCE1 + 0.3 HCE2	$1 \times 10^{10}$	0	31 000
6)	XYHW → 0.35 HCE1 + 0.65 HCE2	$1 \times 10^{10}$	0	28 500
7)	HCE1 → 0.6 XYLAN + 0.2 C <sub>3</sub> H <sub>6</sub> O <sub>2</sub> + 0.12 GLYOX + 0.2 FURF + 0.4 H <sub>2</sub> O + 0.08 H <sub>2</sub> + 0.16 CO	3	1	11 000
8)	HCE1 → 0.4 H <sub>2</sub> O + 0.8 CO <sub>2</sub> + 0.05 HCOOH + 1.6 CO + 1.25 H <sub>2</sub> + 0.3 CH <sub>2</sub> O + 0.625 CH <sub>4</sub> + 0.375 C <sub>2</sub> H <sub>4</sub> + 0.875 CHAR	$1.8 \times 10^{-3}$	1	3000
9)	HCE2 → 0.2 H <sub>2</sub> O + CO + 0.575 CO <sub>2</sub> + 0.4 CH <sub>2</sub> O + 0.1 C <sub>2</sub> H <sub>5</sub> OH + 0.05 HAA + 0.35 ACAC + 0.025 HCOOH + 0.25 CH <sub>4</sub> + 0.3 CH <sub>3</sub> OH + 0.225 C <sub>2</sub> H <sub>4</sub> + 0.725 H <sub>2</sub> + CHAR	$5 \times 10^9$	0	31 500
<b>Lignins</b>				
10)	LIGC → 0.35 LIGCC + 0.1 COUMARYL + 0.08 PHENOL + 0.41 C <sub>2</sub> H <sub>4</sub> + H <sub>2</sub> O + 1.02 CO + 0.7 H <sub>2</sub> + 0.3 CH <sub>2</sub> O + 0.495 CH <sub>4</sub> + 5.735 CHAR	$1 \times 10^{11}$	0	37 200
11)	LIGH → LIGOH + 0.5 ALD3 + 0.5 C <sub>2</sub> H <sub>4</sub> + 0.2 HAA + 0.1 CO + 0.1 H <sub>2</sub>	$6.7 \times 10^{12}$	0	37 500
12)	LIGO → LIGOH + CO <sub>2</sub>	$3.3 \times 10^8$	0	25 500
13)	LIGCC → 0.3 COUMARYL + 0.2 PHENOL + 0.35 HAA + 0.7 H <sub>2</sub> O + 0.65 CH <sub>4</sub> + 0.6 C <sub>2</sub> H <sub>4</sub> + H <sub>2</sub> + 1.8 CO + 6.75 CHAR	$1 \times 10^4$	0	24 800
14)*	LIGOH → 0.9 LIG + H <sub>2</sub> O + 0.45 CH <sub>4</sub> + 0.9 CH <sub>3</sub> OH + 0.9 H <sub>2</sub> + 0.05 CO <sub>2</sub> + 2.1 CO + 0.05 HCOOH + 0.2 C <sub>2</sub> H <sub>4</sub> + 0.025 HMWL + 0.1 ACROL + 4.25 CHAR	$0.4 \times 10^6$	0	30 000
15)	LIG → 0.7 FE2MACR + 0.3 ANISOLE + 0.6 CO + 0.3 CH <sub>3</sub> CHO	4	1	12 000
16)	LIG → 0.6 H <sub>2</sub> O + 2.6 CO + 0.6 CH <sub>4</sub> + 0.4 CH <sub>2</sub> O + 0.5 C <sub>2</sub> H <sub>4</sub> + 0.4 CH <sub>3</sub> OH + 2 H <sub>2</sub> + 6 CHAR	$8.3 \times 10^{-2}$	1	8000
17)	LIG → 0.6 H <sub>2</sub> O + 2.6 CO + 1.1 CH <sub>4</sub> + 0.4 CH <sub>2</sub> O + C <sub>2</sub> H <sub>4</sub> + 0.4 CH <sub>3</sub> OH + 4.5 CHAR	$1 \times 10^7$	0	24 300
<b>Extractives</b>				
18)	TGL → ACROL + 3 FFA	$7 \times 10^{12}$	0	45 700
19)	TANN → PHENOL + CO + H <sub>2</sub> O + ITANN	20	0	10 000
20)	ITANN → 5 CHAR + 3 CO + H <sub>2</sub> O + H <sub>2</sub>	$1 \times 10^3$	0	25 000
<b>H<sub>2</sub>O Evaporation</b>				
21)	H <sub>2</sub> O → H <sub>2</sub> OL	1	1	8000

As seen in Table 4, the biomass pyrolysis mechanism is described with lumped kinetic models, even though this limits the correctness and accuracy of the model. This lumped biomass pyrolysis mechanism represents a rough attempt to describe the complex behavior of pyrolysis products. Also, Ranzi et al. [22] states that several comparisons with experimental data prove the reliability of the multistep kinetic scheme, and also mentions that this multistep kinetic scheme of biomass can be easily modified and revised in order to improve the model correctness and accuracy in case of working with new experimental information. For that reason, the kinetic data for reaction number 14 was adjusted to fit the predicted results for product compositions in pyrolysis step.

**Table 5. Modified reaction from the original multistep kinetic scheme of Ranzi et al. [22]. This table reports the adjustments we made in kinetic data for Reaction 14 with respect to literature**

<i>Reaction</i>		<i>An</i> ( $K^{xn} \cdot s^{-1}$ )	<i>xn</i>	<i>Ea</i> [kcal/kmol]
<i>From literature</i>				
<b>14)</b>	LIGOH → 0.9 LIG + H <sub>2</sub> O + 0.1 CH <sub>4</sub> + 0.6 CH <sub>3</sub> OH + 0.05 G[H <sub>2</sub> ] + 0.3 G[CH <sub>3</sub> OH] + 0.05 CO <sub>2</sub> + 0.65 CO + 0.6 G[CO] + 0.05 HCOOH + 0.85 G[COH <sub>2</sub> ] + 0.35 G[CH <sub>4</sub> ] + 0.2 G[C <sub>2</sub> H <sub>4</sub> ] + 4.25 CHAR	1x10 <sup>8</sup>	0	30000
<i>Adapted value in our work</i>				
<b>14)</b>	LIGOH → 0.9 LIG + H <sub>2</sub> O + 0.45 CH <sub>4</sub> + 0.9 CH <sub>3</sub> OH + 0.9 H <sub>2</sub> + 0.05 CO <sub>2</sub> + 2.1 CO + 0.05 HCOOH + 0.2 C <sub>2</sub> H <sub>4</sub> + 0.025 HMWL + 0.1 ACROL + 4.25 CHAR	0.4x10 <sup>6</sup>	0	30000

In addition, as seen in Table 29 in the Appendix, the original multistep kinetic scheme considers partial trapping species, denoted in the reactions as “G [...]”, in the metaplastic phase. Hence, following the approach taken by Caudle et al. [21], the partial trapping species in the original multistep kinetic scheme are disregarded. Instead, these species are treated as instantaneous and are assumed as seen in Table 4. Regarding the Ash component, it is commonly characterized using a proximate and ultimate analysis approach. This will be true for the gasification process modeling of biomass in Section 2.3. However, for the fast pyrolysis process modeling of biomass, ash will be treated as the chemical compound calcium oxide (CaO). Char is considered as pure carbon (C).

#### Model setup for fast pyrolysis process in Aspen Plus

RCSTR block was used to simulate the fast pyrolysis reactor in Aspen Plus. The biomass feed stream enters the RCSTR block at 2.3 bar and 500°C along with fluidization gases and sand. For simplicity purposes, and due to the long computational times and the multistep kinetic scheme, the fluidization gas stream was attached to a mixer block placed after the fast pyrolysis reactor. Regarding the heat transferred through the recirculation of the stream of sand, it is simulated by the use of a heat stream recovered from the hot flue gas stream coming from the combustor.

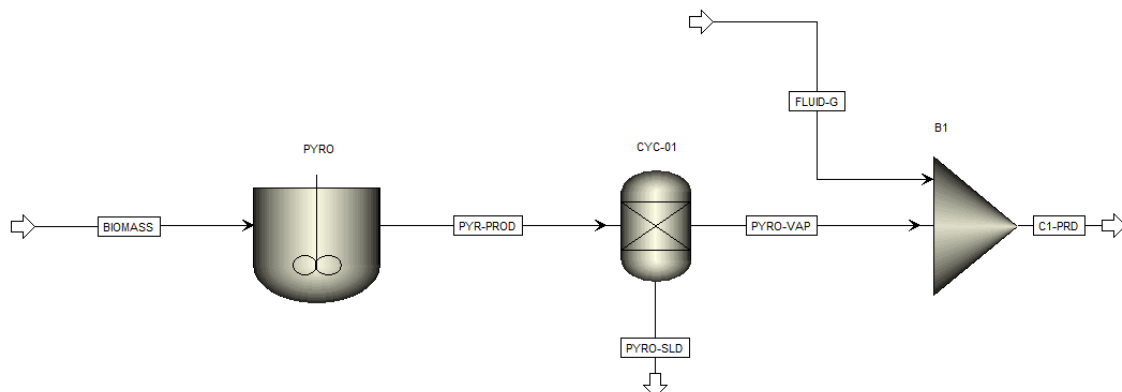


**Figure 5. Fast Pyrolysis reactor model in Aspen Plus.**

As seen in Figure 5, the product streams leaving the fast pyrolysis reactor are separated into two streams: “Pyrolysis vapors” (PYRO-VAP) and “Pyrolysis solids” (PYRO-SLD). The pyrolysis vapor stream is sent to the mixer block where it is mixed with the fluidization gases stream, while the pyrolysis solid stream is sent to the combustor modelled as a RSTOIC reactor where the non-conventional solid components are converted into their elements, such as hydrogen, carbon, and oxygen.

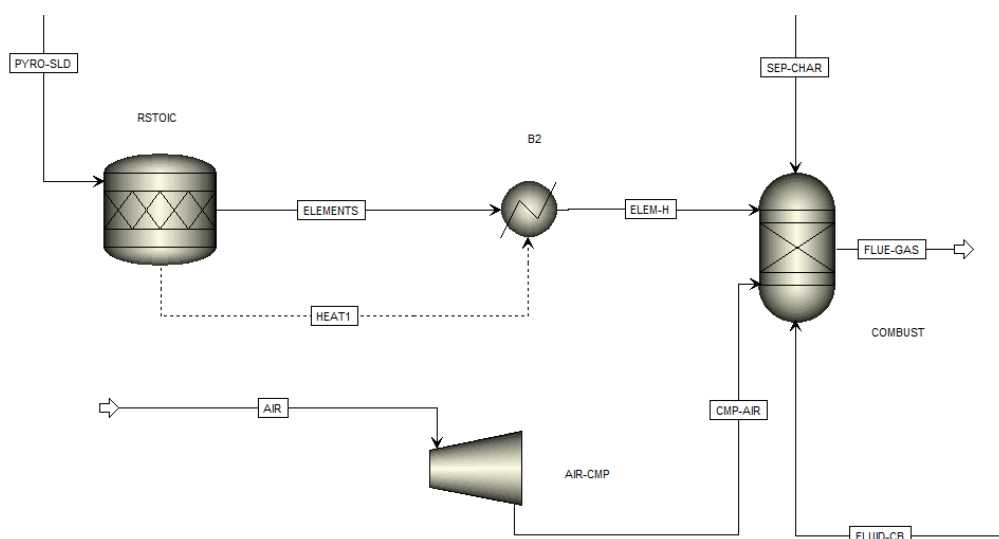


**Figure 6. Conversion of the fast pyrolysis stream to conventional components as modelled in Aspen Plus.**

As seen in Figure 6, these elemental components are combusted with a specific amount of air and provide the sufficient amount of energy required by different sections and processes at the plant.

Biomass pyrolysis model validation

In general, the pyrolysis of biomass results in the production of huge number of chemical compounds. For that reason, for the validation process of different pyrolysis models, reaction products are often lumped into three groups: gases, pyrolytic liquid (bio-oil/tar) and char [26]. According to the work of Di Blasi et al. [26], these groups result from both the primary decomposition of biomass and the secondary reactions of volatile condensable organic products into low-molecular weight gases and char, in addition to numerous factors such as such temperature, pressure, heating rate, biomass composition, ash content, moisture content, particle size, affect the product yields.

Regarding the permanent gases group, it usually comprises CO<sub>2</sub>, CO, CH<sub>4</sub> and lower amounts of H<sub>2</sub> and C<sub>2</sub> hydrocarbons, while the pyrolytic liquid composition is highly dependent on the operating conditions of the thermal treatment, such as temperature and residence time within the reactor of the tar vapors [26]. In our case, the products from the pyrolysis process are lumped into the mentioned groups and compared with experimental data from different studies.

Results from our model were in coherence with results obtained by Caudle et al. [21] as seen in Table 6.

**Table 6. Comparison between the experimental results of Caudle et al. [21] and our model.**

		Caudle. et al. work [21]	Model Results
Liquid	kg/hr	49,90	48,91
Gas	kg/hr	60,40	61,79
Solid	kg/hr	7,30	6,12
Water	kg/hr	7,10	7,00
Ash	kg/hr	0,40	0,37

From the table above, we can appreciate that there is a good agreement between the results obtained by Caudle et al. [21] and our model being the major difference the amount of char (solid) produced in our case.

*Modeling of the ex-situ vapor phase Hydrodeoxygenation (HDO) Process*

The Pyrolysis vapors after being mixed with the fluidization gases, are cooled down until 400°C with the help of a heat exchanger. The cooled down stream enters the HDO block modeled as a RYIELD reactor, where hydrogen enters the block for the respective hydrodeoxygenation process of bio-oil. The product distribution for the RYIELD reactor is specified in Table 33 in the Appendix. Hydrogen consumed in the HDO step is assumed to 10% of the total mass of dried biomass. The HDO process itself is an exothermic process, and the heat released from the process block is used to generate steam at 181°C and 3 bar. A schematic of the process can be seen in Figure 7.

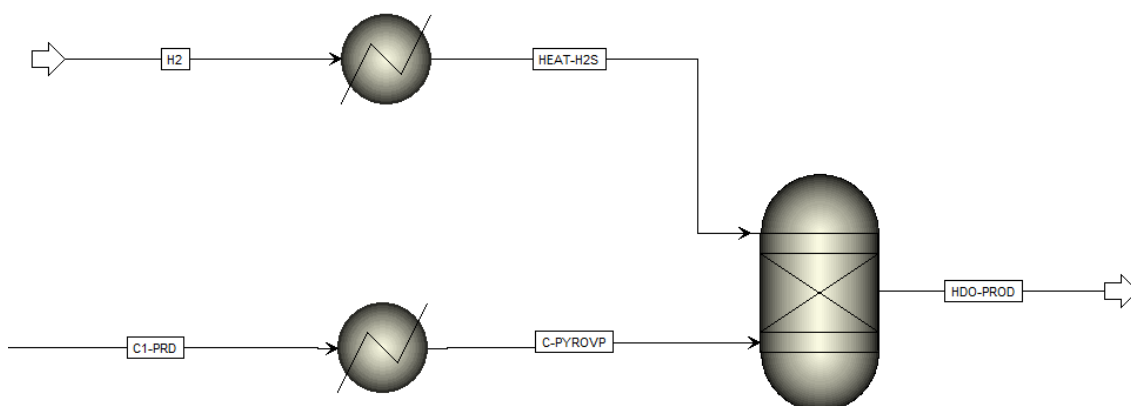


**Figure 7. HDO unit in Aspen Plus.**

As previously mentioned, the modeling of the hydrodeoxygenation of bio-oil under atmospheric pressure in the vapor phase was the main focus. A review of different studies was performed and a summary of the different catalysts which have been tested at atmospheric HDO can be found in Ta-

ble 31 in the Appendix. Also, different studies were reviewed in terms of the type of biomass sample used as feedstock. A summary of these reviews can be seen in Table 32 in the Appendix. Therefore, based on the review, the catalyst and upgraded bio-oil composition from Nolte et al. [17] were chosen for the modeling of the HDO unit. Furthermore, the principal outcomes from the study of Nolte et al. [17] were the following: the bio-oil composition remains the same irrespective of the starting biomass chosen for pyrolysis and HDO upgrading, and the carbon, oxygen and hydrogen wt% was found to be in the same range for different biomass raw materials. Therefore, this proves that the final composition requirements for upgraded bio-oil remains the same irrespective of starting biomass raw material.

#### Modeling of the Pressure Swing Adsorption (PSA) unit

The non-condensable gases stream is sent to a compressor where it is pressurized to 8 bar for the respective recovery of hydrogen in the PSA unit. During the process modeling, the PSA unit was modelled as a normal component separator block. Regarding the total amount of hydrogen recovered from the separator, it was determined according to the following formula provided by Nazir et al. [27], where P1 and P2 are the pressures of the PSA feed-gas and off-gas streams respectively:

Amount of hydrogen recovered in PSA:

$$H_2 \text{ recovery in PSA (\%)} = 100 - \frac{100}{0.2521 \left(\frac{P_1}{P_2}\right) + 1.2706} \quad \text{Eq 1}$$

The hydrogen recovered from the PSA process can be used in the hydrodeoxygenation section in the pyrolysis plant, and the off-gas is sent as fuel to the combustor block for thermal disposal.

#### Heat recovery and Power generation

The heat recovery and power generation section of the plant has the purpose of collecting and distributing heat between different parts of the process and producing electricity from the excess heat generated by the process. At the fast pyrolysis plant there are several process operations that provide a significant amount of heat, which if used efficiently, can positively impact the economics of the overall process. Some of the major sources of heat (latent and sensible heat) at the fast pyrolysis plant are the following: char, char combustor, upgraded pyrolysis vapors, combustor flue gas, and HDO reactor. Remaining heat from the process after using it for pre-heating streams and for endothermic reactions, is recovered in the form of steam that is expanded in the turbine to generate electricity.

Regarding the simulation of the steam cycle process, it was developed in Aspen HYSYS. Following are the assumptions in the model.

- Composition of air and conditions entering to the combustor, from Anantharaman et al [28].
- Pressure drop for different reactors (1% from the inlet pressure), pressure drop for heat exchangers (2% from the inlet pressure), efficiency of the syngas and non-condensable gases compressor (80%), efficiency of the air compressor (92.5%), efficiency of the different pumps in the process (80%).
- H<sub>2</sub> recovery rate in the PSA unit from Nazir et al [27].

- The conditions of the water for steam generation were: 3.4 bar, and 29°C. The conditions of the steam produced were: 3 bar, and 181°C. The conditions for the cooling water for different processes were: an increase of 12°C from 17 to 29°C, and pumped at 3 bar pressure.

## 2.2 MEA SOLVENT BASED CO<sub>2</sub> CAPTURE UNIT

The traditional method to remove CO<sub>2</sub> is to scrub the CO<sub>2</sub> containing stream with a solvent capable of dissolving the gas at a sufficient rate and quantity [29]. This process is performed in counter-current within an absorber column equipped with trays or packings. Then, the solvent loaded with CO<sub>2</sub> is sent to a stripper column where it is flashed under atmospheric temperature conditions. The CO<sub>2</sub> is released and the solvent is regenerated before being used again in the absorption column through recirculation [29].

From the variety of physical and chemical solvents used in the industry, Appl et al. [29] mentions that selecting a specific type depends mostly on the process's operating conditions such as the partial pressure of CO<sub>2</sub>, which when is low, chemical solvents are preferred due to its characteristic to absorb a major quantity of CO<sub>2</sub> than physical solvents. For that reason, for the present work, Monoethanolamine (MEA) was selected as the chemical solvent to capture 90% of CO<sub>2</sub> from the flue gas stream.

### Modeling of the MEA carbon capture unit

The MEA unit was modeled in Aspen Hysys with a carbon capture rate of 90% of the flue gas stream. The carbon capture unit consists of an absorber, a stripper column with a reboiler, a pump for the solvent, and heat exchangers. After the residual ash has been removed from the flue gas with a separator block, it is sent to the absorber column which has 20 stages. The ash free flue gas stream at a temperature around 100°C enters from the bottom part and the lean amine containing 30 wt% MEA and an initial CO<sub>2</sub> loading of 0.3364 is fed from the upper section with a temperature of 40°C and a pressure of 1.09 bar. The mass flow of the MEA stream was set in order to achieve a 90% carbon capture rate.

Hence, the CO<sub>2</sub> rich amine leaving the absorber column is sent to a heat exchanger where it is heated up until a temperature of 80°C before entering the stripper column. The conditions of the steam used for the regeneration of the amine were: temperature of 181°C, 3 bar pressure, requiring 5082,42 kJ/kg of CO<sub>2</sub> captured.

The regenerated amine leaving the stripper unit at a temperature around 100°C preheats the CO<sub>2</sub> loaded amine with the aid of a heat exchanger. It is further cooled in a heat exchanger until reaching a temperature of 40°C, and finally pumped back to the absorber unit for recirculation.

## 2.3 BIOMASS GASIFICATION

### 2.3.1 Overall description of the process

In this study, we assume the same conditions in gasification process of biomass like the fast internally circulating fluidized bed (FICFB) gasifier design used in the plant of Güssing in Austria, which has been operating since 2002 and has a capacity of 8 MW fuel input [30]. A schematic of the process flow can be seen in Figure 8.

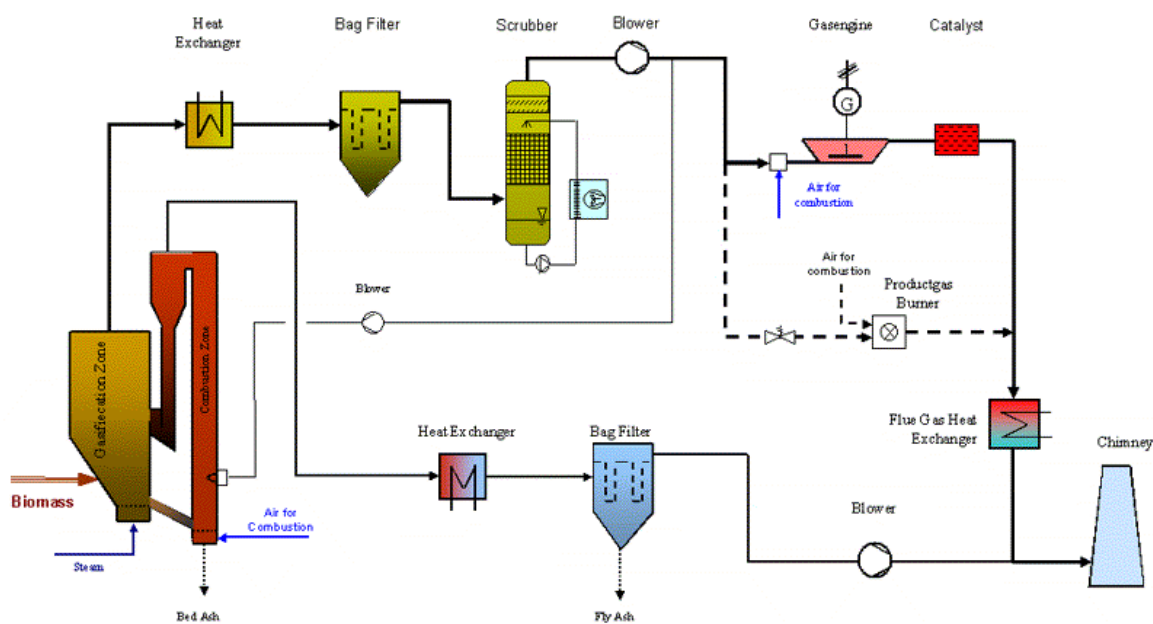


**Figure 8. Biomass gasification process diagram flow in the plant of Güssing, Austria. Source: <https://web.archive.org/web/20120324011457/http://www.ficfb.at/>.**

The plant was capable of producing heat and power, 4.5 MWth and 2 MWeI respectively. At the plant, the biomass is gasified within a circulating fluidized bed reactor. The product gas generated is cooled and cleaned in two stages, and finally used as fuel in a gas engine.

Biomass feedstock is dried before entering the FICFB gasifier. It can be done through different methods. One example is the natural drying method which is achieved by storing the material for a period of time of 1 to 2 years. Then, once the biomass material has been dried to a desired moisture content, it is delivered to the plant and chipped on site. At Güssing, the moisture content of the biomass material used in the plant ranged from 25 to 40%. The biomass chips are transported with the use of a daily hopper and fed into the fluidized bed reactor through screw feeders.

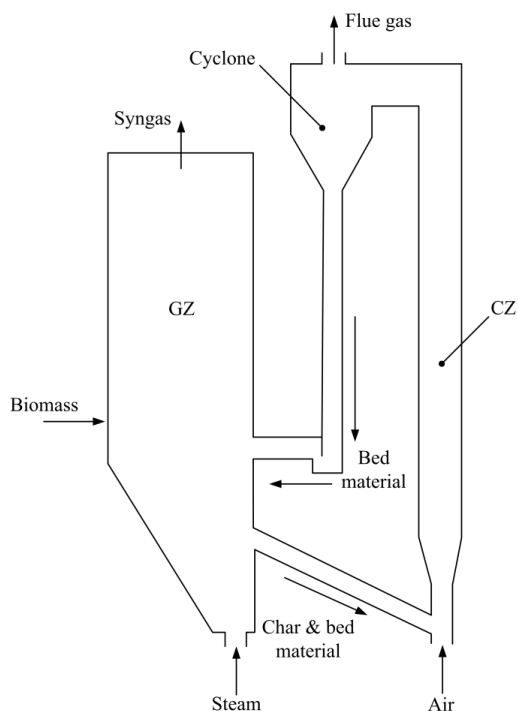


**Figure 9. Fast Internally Circulating Fluidized Bed (FCICFB) schematic diagram (Source: [31]).**

As seen in the schematic of the process shown in Figure 9 [31], the fast internally circulating fluidized bed (FICFB) is divided into two zones, the gasification zone (GZ) and the combustion zone (CZ). This FICFB gasifier operates at atmospheric pressure and the advantages of this configuration is the physical separation of the gasification and combustion reactions, which results in a largely  $N_2$  free syngas [31].

The chipped biomass feedstock enters to the bubbling fluidized bed reactor (GZ), where the bed material provides the necessary heat required by the endothermic gasification reactions and is fluidized with steam generated by recovering waste heat from the process. Biomass is pyrolyzed and gasified with steam producing residual char, which leaves the gasification zone along with the bed material through an inclined chute to the circulating fluidized bed riser (CZ). At the combustion zone, a stream of air is supplied to combust the residual char and fluidize the bed material. The flue gas generated from the process is separated from the bed material with the use of a cyclone, and the bed material is recycled back to the gasification zone through a loop seal [31].

The syngas stream coming out of the gasifier is cooled down from a temperature of  $850^{\circ}\text{C}$ - $950^{\circ}\text{C}$  to about  $150^{\circ}\text{C}$ - $180^{\circ}\text{C}$  with the aid of heat exchangers. The cooled syngas stream is cleaned within a two-stage cleaning process (i) where the first cleaning stage consists of a fabric filter that separates the particles and some tar present in the stream (ii) and the second cleaning stage consists of a scrubber unit that separates any remaining amount of tar from the stream. From the first cleaning stage, the captured solid particles and tar are recycled back to the combustion zone, while from the second stage, the resulting scrubber liquid saturated with tar is vaporized and also sent to the combustion zone for thermal disposal.

Finally, the resulting syngas stream from the scrubber unit is used in a gas engine, and it is also catalytically oxidized to reduce the emissions of carbon monoxide. The sensible heat released in this

process is used to produce district heat, and the flue gas is used to pre heat the stream of air going to the combustor. The details for modelling the gasification process are available in the Appendix.

### Water Gas Shift Section

The syngas stream leaving the gasifier reactor contains a little but non-negligible amount of CO produced during the biomass gasification. Hence, a conversion from CO to CO<sub>2</sub> is crucial for further downstream processes. The diagram flow of the process is shown in Figure 10.

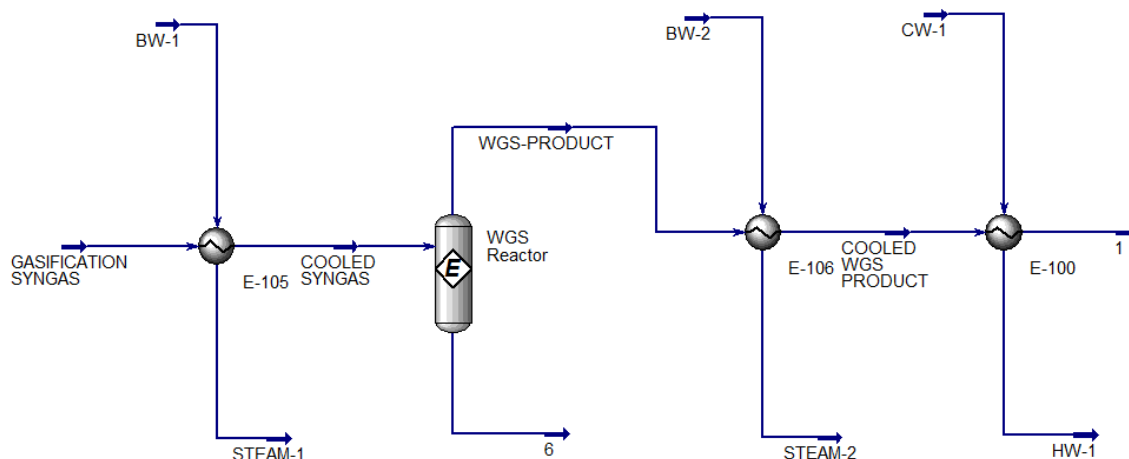


**Figure 10. Water gas shift section diagram flow as modelled in Aspen Plus.**

An equilibrium reactor “WGS Reactor” was used for the modeling of the water gas shift conversion of CO to CO<sub>2</sub>, this conversion is achieved through the input of the following reaction in the equilibrium reactor:



The water gas shift conversion in general is performed in two stages, the first stage is performed in a high temperature reactor (HT), and the second stage in a low temperature reactor (LT). However, for the present work, the water gas shift conversion is performed in only one stage, where the syngas enters with a temperature of 250°C to the WGS reactor, and leaves at approximately 292°C. The heat of the water gas shift product stream is recovered through the use of two heat exchangers, one is used to generate steam and the other to further cooldown the syngas coming from the first heat exchanger for the next stages, syngas compression train and PSA section. Nearly 97% of the total CO content in the initial syngas stream was converted into CO<sub>2</sub>.

### Pressure Swing Adsorption Section

The cooled down syngas stream from the water gas section is compressed through a three-stage intercooled compressor with a polytropic efficiency of 80% up to a final pressure of 25 bar before entering the Pressure Swing Adsorption unit. Then the compressed syngas is sent to the Pressure Swing Adsorption (PSA) unit where hydrogen is recovered. The amount of hydrogen recovered is estimated similarly as discussed before, according to the equation presented by Nazir, Cloete [27].

As mentioned previously, the hydrogen recovered from the PSA process can be used in the hydrode-oxygenation section in the pyrolysis plant, and the off-gas is used as fuel in combustion. A schematic of the PSA section in Aspen can be seen in Figure 11.

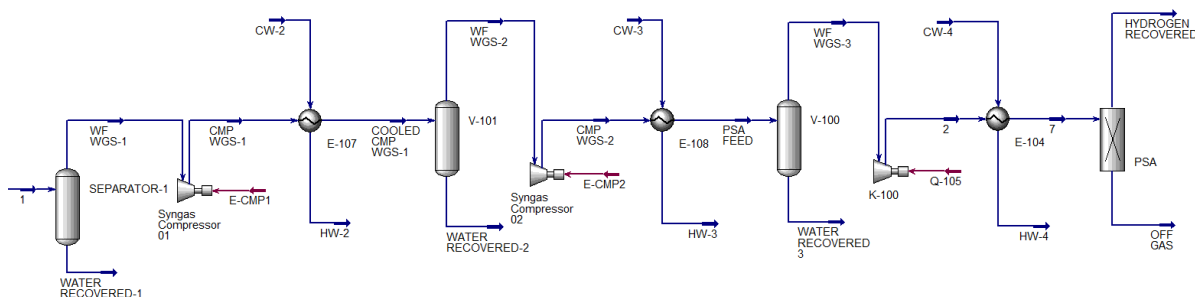


Figure 11. Intercooled syngas compressor train and PSA section as modelled in Aspen Plus.

## 2.4 HYDROGEN PRODUCTION FROM NATURAL GAS REFORMING

Hydrogen is produced by reforming of natural gas using a fired tubular reformer (FTR). The process is similar to the one presented by Nazir et al. [27] and Martinez et al. [32]. The schematic of the process can be seen in Figure 12.

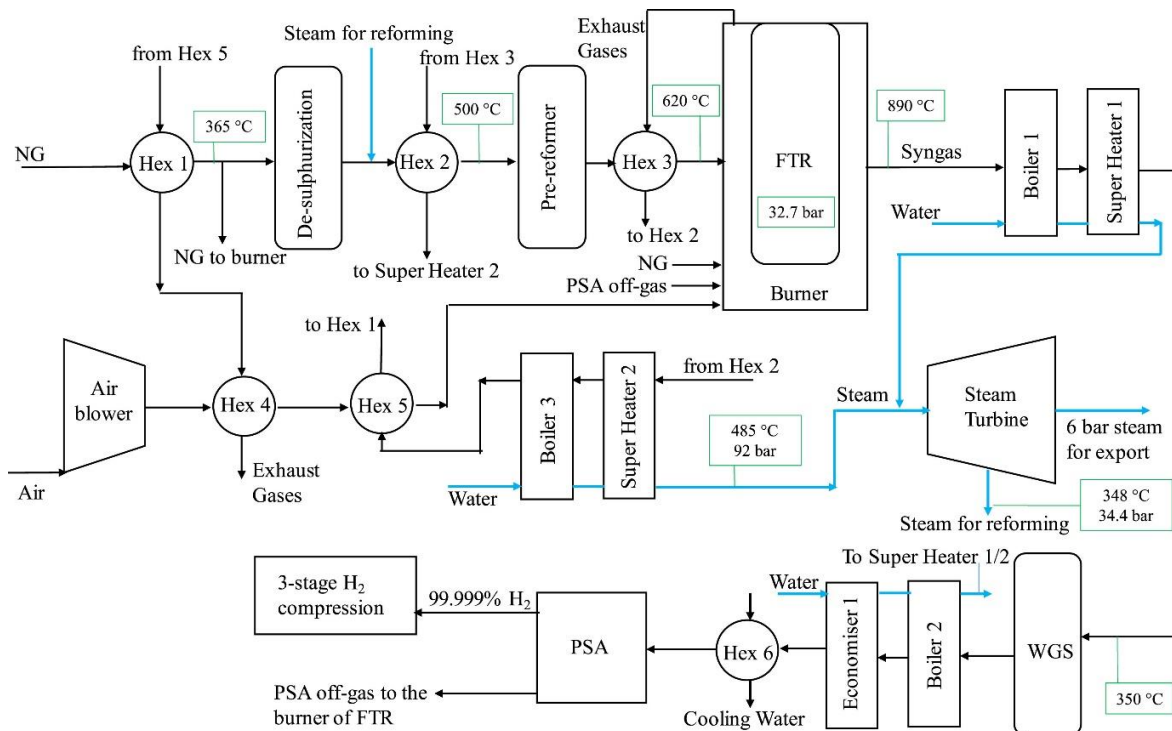


Figure 12. Schematic of the SMR plant using FTR for the reforming of Natural gas – Reproduced from Nazir et al. [27].

Natural gas is de-sulphurized, mixed with steam and sent to a pre-reformer to convert the higher hydrocarbons. The resulting stream is sent to the reforming unit (FTR) with the following operating conditions: a pressure of 32.7 bar and a ratio of steam to carbon (S/C) of 2.7. A fraction of the natural gas stream (3%) is extracted after the desulphurization process and combusted along with the

off-gas produced from pressure swing adsorption (PSA) unit in order to provide the heat required by the endothermic reactions of the reforming section. After the reforming process, approximately 80% of the methane content of natural gas is converted into syngas, which is further cooled down and treated in a WGS unit to convert any content of CO and H<sub>2</sub>O in the syngas into CO<sub>2</sub> and H<sub>2</sub> before entering the PSA unit, where 99.99% of pure H<sub>2</sub> is recovered.

## 2.5 HYDROGEN PRODUCTION FROM ELECTROLYSIS

In this project, we assume hydrogen is generated from an alkaline electrolyser, similar to the one available with NEL [33]. The energy required to produce 1 kg H<sub>2</sub> with greater than 99.9% purity is assumed to be 42 kWh. This is the best available technology and can be scaled and customized according to use case specification. The system is scaled depending on the hydrogen needed for HDO step.

## 2.6 IH2 PROCESS

IH2 is a two-stage, catalytic fast hydrolysis process integrated with a downstream hydrotreatment reactor to produce a fungible gasoline/diesel blendstock using various biomass and plastic waste feedstocks. A simple schematic for the IH2 process is shown in Figure 13. Hydrogen and biomass are introduced into the catalytic pyrolysis fluidized bed reactor at 20-35 bar and 350-500°C. The biomass is converted into low oxygen content hydro-carbon vapors and char. Here, hydrogen acts as both fluidizing and deoxygenation agent. The second stage is a fixed bed reactor and designed at similar pressures as the first fluidized bed reactor, but having slightly lower design temperatures (260-430°C). The purpose of the second reactor is to remove any hetero atoms like nitrogen and Sulphur from the hydrocarbons. The vapors are then sent through a series of high- and low-pressure separators and condensers where water, condensable hydrocarbons and non-condensable gases are separated. The condensed hydrocarbon stream is having suitable quality to be used as gasoline and diesel blendstocks for further downstream processing. The non-condensable gases are reformed to generate hydrogen needed for IH2 process. More details regarding the process and its performance are presented in Subramaniam [14].

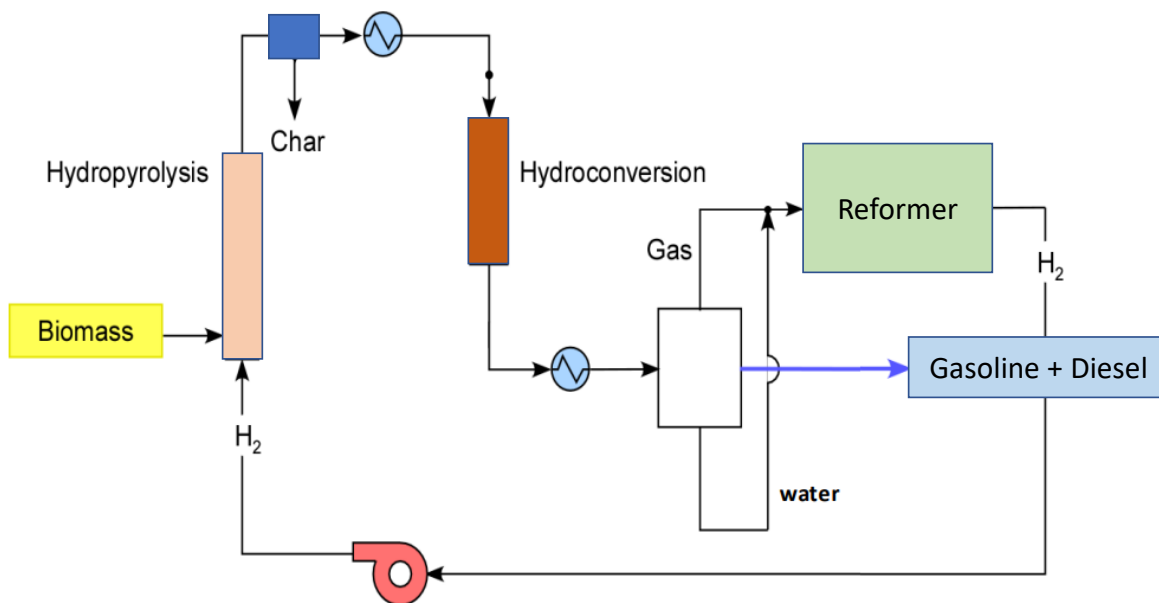


Figure 13. Simple process flow schematic of IH2 process as proposed by GTI (Source: [34]).

### 2.7 BIOOIL TO TRANSPORTATION FUELS

The mass and energy balances of the downstream refinery processing of the deoxygenated bio-oil was based on [35], which assumes hydroprocessing via a SynSat process to meet applicable fuel standards. The mass balance is shown in Figure 14. As can be seen, the final product split based on mass is 35 % diesel and 65 % gasoline. The hydrogen demand is 0.15 MJ/MJ diesel (LHV), or about 0.02 kg hydrogen per kg fuel (diesel + gasoline).

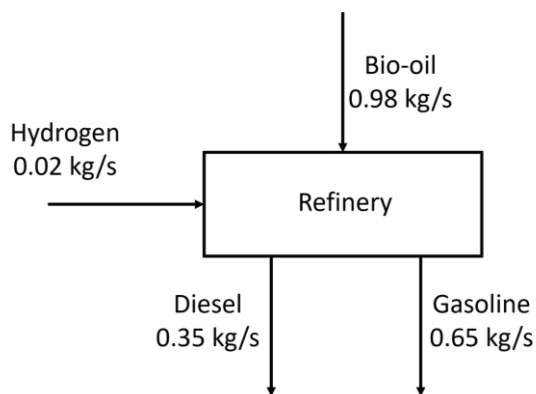


Figure 14. Assumed mass balance for refinery processing of the produced deoxygenated bio-oil.

### 3 PROPOSED PROCESS SCENARIOS

Different process scenarios have been studied as part of this project. These scenarios are described as cases below in Table 7.

**Table 7. Definition of different process scenarios.**

Case	Definition
Reference case scenarios	
Ref1	HDO step uses hydrogen generated from natural gas reforming process
Ref2	HDO step uses hydrogen generated from electrolysis
Ref3	HDO step uses hydrogen generated from biomass gasification
Ref4	HDO step uses hydrogen generated from gasification of biochar from the process and additional biomass
CCS case scenarios – These scenarios have a post-combustion MEA absorption-based CCS process integrated with the bio-oil production process	
CCS1	CO <sub>2</sub> is captured from the NG reforming process that generates hydrogen for the HDO step. The remaining process is similar to case Ref1
CCS2	CO <sub>2</sub> is captured only from the combustion exhaust gases from pyrolysis step. The remaining process is similar to case Ref3
CCS3	CO <sub>2</sub> is captured from the combustion exhaust gases from both pyrolysis and gasification step. The remaining process is similar to case Ref3.
CCS4	CO <sub>2</sub> is captured from the combustion exhaust gases from both pyrolysis and gasification step. The remaining process is similar to case Ref4.
CCS5	CO <sub>2</sub> is captured from the combustion exhaust gases from gasification step. The remaining process is similar to case Ref3.
IH2	Bio-oil is produced in the IH2 process

## 4 METHODOLOGY

In this section we describe the methods used to estimate the process and techno-economic performance followed by greenhouse gas emissions assessment,

### 4.1 PROCESS PERFORMANCE

The main key performance indicators (KPIs) to assess the process performance of the proposed process routes are defined below.

- Carbon recovery in bio-oil product: We have defined two indicators for carbon recovery in bio-oil. Carbon recovery is defined as the ratio between carbon recovered in the hydrode-oxygenated bio-oil to the total input carbon in the biomass feed to the pyrolysis step. System level carbon recovery is defined as the ratio between the carbon recovered in bio-oil and the total carbon input to the system. The total carbon input to the system also includes the carbon input in producing hydrogen for the HDO step.

$$\text{Carbon Recovery} = \frac{\text{Mass of Carbon in bio-oil}}{\text{Mass of Carbon in biomass feed to pyrolysis}} \quad \text{Eq 2}$$

$$\text{System level carbon recovery} = \frac{\text{Mass of Carbon in bio-oil}}{\text{Mass of Carbon input to the entire system}} \quad \text{Eq 3}$$

- Bio-oil yield: This is defined as the ratio between the mass of hydro-deoxygenated bio-oil produced and the mass of dry biomass feed to the pyrolysis process. The system level yield is defined as the ratio of mass of deoxygenated bio-oil produced and the mass of total biomass input to the system (biomass for pyrolysis and biomass for gasification).

$$\text{Yield}_{\text{biooil}} = \frac{\text{Mass of bio-oil}}{\text{Mass of dry biomass feed to pyrolysis}} \quad \text{Eq 4}$$

$$\text{System level yield}_{\text{biooil}} = \frac{\text{Mass of bio-oil}}{\text{Mass of dry biomass feed to the system}} \quad \text{Eq 5}$$

- Energy efficiency: The energy efficiency of the process system is defined through conversion efficiency and system efficiency as described below.
  - Conversion Efficiency: This is defined as the ratio between the energy content of bio-oil produced (LHV basis) and the energy content (LHV basis) of the biomass feed (biomass dry basis).

$$\eta_{\text{conversion}} = \frac{\text{Biooil Product Energy}}{\text{Feedstock Energy}} \quad \text{Eq 6}$$

- System Efficiency: This is defined as the ratio between the total output energy from the system to the total input energy. The total output energy includes the energy content in bio-oil, net electricity generated within the system and steam exports. The total input energy includes the energy content in biomass feed (dry), fuel for hydrogen generation and electricity. In the case of IH2 process, the total input energy includes the energy content in biomass feed (dry) and electricity.

$$\eta_{\text{system}} = \frac{\text{Output Energy}}{\text{Input Energy}} \quad \text{Eq 7}$$

## 4.2 ECONOMIC AND GHG ASSESSMENT

This section describes the methodology, tools and input data used for the economic and GHG assessments of the process routes investigated in the present work. The ENPAC-tool (described below) was the main tool used to establish consistent price and emission factor data for evaluated process routes. The economic and GHG assessment below covers all reference cases (Ref1-4) and two CCS-cases (CCS1 and CCS4). CCS1 is the natural gas case and CCS4 is the case combining utilization of bio-char in gasification, and CCS applied to both the pyrolysis process and the gasification process. The remaining CCS-cases (CCS2,3 and 5) are similar to CCS4, but proved less promising in a preliminary analysis considering economic and environmental parameters, why CCS4 was selected as the only (BE)CCS case considered in this section.

The process modeling described above only considers production of deoxygenated bio-oil. However, the economic and GHG assessments are based on comparison to the final motor fuels gasoline and diesel.

### ENPAC Scenarios

The present work used scenarios of the ENPAC-tool [36], [37] to generate energy carrier prices and GHG emission factors. The ENPAC-tool was developed to generate consistent energy market scenarios, i.e., scenarios where key parameters are clearly linked by means of e.g., conversion technologies or substitution principles. Input data – required for all scenario years – are fossil fuel prices on the world market (crude oil, natural gas and coal), charge for emitting CO<sub>2</sub> and optional policy support instruments. Based on this input data and a few additional user options, the tool calculates GHG emission factors and price data for industrially relevant energy carriers using the modules described below (only modules of relevance to this project are described).

In general, the prices and emission factors produced by ENPAC reflect the long-term marginal effect of increased use of energy carriers/sources. The tool uses system expansion and assumptions about marginal changes in the surrounding system to assess the system impact of changes in energy use. The emission factors include Well-to-Gate<sup>2</sup> and combustion emissions. Note that only fossil CO<sub>2</sub> emissions are included (i.e., emission of fossil carbon atoms). However, bio-based energy carriers still have non-zero emission factors since Well-to-Gate emissions are considered - for example, fossil fuels may be used for collecting and transporting biomass. Since the tool assesses the marginal impact of increased use of an energy carrier, biomass utilization can sometimes cause significant CO<sub>2</sub> emissions, if it redirects biomass from an existing use (see the description of the wood energy module below).

- **Fossil fuel module:** The prices of light and heavy heating fuel oil for industrial users are calculated from the crude oil price using correlations based on historical data. The price of natural gas and coal for industrial users is calculated similarly.

---

<sup>2</sup> “Well-to-Gate” covers emissions associated with the supply of raw materials and with the production/refining stage but does not include the transportation and distribution of final products. The scope of Well-to-Gate ends when the products leave the production plant or refinery and is thus narrower than the scope of “Well-to-tank”.

- **Motor fuel module:** The prices of diesel and gasoline at pump are calculated from the crude oil price using correlations based on historical data. The biofuel sale price at gate is calculated assuming that the price at pump must be the same, i.e., by subtracting distribution costs and adding biofuel support revenues to the fossil fuel price at pump.
- **Electricity module:** The electricity price and emission factor of electricity is calculated using the concept of build margin. The underlying assumption is that increased electricity consumption in the system will eventually lead to the construction of new base-load plants. The power generation technology with the lowest levelized cost of electricity generation (including investment costs) will be selected and constitutes the build-margin technology which determines the cost and emission factor of electricity in ENPAC scenarios. The calculation is based on fuel prices and technical and economic data built into the tool. Natural Gas Combined Cycle (NGCC) and Coal are always included as potential build-margin technologies in ENPAC, and the user can choose to include Nuclear and Wind as options, as well as a CCS option for the fossil technologies.
- **Wood energy module:** The price of wood fuel (biomass) is calculated using the concept of willingness-to-pay and assumed future marginal users of wood fuel. There are two possible marginal uses of biomass in ENPAC: co-firing in coal power plants and conventional bio-fuel production in a biorefinery. The price that these users are willing to pay for biomass is related to the price of the alternative fossil energy carrier (coal or motor fuel, including CO<sub>2</sub> charges) and sets the price of wood energy in ENPAC.

For the calculation of the emission factor of wood fuel the user has the choice to treat biomass either as a limited or an unlimited resource, a distinction that has a significant impact on the emission factor. If biomass is treated as an unlimited resource, the only emissions associated with biomass use are the emissions from activities required to deliver a unit of biomass to the production plant (for forest residues: collection and transportation). However, if biomass is considered a limited resource, any new biomass user will effectively use biomass that would otherwise be used by the marginal biomass user in the system. In ENPAC it is assumed that this will cause the marginal biomass user to use fossil energy sources instead (e.g., power plants co-firing bio-pellets and coal will increase the share of coal in combustion), which is reflected by a considerably higher emission factor for biomass usage.

Treating biomass as a limited resource is representative of a future where the use of biomass has increased drastically due to ambitious climate policies during the transition to a sustainable society, up to a point where all sustainably produced biomass is used. At this point, any new use of biomass will divert biomass from an existing marginal user. Consequently, it is crucial that any new use of biomass is better (from a GHG emission perspective) than the existing use it displaces. By considering the marginal effects that arise when biomass is treated as a limited resource, it is possible to make sure that an investigated prospective project is not only “better” than current fossil processes, but also represents a good way of using limited biomass resources to reach climate targets.

Combustion emissions of biomass are always treated as zero.

In the present work, two ENPAC scenarios for 2030 were used. The scenarios use fossil fuel price data from the 2019 World Energy Outlook [38] scenarios “Sustainable development” (SD) and

“New policies” (NP). The ENPAC scenario inputs and outputs are summarized in Table 8. Note that hydrogen is not included in ENPAC. The price has been estimated as 3.564 times the price of natural gas (excl. CO<sub>2</sub> charge) based on [39]. The value reflects hydrogen production via SMR of natural gas. This value was only used to calculate the hydrogen cost at the refinery where bio-oil is processed into diesel and gasoline. The cost of hydrogen required for production of bio-oil was instead based on the biomass, power or natural gas demand (depending on process setup) as determined by process modeling.

In the SD Scenario, biomass is considered a limited resource. This is motivated by the fact that the ambitious policies required to bring about a sustainable development may lead to an energy system where all biomass that can be sustainably and cost-effectively utilized is used. In the NP Scenario, climate policies are less ambitious, and it is assumed that there will be un-utilized biomass that can be used cost-effectively by new biofuel plants. Thus, biomass is considered an unlimited resource in this scenario.

**Table 8. Input data used to generate ENPAC scenarios, and the resulting output data used in GHG and economic assessments in this work.**

ENPAC data	2030-SD	2030-NP
Input		
Fossil fuel prices data source	WEO-2019: 2030-SD	WEO-2019: 2030-NP
Biomass as a limited resource?	Yes	No
Support for renewable electricity (EUR/MWh)	5	5
EU ETS CO <sub>2</sub> charge (EUR/tonne)	79	29
CO <sub>2</sub> charge for gasoline (EUR/tonne)	99	99
CO <sub>2</sub> charge for diesel (EUR/tonne)	110	110
Support for gasoline biofuel (EUR/MWh-LHV)	43	43
Support for diesel biofuel (EUR/MWh-LHV)	25	25
Output		
Energy carrier	Energy price (EUR/MWh-LHV)	
Grid electricity (buyer)	48	48
Grid electricity (seller)	45	45
Biomass (buyer)	27	16
Hydrogen (from SMR)	67	57
Natural gas incl. CO <sub>2</sub> charge (buyer)	48	41
Biofuel (gasoline), incl. support – sale price at gate	114	128
Biofuel (gasoline), excl. support – sale price at gate	71	85
Biofuel (diesel), incl. support – sale price at gate	106	122
Biofuel (diesel), excl. support – sale price at gate	81	97
Energy carrier	Emission factor (kgCO <sub>2</sub> eq./MWh-LHV)	
Grid electricity	0	0
Biomass usage	405	8
Natural gas	248	
Gasoline (Well-to-Gate and Combustion emissions)	286	
Diesel (Well-to-Gate and Combustion emissions)	289	

### Economic assessment

The economic feasibility of the investigated process routes was assessed by estimating the maximum total capital investment (TCI) that allows a prospective plant to be profitable, i.e., the total

investment opportunity. The total capital investment (TCI) includes the total cost of building the plant, including the direct costs of installed equipment on-site, as well as indirect costs (engineering, contingency etc.) To estimate the total investment opportunity, the specific operating costs (OPEX) were compared to the potential fuel sales price, according to:

$$\text{Total investment opportunity} \left( \frac{\text{EUR}}{\text{GJ}} \right) = \text{Fuel sales price} \left( \frac{\text{EUR}}{\text{GJ}} \right) - \text{OPEX} \left( \frac{\text{EUR}}{\text{GJ}} \right) \quad \text{Eq 8}$$

Given the fuel sales price and the specific operating costs (OPEX) of the production plant, the total investment opportunity calculated according to equation Eq 8 gives the maximum specific annualized TCI (in EUR/GJ) that allows the plant to break even. The corresponding total TCI (in EUR) can be calculated using the annual fuel production (in GJ) and the annuity factor<sup>3</sup>. With this approach, the high uncertainty associated with capital cost (TCI) estimates of new technologies can be avoided. When the total investment opportunity has been estimated, a rough TCI estimate is often enough to determine whether the investigated process is likely to be economically feasible.

The OPEX estimates used in the present work were calculated per unit of produced biofuel energy (EUR/GJ biofuel-LHV), with biofuel output taken as the sum of diesel and gasoline production. The OPEX estimates were based on mass and energy balances from the process modeling, additional assumptions for the refinery processing (see Figure 14), feedstock and energy prices from the ENPAC scenarios, and the assumptions outlined in Table 9. For energy prices, see Table 8.

For cases with (BE)CCS, a concept similar to the Northern Lights project was considered. In this concept, the captured CO<sub>2</sub> is liquefied and stored temporarily at the biofuel plant site (total storage capacity equals four days of production) before being loaded onto ships and taken to a central hub where it is injected to storage via pipeline. The off-site costs (ship transport, central hub storage, pipeline transport and final storage) were assumed to be 42.5 EUR/tonne reflecting the mid-point of estimates given for 2030 by the Northern Lights project [40]. Compression was included in the modeling in the present work, and the liquefaction power demand was assumed to be 19.6 kWh/tonne based on [41]. In the present work, capture of fossil CO<sub>2</sub> was assumed to decrease the price of natural gas bought by the biofuel plant by an amount equal to the product of the amount of CO<sub>2</sub> captured and the EU ETS CO<sub>2</sub> charge.

There is currently no market for negative emissions. However, it is likely that such a market will develop or that government subsidies will be used to incentivize negative emissions. From a European perspective, it is reasonable to assume that market prices (or the size of the subsidies) will be linked to the EU ETS CO<sub>2</sub> charge. For example, allowing negative emission credits for compliance within EU ETS would tie the value of negative emission credits directly to the CO<sub>2</sub> charge. However, as pointed out in Zetterberg, Johnsson [42], EU ETS charges will likely not be high enough to support early BECCS-projects. This could be solved by keeping markets for negative emissions separate from the EU ETS and use e.g., procurement to create a premium on negative emissions compared to the EU ETS charge. In the present work, negative emissions were assumed to give "negative emission credits" priced at a 25 % premium compared to the EU ETS CO<sub>2</sub> charge.

<sup>3</sup> Calculated according to  $(1 - (1 + r)^{-n}) / r$ , where n is the lifetime of the investment and r is the discount rate.

Refinery OPEX was estimated based on increased hydrogen demand at the refinery due to processing of bio-oil to gasoline and diesel. A hydrogen demand of 0.15 MJ/MJ diesel (LHV) was assumed based on [35]. (see also Figure 14).

**Table 9. Parameters and data used in the economic assessment.**

Variable costs (EUR/GJ LHV biofuel)		
Parameter	Value	Comment
Catalysts	4.25	Re-calculated from 0.18 EUR/kg biofuel given for HDO of pyrolysis oil in [39].
Feed sizing	0.31	Added to biomass cost from ENPAC following the approach of [35].
Miscellaneous	0.29	Based on [35]. Includes e.g., waste-water treatment and boiler operations.
Fixed costs (EUR/GJ LHV biofuel)		
Parameter	Value	Comment
Labour	0.48	From Jones et al. [43] escalated from USD2011 to EUR2019 using the Chemical Engineering Plant and Cost (CEPCI) labour index.
Overhead	0.43	90 % of labour cost.
Maintenance		5 % of average annualised TCI estimate.
- Natural gas	0.40	
- Electrolysis	0.42	
- Gasification	0.40	
Operational and financial parameters		
Parameter	Value	Comment
Plant availability	96 %	-
Discount rate	8 %	-
Plant life (years)	20	-
Biofuel capacity (MW-LHV)	256.5	Average of studies underlying the TCI estimates. 35.8 % diesel (energy basis), balance gasoline.
Other		
Parameter	Value	Comment
Negative emissions premium	25 %	Capture of biogenic CO <sub>2</sub> valued at 125% of the EU ETS CO <sub>2</sub> charge
CO <sub>2</sub> transport and storage cost (EUR/tonne)	42.5	Estimated value for 2030 based on [40].

As indicated in Table 9, the maintenance cost was estimated from the total capital investment (TCI) meaning that an indicative estimate of this value was needed. The procedure used to generate this estimate is described below and summarized in Table 10. Note however that only an indicative estimate was developed in this work, as this was required to estimate maintenance cost and hence the total OPEX. A more rigorous approach should be used if more accurate estimates are required.

TCI for bio-oil processes similar to those studied in the present work were estimated by [43] and [15] and the average of the two estimates was used in this work to develop indicative TCI values. The values given by [43] and [15] include hydrogen generation via steam methane reforming and have been used for the natural gas process routes (Ref1 and CCS1) without adjustments other than escalation to 2019 money value using the CEPCI composite index.

For process routes with alternative hydrogen supply (electrolysis (Ref2) and gasification (Ref 3-4, CCS4)) the cost of steam methane reforming has been replaced in the installed equipment cost (IEC) estimates by cost estimates for the alternative technologies and the TCI has been recalculated.

lated. For electrolysis the purchased equipment cost estimate was based on cost functions derived from data for alkaline electrolyzers given in [44], resulting in a purchased equipment cost of about 460 EUR/kW<sub>el</sub> for the capacities considered in the TCI estimates. The electrolyser LHV system efficiency was taken as 65 % and the installation factor was taken as 1.2. For gasification, installed equipment cost for hydrogen production via gasification were based on [45] and scaled to the capacities of [43] and [15] using a cost-escalation factor of 0.6.

Installed equipment costs for the carbon capture process (without compression and storage) were based on cost functions developed by [46], while liquefaction and on-site storage costs were based on [41]. Costs occurring during transport to the final storage site are external to the project and were treated as a variable OPEX item at 42.5 EUR/tonne as described above.

Details regarding the TCI estimates for the various cases are summarized in Table 10. The average of the annualized specific TCI estimates was used to calculate the specific (EUR/GJ-LHV) maintenance costs given in Table 9.

**Table 10. Summary of Total Capital Investment (TCI) estimates for the investigated process routes. The studies by Jones et. al. and Dutta et.al. considered production of deoxygenated bio-oil with hydrogen supply via steam methane reforming (i.e., Ref1 in the present study). An average of their TCI estimates was used directly for Ref1. For other routes, TCI values were adjusted to account for differences in hydrogen supply and the use of (BE)CCS, where relevant. All monetary values have been escalated to EUR-2019 using the CEPCI composite index and annual average currency exchange rates. IEC: Installed Equipment Cost, PEC: Purchased Equipment Cost.**

	Jones et al. 2013 [43]	Dutta et al. 2015 [15]
<b>Hydrogen supply via natural gas reforming</b>		
Capacity (MW LHV biofuel)	259	254
Annual production (GJ LHV biofuel)	7 841 111	7 689 738
Hydrogen demand (MW LHV)	118	86
TCI – natural gas route, Ref1 (MEUR)	650	556
IEC (MEUR)	359	300
IEC without hydrogen production (MEUR)	295	237
<b>Alternative hydrogen supply - electrolyser</b>		
Specific electrolyser cost, PEC (EUR/kW <sub>el</sub> )	460	
Electrolyser installation factor	1.2	
Electrolyser LHV efficiency	65 %	
Electrolyser IEC	100	73
TCI – electrolysis route, Ref2 (MEUR)	718	575
<b>Alternative hydrogen supply – biomass gasification</b>		
Gasifier thermal input (MW <sub>th</sub> LHV)	149	108
Gasifier thermal input (MW <sub>th</sub> LHV) – NREL cost estimate	478	
Cost escalation factor	0.6	
Gasifier IEC	73	60
TCI – gasifier routes, Ref 3-4, CCS4 (MEUR)	668	550
<b>(BE)CCS costs</b>		
Carbon capture IEC (EUR/tonne)	Natural gas: 202 Gasification (integrated): 134	
Liquefaction cost IEC (EUR/tonne)	93	
Intermediate storage cost (EUR/tonne)	5	
TCI – carbon capture routes, CCS1+4 (MEUR)	Natural gas: 685 Gasification (integrated): 766	Natural gas: 595 Gasification (integrated): 655
<b>Summary – specific annualised<sup>1</sup> TCI</b>		
Natural gas route, Ref1 (EUR/GJ-LHV)	8.46	7.38
Natural gas + CCS route, CCS1 (EUR/GJ-LHV)	9.00	7.80
Electrolyser route, Ref2 (EUR/GJ-LHV)	9.43	7.55
Gasification route, Ref3-4 (EUR/GJ-LHV)	8.77	7.21
Gasification + BECCS route, CCS4 (EUR/GJ-LHV)	10.06	8.60

<sup>1</sup> Annuity factor 0.102 (discount rate 8 %, lifetime 20 years).

### GHG assessment

Greenhouse gas emissions were evaluated per energy unit of fuel (gCO<sub>2</sub>eq./MJ-LHV fuel) including Well-to-Gate and combustion emissions. The considered system boundaries and included inputs and outputs for the investigated process routes are shown in Figure 15. Emission factors were taken from ENPAC for the two scenarios introduced in Table 8. Emissions related to transportation of the bio-oil intermediate to the refinery were neglected.

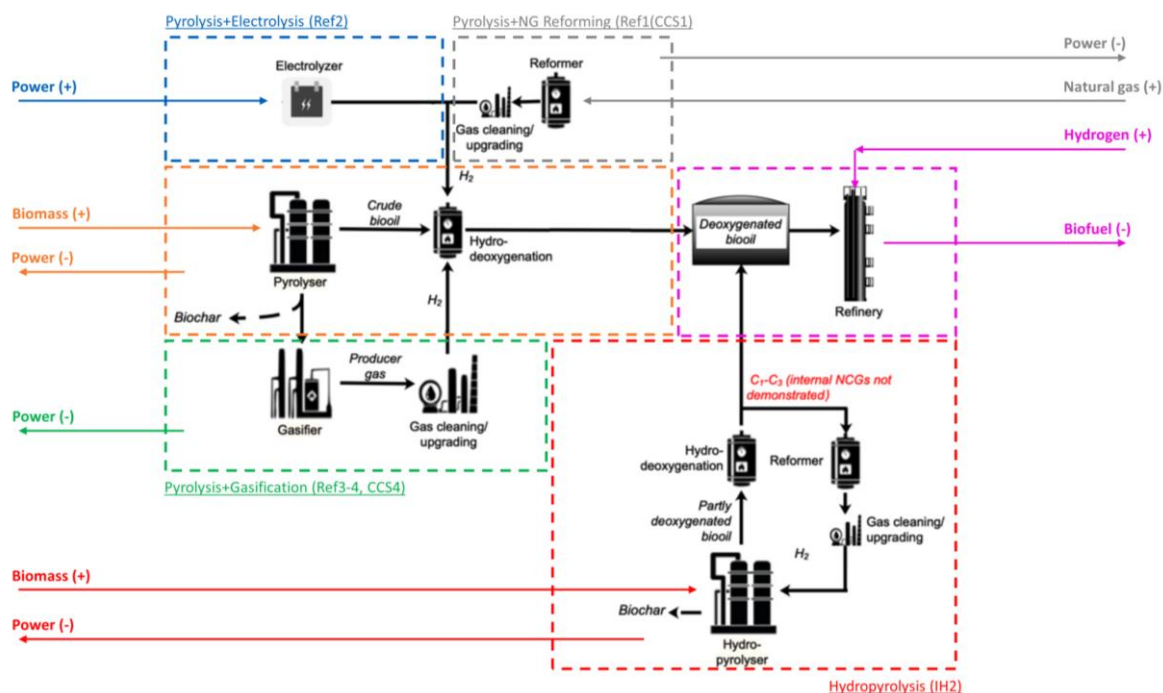


**Figure 15. System boundaries and inputs/outputs considered for the GHG assessment. PINK: Included in all process routes, ORANGE: Included in all fast pyrolysis routes, BLUE: Pyrolysis/electrolysis route (Ref2), GREY: Pyrolysis/steam reforming route (Ref1, CCS1), GREEN: Pyrolysis/gasification route (Ref3-4, CCS4), RED: Hydro pyrolysis route (IH2). (+) denotes inputs and (-) denotes outputs/products.**

Emission factors for the main process inputs are summarized in Table 11, and were combined with mass and energy balance data from simulation and Figure 14 to calculate the total Well-to-Gate<sup>4</sup> emissions of the studied biofuel process routes. The emission factor for hydrogen is not given by ENPAC and was estimated as 91.4 gCO<sub>2</sub>eq./MJ-LHV following the approach used by [35] reflecting SMR of natural gas. This value was only used for hydrogen used at the refinery where bio-oil is processed into diesel and gasoline. The emissions related to hydrogen required for production of bio-oil were instead based on the biomass, power or natural gas demand (depending on process setup) as determined by process modeling. System expansion was used to account for co-produced electricity which was assumed to replace grid electricity. To account for the effect of (BE)CCS, calculated Well-to-Gate emissions were reduced by an amount corresponding to 97.5 % of the captured CO<sub>2</sub>. The remaining 2.5 % represent downstream emissions in the CCS value chain (i.e., emissions during distribution and final storage – including CO<sub>2</sub> leakage).

<sup>4</sup> Well-to-Gate covers emissions associated with the supply of raw materials and with the production/refining stage but does not include the transportation and distribution of final products. The scope of Well-to-Gate ends when the products leave the production plant or refinery and is thus narrower than the scope of Well-to-tank.

**Table 11. ENPAC GHG emission factors used in the GHG assessment.**

Emission factor (gCO <sub>2</sub> eq./MJ-LHV)		
	2030-SD	2030-NP
Grid electricity	0	0
Biomass usage	112.5	2.2
Hydrogen <sup>1</sup>	91.4	
Gasoline WTG+C	79.4	
Diesel WTG+C	80.3	

Emission factor not included in ENPAC. Estimate following the approach used by [35] reflecting SMR of natural gas.

## 5 RESULTS AND DISCUSSION

In the present section the results of the different proposed cases in our study

In the present section the results of the different proposed cases in our study. The results are divided into two parts: (i) process performance of the proposed routes to produce hydrodeoxygenated bio-oil (ii) economic and GHG assessment for producing hydrodeoxygenated bio-oil and final gasoline and diesel fractions.

### 5.1 RESULTS FOR PROCESS PERFORMANCE

Table 12 presents the main results for process performance of bio-oil production processes. In the discussion here, the system boundary includes only the deoxygenated bio-oil production. The refinery process is excluded in the analysis here since it is similar to all the process scenarios defined in Table 7.

As seen in Table 12, the IH2 process outperforms the other process routes for all the KPIs including carbon recovery, yield, conversion efficiency and system efficiency. The IH2 process is a catalytically driven in-site hydro-pyrolysis process operating at elevated pressures (20-35 bar), which favors hydro-deoxygenation resulting higher bio-oil yields. The pyrolysis-based process routes are designed for lower pressure (2-3 bar) which favors more CO<sub>2</sub> formation when compared to liquid hydrocarbons. In addition, the pyrolysis process considered in this study is not catalytic, but rather sand is assumed to be the bed material.

Table 12 compares the results from the four reference cases (Ref1-4) which have different hydrogen generation processes for the HDO step. The carbon recovery in bio-oil with respect to the biomass input to the pyrolysis step was assumed to be same in all the cases. However, Ref 2 (electrolysis for H<sub>2</sub> generation) has the highest system level carbon recovery when compared to NG reforming and biomass gasification-based processes to meet the H<sub>2</sub> demands in the HDO step. The HDO process that is integrated with the NG reforming process to meet the demands of H<sub>2</sub> as defined as case Ref1, is next to Ref2 in system level carbon recovery, since the carbon in NG is also accounted for. Finally, the biomass gasification-based cases have lower system level carbon recovery as the carbon in gasification process is emitted in the form of CO<sub>2</sub>. Therefore, the processes with lower carbon recovery, have higher CO<sub>2</sub> emissions.

The bio-oil yield is assumed to be same for the cases Ref1-4. However, the system level yield is higher for Ref1-2 when compared to Ref3-4, because the biomass input to the system is higher in the cases Ref3-4. The conversion efficiency is considered same for the cases Ref1-4. However, the system efficiency is higher for the case with NG reforming for H<sub>2</sub> generation (Ref1) followed by the case with electrolysis for H<sub>2</sub> generation (Ref2). The hydrogen generation efficiency of NG reforming process is highest (79-80% [27]) when compared to electrolysis and biomass gasification processes. The system efficiency in cases Ref1-4 is also low when compared to IH2 process, because our analysis does not include the energy losses in the exhaust gases which still contain 4-5% water vapor. Additional heat can be recovered through water vapor condensation in exhaust gases and integrated with district heating systems. Heat recovery can significantly improve (up to 20%-points) the system efficiency of cases Ref1-4. The carbon recovery, system level bio-oil yield and the system efficiency improves in the case with biomass gasification, if a fraction of char from the

pyrolysis step is also gasified to produce hydrogen (as in Ref4). The system efficiency for the IH2 process is higher than its conversion efficiency because of the additional net electricity exports from the process considered while evaluating system efficiency.

Table 12 also presents the results for process scenarios with CO<sub>2</sub> capture and storage. The CO<sub>2</sub> capture process is integrated with Ref1 (CCS1), Ref3 (CCS2, CCS3, CCS5) and Ref4 (CCS4). Captured CO<sub>2</sub> is compressed until 110 bar and transported for permanent storage. In the case CCS1, the CO<sub>2</sub> capture and compression accounts for 4%-point drop in system efficiency when compared to Ref1. When CO<sub>2</sub> capture and compression is integrated with process with biomass gasification, the system efficiency penalty is between 2-5%-point depending on the point of CO<sub>2</sub> capture and the capture rate.

The results obtained for the cases Ref1-4 and CCS1-5 are from the inhouse developed process models for pyrolysis, HDO and biomass gasification. Process models have been validated against experimental results published in scientific literature. The mass balance for the HDO step has been established using the experimental studies reported by Nolte, Zhang [10].

**Table 12. Main results from process analysis.**

Case	Ref1	Ref2	Ref3	Ref4	CCS1	CCS2	CCS3	CCS4	CCS5	IH2
Wet biomass input (including biomass for gasification in respective cases) (kg/kg-bio-oil)	8.4	8.4	22.3	19.9	8.4	22.3	22.3	19.9	22.3	5.6
NG (kg/kg-bio-oil)	2.1	-	-	-	2.1	-	-	-	-	-
Biogenic CO <sub>2</sub> emitted (kg/kg-bio-oil)	4.1	4.1	22.5	19.7	4.1	18.8	2.3	2.0	6.0	4.0
Fossil CO <sub>2</sub> emitted (kg/kg-bio-oil)	5.6	-	-	-	0.6	-	-	-	-	-
Carbon recovery (Eq 2)	0.286	0.286	0.286	0.286	0.286	0.286	0.286	0.286	0.286	0.45
System level carbon recovery (Eq 3)	0.191	0.286	0.109	0.122	0.191	0.109	0.109	0.122	0.109	0.45
Yield (Eq 4)	0.171	0.171	0.171	0.171	0.171	0.171	0.171	0.171	0.171	0.243
System level yield (Eq 5)	0.171	0.171	0.064	0.072	0.171	0.064	0.064	0.072	0.064	0.243
Conversion efficiency (Eq 6)	0.372	0.372	0.372	0.372	0.372	0.372	0.372	0.372	0.372	0.574
System efficiency (Eq 7)	0.255	0.212	0.181	0.187	0.211	0.162	0.134	0.148	0.137	0.599

## 5.2 ECONOMIC AND GHG ASSESSMENT RESULTS

Total OPEX and fuel sales price (with support) are given in Figure 16. The hydrogen supply cost was calculated from the cost of natural gas (Ref1, CCS1), power (Ref2) or biomass (Ref3-4, CCS4) used for hydrogen production. This means that the use of power (Ref2) or biomass (Ref3-4, CCS4) for hydrogen production is not included in the bars for power or biomass cost for these cases, but rather in the cost for hydrogen supply. The BECCS case included in the figure refers to the case where BECCS is applied to flue gases of both the gasification and the pyrolysis process, and bio-char is used in gasification (CCS4). The distance between the total OPEX and the sales price reflects the investment opportunity. In most production pathways and scenarios analyzed in this work, the OPEX is higher than the fuel sales price and there is no investment opportunity. In the SD Scenario, there is a 3.7 EUR/GJ investment opportunity for the pathway with gasification and BECCS (CCS4). However, the annualized TCI estimate developed in this work is 8.6-10.1 EUR/GJ (see Table 10) and the production pathway is unlikely to be profitable. In the NP Scenario, there is a 5.2 EUR/GJ investment opportunity for the pathway with char utilization in gasification (Ref4) and a 3.3 EUR/GJ opportunity for the gasification pathway without char utilization (Ref3). The estimated annualized TCI for both cases is 7.2-8.8 EUR/GJ (see Table 10).

As can be seen, production costs are considerably higher than for the IH2 process evaluated by [35]. The high production costs are mainly due to a high hydrogen demand leading to significant costs for hydrogen feedstock (biomass, electricity or natural gas, depending on process configuration). As can be seen in the figure, there are no variable costs associated with hydrogen supply in the IH2-process. This is because the hydrogen demand can be met by hydrogen present in the biomass feedstock, obtained by reforming non-condensable cases from the pyrolysis step.

Production costs are generally higher in the SD Scenario, except for the case with BECCS applied to biogenic CO<sub>2</sub> from the pyrolysis and gasification processes (CCS4). In this case, the high CO<sub>2</sub>-charge in the SD Scenario implies a high value for the negative emissions of the BECCS process.

The results are not sensitive to the assumed biomass feedstock, and results for all pathways and scenarios vary less than +/- 5 % for the various feedstocks discussed in here.

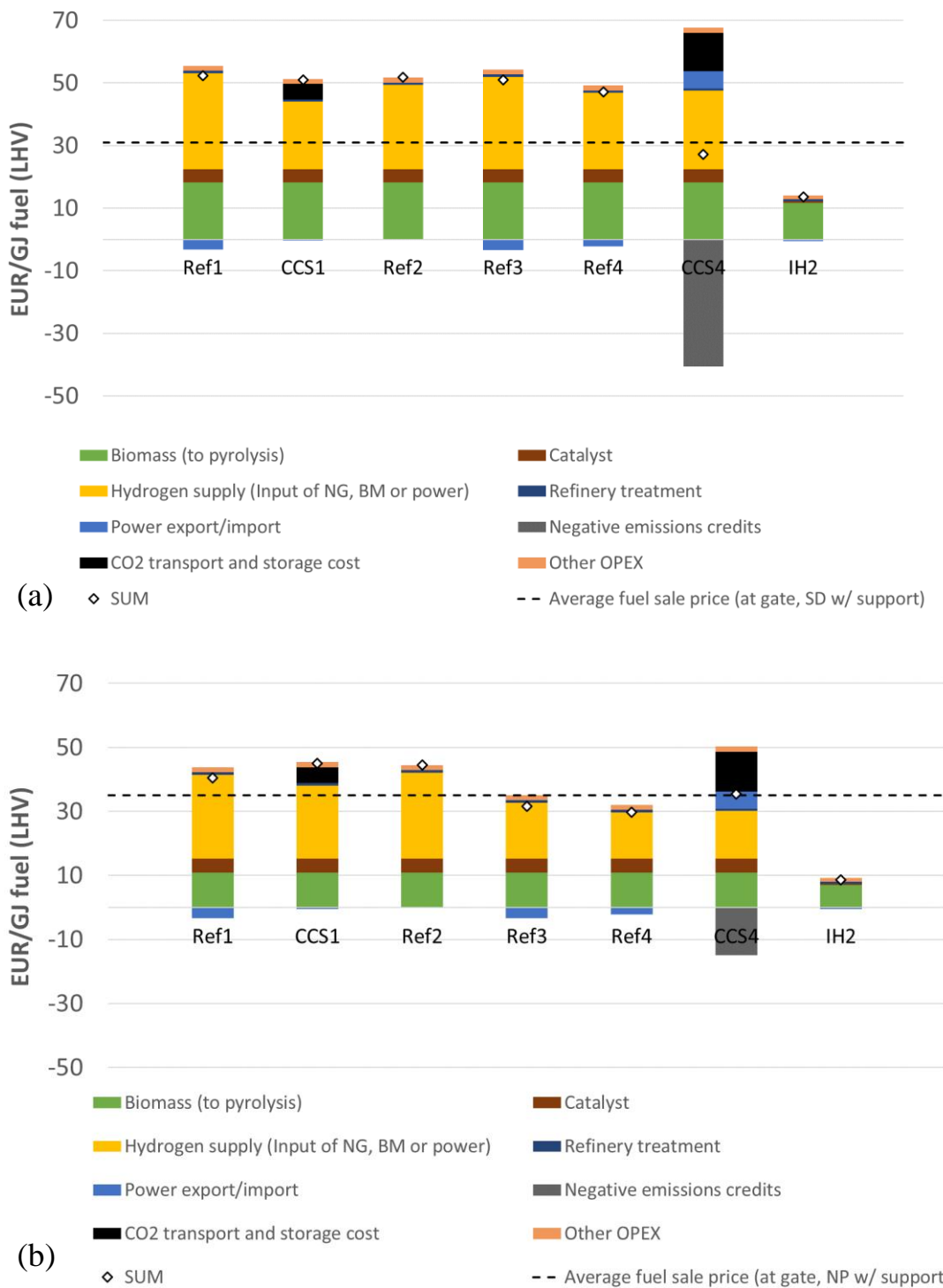


**Figure 16. Total fuel production OPEX for the investigated biofuel pathways in the ENPAC (a) SD Scenario and (b) NP Scenario. The resulting investment opportunity (in terms of annualized TCI) is calculated as the fuel sale price (dashed line) minus the OPEX sum (diamonds). If OPEX is lower than the sales price, the investment opportunity can be read as the distance between the OPEX sum and the dashed lines in the figure. The fuel sale price is the average biofuel sale price at gate calculated from diesel and gasoline prices and the diesel/gasoline product split. Ref1: Natural gas, CCS1: Natural gas with CCS applied to fossil CO<sub>2</sub>-emissions, Ref2: Electrolysis, Ref3: Gasification, Ref4: Gasification with char utilization, CCS4: Gasification with char utilization and BECCS applied to all CO<sub>2</sub> emissions. IH2: IH2 process based on work by [35].**

The resulting Well-to-Gate plus combustion GHG emission of the three HDO-pathways are shown in Figure 17 and compared to the fossil fuel counterparts and fuel produced using the IH2 process. Following the approach used by [35], all refinery emissions have been allocated to the diesel fuel, while all other emissions are distributed between gasoline and diesel proportionally to the amount (MJ-LHV) produced of each fuel. Only results for diesel are shown, but the gasoline results are identical except for the refinery contribution. The BECCS case included in the figure refers to the case where BECCS is applied to flue gases of the gasification and the pyrolysis process (CCS4). The hydrogen supply emissions were calculated from the emission factors of natural gas (Ref1, CCS1), power (Ref2) or biomass (Ref3-4, CCS4) used for hydrogen production. This means that the use of power (Ref2) or biomass (Ref3-4, CCS4) for hydrogen production is not included in the bars for power or biomass emissions for these cases, but rather in the emissions for hydrogen supply.

The results are heavily dependent on the emission factor attributed to biomass (see also the introduction of the ENPAC scenarios in Section 4.2. In the scenario 2030-SD, biomass is considered a limited resource with co-fired coal/biomass power plants as the marginal user. Consequently, the marginal effect of the use of biomass for biofuel production is an increased use of coal in power plants, resulting in a very high emission factor for biomass and Well-to-Gate emissions for biofuels that are considerably higher than for fossil fuels. The high emissions attributed to the produced biofuel in this case indicates that if future societies utilize all sustainably available biomass (i.e., biomass is a limited resource), that biomass would be better used for co-firing in power plants (displacing coal) than for biofuel production using the process routes evaluated in this study.

If biomass is instead treated as an unlimited resource (scenario NP-2030), the emissions reduction compared to fossil fuels is 88 % for the electrolysis route (Ref2), 77 % for the gasification route without char utilization (Ref3) and 79% for gasification with char utilization (Ref4). With gasification, char utilization and BECCS (CCS4), the emission reduction is close to 600 %. Due to the high hydrogen demand of the process, the natural gas pathway (Ref1 and CCS1) leads to significantly higher emissions than fossil diesel, even if CCS is used.

In the NP scenario, all routes except those based on natural gas fulfill the REDII requirement of 65% emission reduction compared to fossil fuel comparators. Note however that the methodology and emission factors used in the NP scenario differ slightly from REDII legislation. Therefore, the results are only indicative of actual performance under REDII. The assumptions regarding biomass in the SD scenario differ greatly from the REDII methodology, why a comparison to REDII is not relevant in this scenario.

In a scenario developed by the Swedish Energy Agency to illustrate a pathway to fulfilling the legislation *Reduktionsplikten* (see [47], availability of high-blending biodiesel and biogasoline with emission factors around 5 gCO<sub>2eq</sub>/MJ is assumed by 2030. Of the routes and scenarios analyzed in the present work, an emission factor lower than 5 gCO<sub>2eq</sub>/MJ is only achieved by route CCS4 in scenario NP, due to the implementation of BE(CCS) and a low emission factor of biomass.

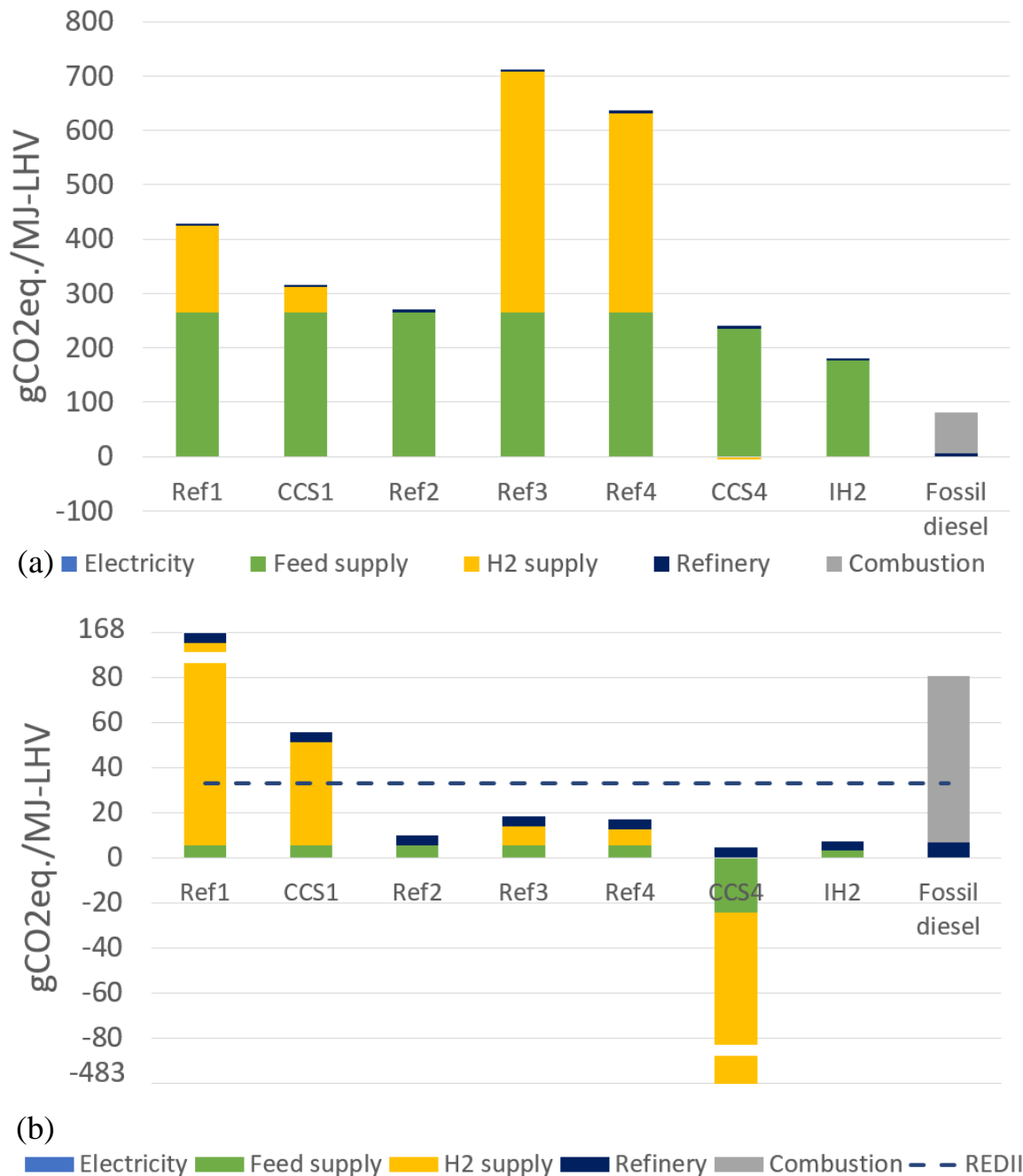


**Figure 17. Well-to-gate + combustion emissions for the process routes investigated in this work. (a): emission factors from ENPAC Scenario SD. The dashed line represents the 65% emission reduction limit for transportation fuels in REDII. The comparison to REDII is only relevant for scenario NP. (b): emission factors from ENPAC Scenario NP. Ref1: Natural gas, CCS1: Natural gas with CCS applied to fossil CO<sub>2</sub>-emissions, Ref2: Electrolysis, Ref3: Gasification, Ref4: Gasification with char utilization, CCS4: Gasification with char utilization and BECCS applied to all CO<sub>2</sub> emissions. IH2: IH2 process based on work by [P5]. Note the y-axis breaks in the positive and negative direction, since the values are significantly higher for two points. Results for diesel are shown. Results for gasoline are identical except for the contribution from refinery operations, which is zero for the bio-gasoline pathways.**

## 6 CONCLUSIONS

In this work we carried out techno-economic and greenhouse gas emissions analysis for the process routes to produce biofuels via deoxygenated bio-oils. Analysis have been performed for process scenarios with different hydrogen generation routes that are integrated with vapor phase hydrodeoxygenation (HDO) of pyrolysis vapors. These include ex-situ HDO of pyrolysis vapors and in-situ hydro-pyrolysis/hydro-conversion (IH2) processes.

The IH2 process developed by GTI outperforms the other process routes techno-economically investigated in this study. IH2 process has ~17%-point higher carbon recovery than the other process that have ex-situ vapor phase HDO step integrated with pyrolysis process. Higher carbon recovery in bio-oils results in higher yield and conversion efficiency of the process. The IH2 process has 7% and 20% higher yield and conversion efficiency respectively when compared to other process routes. The IH2 process also has the highest system level efficiency. However, the system efficiency of the pyrolysis and HDO route can be improved with better heat integration and recovery. Nearly 20%-point of system efficiency is lost through the exhaust gases leaving at temperature >100°C.

In the cases with pyrolysis an ex-situ HDO step, the hydrogen generation process and its efficiency have a significant impact on the system level carbon recovery, system level yield and system efficiency. Electrolysis is better route to generate hydrogen for HDO step with respect to system level carbon recovery, followed by NG reforming and biomass gasification. In terms of system level yield, generating hydrogen with electrolysis and NG reforming perform equally and better than biomass gasification. However, generating hydrogen from NG reforming for HDO has a better overall system level efficiency, followed by electrolysis (4%-points less) and biomass gasification (7%-points less). Integrating CCS reduces the system level efficiency of the processes by 4-5%-points.

The techno-economic analysis for the processes has been presented for two scenarios: Sustainable Development (SD) and New Policies (NP) scenarios. Similar to process performance, the IH2 process outperforms the other processes significantly in terms of fuel production costs in both the SD and the NP scenario. The IH2 process OPEX is also significantly lower than the sales price of fuels, leaving a high investment opportunity. Regardless of scenario, the best performing routes based on pyrolysis and HDO are the routes using biomass gasification for hydrogen supply, while routes based on electrolysis or natural gas reforming give higher costs. This is true despite the higher energy and carbon efficiencies of the electrolysis and natural gas pathways, and is explained by the lower energy price of biomass compared to electricity and natural gas. In the SD scenario, the high value of negative emissions implies significantly lower OPEX for the route with gasification and BECCS (CCS4) than for the other pyrolysis+HDO routes. In the NP scenario, CO<sub>2</sub> charges are lower and gasification-based routes without BECCS (Ref3-4) outperform CCS4. However, all gasification based routes still perform better than routes based on electrolysis or natural gas reforming.

A GHG assessment of the process routes was made using the same two scenarios (SD and NP) that were used for the economic assessment. In the SD scenario, high emissions are attributed to the use of biomass and all process routes perform worse than fossil diesel. In the NP scenario, the performance of the natural gas based routes is still poor and even if CCS is used, emissions are only reduced by 36 % compared to fossil diesel. All other investigated process routes perform well in the

NP scenario. In particular, the IH2 process and Ref2 (electrolysis for hydrogen supply) achieve emission reductions of around 90 %. Processes using gasification for hydrogen supply (Ref 3-4) give higher emissions due to upstream emissions associated with biomass supply, and achieve emission reductions of 77-84%. The higher number (84%) is achieved by Ref4 and is explained by the better biomass utilization due to utilization of pyrolysis char in biomass gasification. If (BE)CCS is applied to the gasification-based process (CCS4) emission reductions exceeding 100% are achieved.

Although the IH2 process performs better in techno-economics, further research is required in evaluating the performance of vapor phase HDO step. Research should be directed towards developing high performance catalysts, experimental trials to obtain suitable design conditions for vapor phase HDO step. This will result in higher carbon recovery and system efficiency. It is also observed that >55% of carbon is emitted in the form of CO<sub>2</sub> from the processes (including the IH2). Therefore, there is a need to develop and demonstrate processes and technologies that enable CO<sub>2</sub> recycling within the process or ex-situ downstream conversion to biofuels.

## REFERENCES

1. European Technology and Innovation Platform Bioenergy (ETIP Bioenergy), *Biofuel fact sheet*. 2020, European Technology and Innovation Platform Bioenergy (ETIP Bioenergy).
2. European Technology and Innovation Platform Bioenergy (ETIP Bioenergy), *Hydrogenated vegetable oil (HVO)*. 2020, European Technology and Innovation Platform. p. 4.
3. Lohri, C.R., et al., *Treatment technologies for urban solid biowaste to create value products: a review with focus on low- and middle-income settings*. *Reviews in Environmental Science and Bio/Technology*, 2017. **16**(1): p. 81-130.
4. Demirbaş, A., *Biomass resource facilities and biomass conversion processing for fuels and chemicals*. *Energy Conversion and Management*, 2001. **42**(11): p. 1357-1378.
5. Basu, P., *Chapter 3 - Biomass Characteristics*, in *Biomass Gasification, Pyrolysis and Torrefaction (Second Edition)*, P. Basu, Editor. 2013, Academic Press: Boston. p. 47-86.
6. Mohan, D., C.U. Pittman, and P.H. Steele, *Pyrolysis of Wood/Biomass for Bio-oil: A Critical Review*. *Energy & Fuels*, 2006. **20**(3): p. 848-889.
7. De Miguel Mercader, F., *Pyrolysis oil upgrading for Co-processing in standard refinery units*. *Enschede: University of Twente*. <https://doi.org/10.3990/1.9789036530859>. 2010.
8. Paul Adams et al. \Chapter 8 - Biomass Conversion Technologies BT - Greenhouse Gas Balances of Bioenergy Systems". In: *Greenhouse Gas Balances of Bioenergy Systems*. 2018.
9. Furusjö, E., et al., *Techno-economics of long and short term technology pathways for renewable transportation fuel production – Detailed report*. 2017: Report No 2018:09, f3 The Swedish Knowledge Centre for Renewable Transportation Fuels, Sweden. Available at [www.f3centre.se](http://www.f3centre.se).
10. Nolte, M.W., J. Zhang, and B.H. Shanks, *Ex situ hydrodeoxygenation in biomass pyrolysis using molybdenum oxide and low pressure hydrogen*. *Green Chemistry*, 2016. **18**(1): p. 134-138.
11. Paasikallio, V., *Bio-oil production via catalytic fast pyrolysis of woody biomass*, in *Department of Biotechnology and Chemical Technology*. 2016, Aalto University.
12. Paasikallio, V., et al., *Product quality and catalyst deactivation in a four day catalytic fast pyrolysis production run*. *Green Chemistry*, 2014. **16**(7): p. 3549-3559.
13. Marker, T.L., et al., *Integrated hydrolysis and hydroconversion (IH2) for the direct production of gasoline and diesel fuels or blending components from biomass, part 1: Proof of principle testing*. *Environmental Progress & Sustainable Energy*, 2012. **31**(2): p. 191-199.

14. Subramaniam, G., *Greenhouse gas and techno-economic evaluation of transportation fuels from Integrated Hydrolysis and Hydroconversion (IH2)*, in *Institutionen för rymd-, geo- och miljövetenskap*. 2021, Chalmers tekniska högskola.
15. Dutta, A., et al., *Process Design and Economics for the Conversion of Lignocellulosic Biomass to Hydrocarbon Fuels Thermochemical Research Pathways with In Situ and Ex Situ Upgrading of Fast Pyrolysis Vapors*. 2015, National Renewable Energy Laboratory (NREL).
16. Nunes, D., *Thermochemical conversion of lignocellulosic biomass into biofuels with Aspen Plus simulation*, in *Department of Chemical Engineering*. 2015, Universidade de Coimbra.
17. Nolte, M., *In situ and ex situ catalysis in biomass fast pyrolysis*, in *Chemical and Biological Engineering*. 2016, Iowa State University of Science and Technology.
18. Humbird, D., et al., *One-Dimensional Biomass Fast Pyrolysis Model with Reaction Kinetics Integrated in an Aspen Plus Biorefinery Process Model*. *ACS Sustainable Chemistry & Engineering*, 2017. **5**(3): p. 2463-2470.
19. Trendewicz, A.A., *Development of a circulating fluidized bed reactor model for the fast pyrolysis of biomass for process simulation*. 2015, Colorado School of Mines.
20. Ranzi, E., et al., *Chemical Kinetics of Biomass Pyrolysis*. *Energy & Fuels*, 2008. **22**(6): p. 4292-4300.
21. Caudle, B.H., M.B. Gorenssek, and C.-C. Chen, *A rigorous process modeling methodology for biomass fast pyrolysis with an entrained-flow reactor*. *Journal of Advanced Manufacturing and Processing*, 2020. **2**(1): p. e10031.
22. Ranzi, E., P.E.A. Debiagi, and A. Frassoldati, *Mathematical Modeling of Fast Biomass Pyrolysis and Bio-Oil Formation. Note I: Kinetic Mechanism of Biomass Pyrolysis*. *ACS Sustainable Chemistry & Engineering*, 2017. **5**(4): p. 2867-2881.
23. Swedish Wood. *The forest and sustainable forestry*. 2020 [cited 2021 December 21st]; Available from: <https://www.swedishwood.com/wood-facts/about-wood/wood-and-the-environment/the-forest-and-sustainable-forestry/>.
24. Debiagi, P.E.A., et al., *Extractives Extend the Applicability of Multistep Kinetic Scheme of Biomass Pyrolysis*. *Energy & Fuels*, 2015. **29**(10): p. 6544-6555.
25. Gorenssek, M.B., R. Shukre, and C.-C. Chen, *Development of a Thermophysical Properties Model for Flowsheet Simulation of Biomass Pyrolysis Processes*. *ACS Sustainable Chemistry & Engineering*, 2019. **7**(9): p. 9017-9027.
26. Di Blasi, C., *Modeling chemical and physical processes of wood and biomass pyrolysis*. *Progress in Energy and Combustion Science*, 2008. **34**(1): p. 47-90.
27. Nazir, S.M., et al., *Efficient hydrogen production with CO<sub>2</sub> capture using gas switching reforming*. *Energy*, 2019. **185**: p. 372-385.
28. Anantharaman, R., et al., *Cesar deliverable D2.4.3. European Best Practice Guidelines for Assessment of CO<sub>2</sub> Capture Technologie s*. 2018. p. 112.
29. Appl, M., *Ammonia, 2. Production Processes*. *Ullmann's Encyclopedia of Industrial Chemistry*, 2011.

30. Hermann, H., et al. *Biomass CHP Plant Güssing - A Success Story*. 2002.
31. Doherty, W., A. Reynolds, and D. Kennedy, *Aspen Plus simulation of biomass gasification in a steam blown dual fluidised bed*. Book Chapter: Materials and Processes for Energy: Communicating Current Research and Technological Developments, 2013: p. 212-220.
32. Martínez, I., et al., *Hydrogen production through sorption enhanced steam reforming of natural gas: Thermodynamic plant assessment*. International Journal of Hydrogen Energy, 2013. **38**(35): p. 15180-15199.
33. NEL, <https://nelhydrogen.com/product/atmospheric-alkaline-electrolyser-a-series/> [Accessed on 11 Feb 2022]. 2022.
34. John, T.M.M.R.M.L.L.F.P.O.-T.J.W.C.M.A.D.P.J.T.J.G.C.J.S., *Long Term Processing using Integrated Hydropyrolysis plus Hydroconversion (IH2) for the Production of Gasoline and Diesel from Biomass*. 2012.
35. Subramaniam, G., *Greenhouse gas and techno-economic evaluation of transportation fuels from integrated hydropyrolysis and hydroconversion (IH2)*, in *School of Engineering*. 2021, Aalto University. p. 70.
36. Harvey, S., E. Axelsson, and S. Axelsson, *Scenarios for assessing profitability and carbon balances of energy investments in industry*. 2010.
37. Axelsson, E. and K. Pettersson. *Energy price and Carbon Balances Scenarios tool (ENPAC)@ a summary of recent updates*. 2014.
38. IEA, *World Energy Outlook 2019*. 2019, International Energy Agency: Paris.
39. Jafri, Y., et al., *Multi-aspect evaluation of integrated forest-based biofuel production pathways: Part 2. economics, GHG emissions, technology maturity and production potentials*. Energy, 2019. **172**: p. 1312-1328.
40. Aasen, E.Y., *Northern Lights A European CO2 transport and storage network*. 2020, Northern Lights CCS.
41. Durusut, E. and M. Joos, *Shipping CO2 – UK Cost Estimation Study*. 2018, Element Energy Limited: Cambridge, UK. p. 65.
42. Zetterberg, L., F. Johnsson, and K. Möllersten, *Incentivizing BECCS—A Swedish Case Study*. Frontiers in Climate, 2021. **3**.
43. Jones, S., et al., *Process Design and Economics for the Conversion of Lignocellulosic Biomass to Hydrocarbon Fuels: Fast Pyrolysis and Hydrotreating Bio-oil Pathway*. 2013: United States. p. Medium: ED; Size: 97 p.
44. Proost, J., *State-of-the art CAPEX data for water electrolyzers, and their impact on renewable hydrogen price settings*. International Journal of Hydrogen Energy, 2019. **44**(9): p. 4406-4413.
45. Kinchin, C.M. and R.L. Bain, *Hydrogen Production from Biomass via Indirect Gasification: The Impact of NREL Process Development Unit Gasifier Correlations*. 2009: United States. p. Medium: ED; Size: 27 pp.
46. Garðarsdóttir, S.Ó., et al., *Investment costs and CO2 reduction potential of carbon capture from industrial plants – A Swedish case study*. International Journal of Greenhouse Gas Control, 2018. **76**: p. 111-124.

47. Energimyndigheten, *Komplettering till Kontrollstation 2019 för reduktionsplikten 2019*.
48. Olcese, R.N., et al., *Hydrodeoxygenation of Guaiacol, A Surrogate of Lignin Pyrolysis Vapors, Over Iron Based Catalysts: Kinetics and Modeling of the Lignin to Aromatics Integrated Process*. Energy & Fuels, 2013. **27**(2): p. 975-984.
49. Sun, J., et al., *Carbon-supported bimetallic Pd–Fe catalysts for vapor-phase hydrodeoxygenation of guaiacol*. Journal of Catalysis, 2013. **306**: p. 47-57.
50. Pichaikaran, S. and P. Arumugam, *Vapour phase hydrodeoxygenation of anisole over ruthenium and nickel supported mesoporous aluminosilicate*. Green Chemistry, 2016. **18**(9): p. 2888-2899.
51. Chen, C.-J., W.-S. Lee, and A. Bhan, *Mo<sub>2</sub>C catalyzed vapor phase hydrodeoxygenation of lignin-derived phenolic compound mixtures to aromatics under ambient pressure*. Applied Catalysis A: General, 2016. **510**: p. 42-48.
52. Wan, S., et al., *Direct catalytic upgrading of biomass pyrolysis vapors by a dual function Ru/TiO<sub>2</sub> catalyst*. AIChE Journal, 2013. **59**(7): p. 2275-2285.
53. Yeboah, I., et al., *Tandem Hydrodeoxygenation Catalyst System for Hydrocarbons Production from Simulated Bio-oil: Effect of C–C Coupling Catalysts*. Industrial & Engineering Chemistry Research, 2021. **60**(5): p. 2136-2143.
54. Yung, M.M., G.S. Foo, and C. Sievers, *Role of Pt during hydrodeoxygenation of biomass pyrolysis vapors over Pt/HBEA*. Catalysis Today, 2018. **302**: p. 151-160.
55. Eschenbacher, A., et al., *Enhancing bio-oil quality and energy recovery by atmospheric hydrodeoxygenation of wheat straw pyrolysis vapors using Pt and Mo-based catalysts*. Sustainable Energy & Fuels, 2020. **4**(4): p. 1991-2008.
56. Venkatakrishnan, V.K., et al., *Oxygen removal from intact biomass to produce liquid fuel range hydrocarbons via fast-hydropyrolysis and vapor-phase catalytic hydrodeoxygenation*. Green Chemistry, 2015. **17**(1): p. 178-183.
57. Au - Wang, H., et al., *Biomass Conversion to Produce Hydrocarbon Liquid Fuel Via Hot-vapor Filtered Fast Pyrolysis and Catalytic Hydrotreating*. JoVE, 2016(118): p. e54088.
58. Wang, H., J. Male, and Y. Wang, *Recent Advances in Hydrotreating of Pyrolysis Bio-Oil and Its Oxygen-Containing Model Compounds*. ACS Catalysis, 2013. **3**(5): p. 1047-1070.
59. Auersvald, M., et al., *Quantitative Study of Straw Bio-oil Hydrodeoxygenation over a Sulfided NiMo Catalyst*. ACS Sustainable Chemistry & Engineering, 2019. **7**(7): p. 7080-7093.
60. Elliott, D.C., et al., *Production of liquid hydrocarbon fuels from peat*. Energy & Fuels, 1988. **2**(2): p. 234-235.
61. Murni, M.A., M.F.R. Nordin, and M.T. Azizan, *Upgrading of Bio-Oil into High-Value Hydrocarbons via Hydrodeoxygenation*. American Journal of Applied Sciences, 2010. **7**(6).
62. Huber, G.W. and A. Corma, *Synergies between Bio- and Oil Refineries for the Production of Fuels from Biomass*. Angewandte Chemie International Edition, 2007. **46**(38): p. 7184-7201.

63. Roberts, M. and T.y. Marker, *Refinery Upgrading of Hydropyrolysis Oil from Biomass*. 2015, U.S. Department of Energy.

## APPENDIX

### DETAILED PROCESS ANALYSIS OF BIOMASS FAST PYROLYSIS AND HDO

As mentioned previously, the biomass fast pyrolysis model was modelled based on the work of Caudle et al. [21], and the operating conditions for the fast pyrolysis reactor were set to a temperature of 500°C, pressure of 1 bar and residence time of 1.5 seconds. Thus, the base case that we studied was the simulation of the fast pyrolysis process with the same biomass composition used in the work of Caudle et al. [21] without considering carbon capture for the flue gas stream leaving the combustor. The second case studied considers the same biomass feedstock and operating conditions as the first case but this time considering a MEA unit with 90% carbon capture rate for the flue gas stream leaving the combustor. The third case considers the same biomass feedstock and operating conditions as the first case but with variations of the total amount of hydrogen supplied to the hydrodeoxygenation (HDO) unit, this was done in order to study the changes in the total amount of bio-oil produced based on the total amount of hydrogen supplied for the hydrodeoxygenation process. Finally, the last case considers the same operating conditions as the other cases but with a change of the composition of the biomass feedstock, we proceeded to change the composition accordingly to the number of Spruce and Pine samples summarized in Table 24 and Table 25 in the Appendix. The aim of the change of feedstock composition was to study the variations in the total amount of bio-oil produced based on the composition of biomass supplied to the fast pyrolysis process.

Hence, the main results obtained for the reference case pyrolysis and HDO process (without specifying the source of hydrogen) are summarized in Table 13.

**Table 13. Analysis of reference case pyrolysis process with HDO (irrespective of the source of hydrogen).**

<i>Wet biomass input</i>	<i>kg/hr</i>	116.6000
<i>Dry biomass input</i>	<i>kg/hr</i>	83.4000
<i>Biomass moisture (after drying process)</i>	<i>kg/hr</i>	1.7000
<i>Dry biomass entering gasification plant</i>	<i>kg/hr</i>	81.7000
<i>Amount of Hydrogen used in HDO</i>	<i>kg/hr</i>	13.4300
<i>PSA feed pressure</i>	<i>bar</i>	8.1568
<i>PSA off gas pressure</i>	<i>bar</i>	2.3460
<i>Calculated % of H<sub>2</sub> recovery</i>	<i>%</i>	53.4200
<i>Pure H<sub>2</sub> recovered from PSA</i>	<i>kg/hr</i>	4.5832
<i>Bio-oil with water</i>	<i>kg/hr</i>	72.4668
<i>Bio-oil without water</i>	<i>kg/hr</i>	13.9221
<i>Char to combustor</i>	<i>kg/hr</i>	2.5201 (from HDO process) + 10.6797 (pyrolysis solids)
<i>SYNGAS mass flow</i>	<i>kg/hr</i>	37.0174 (non-condensable gases)
<i>Electrical Input</i>	<i>kW</i>	14.2418
<i>Electrical Output</i>	<i>kW</i>	49.6100
<i>Net electricity</i>	<i>kW</i>	35.3682
<i>Biogenic CO<sub>2</sub> present in flue gas</i>	<i>kg/hr</i>	57.7673
<i>Biogenic CO<sub>2</sub> emitted to atmosphere</i>	<i>kg/hr</i>	57.7673

As seen in the table, the total amount of feedstock supplied to the pyrolysis plant was 116.6 kg/hr of biomass, which contained 30% of moisture content. For that reason, a drying process was required before the biomass feedstock could enter the fast pyrolysis reactor. Thus, the wet biomass was dried using heat recovered from the high temperature flue gas stream coming from the combustor. The drying process was performed until reaching a feedstock moisture content of 2.03%. Resulting in this manner in a total amount of dried biomass supplied to the process of 83.4 kg/hr. After the dried biomass was pyrolyzed within the fast pyrolysis reactor, the resulting product consisted of a mixture of solid and vapor components. Hence, from the product stream, the solid components were separated and sent to the combustor, while the vapor components were sent to the hydrodeoxygenation (HDO) reactor.

At the HDO reactor, a total amount of 13.43 kg/hr of hydrogen was supplied for the hydrodeoxygenation process of bio-oil. The resulting products from the process were 37.01 kg/hr of non-condensable gases, 2.52 kg/hr of char, and 72.46 kg/hr of bio-oil mixed with water. The product stream of bio-oil was separated from water and resulted in 13.92 kg/hr. The generated non-condensable gases stream was compressed until 8 bar and sent to the pressure swing adsorption (PSA) unit where a total amount of 4.58 kg/hr of hydrogen was recovered. The amount of hydrogen recovered from the process is then pre heated and used in the HDO reactor, and from the total off-gas stream generated from the process, a specific amount was used to fluidize the fast pyrolysis reactor and the remaining amount was sent to the combustor for thermal disposal along with the 2.51 kg/hr of char generated from HDO process, and the solid product stream from the fast pyrolysis reactor.

Then, at the combustor, the combustion of the previous mentioned stream with a specific amount of compressed air resulted in a high temperature flue gas stream, which was used to pre heat different streams and sections at the pyrolysis plant. More specifically, the flue gas stream was used to provide the necessary heat required by the endothermic reactions at the fast pyrolysis reactor, pre heat the fluidization gases stream going to the fast pyrolysis reactor, pre heat the recovered amount of hydrogen from the PSA unit going to the HDO reactor, produce steam at 180°C and 3 bar, and finally to dry the wet biomass feedstock. Since in this case the MEA carbon capture unit is not considered for the flue gas stream, a total amount of 57.76 kg/hr of biogenic CO<sub>2</sub> was released to the atmosphere.

In terms of the electrical requirements by the different equipment's used in the plant, the total electrical input for the fast pyrolysis plant was in total 14.24 kW, while the electrical output generated using turbines and the steam generated from the heat recovered from the flue gas stream was in total 49.61 kW. Resulting in this manner in a net electricity balance of 35.36 kW.

The main results obtained for the reference case pyrolysis and HDO process that is integrated with CO<sub>2</sub> capture unit for combustion exhaust gases from pyrolysis unit are summarized in Table 14.

**Table 14. Analysis of reference case pyrolysis process with HDO (irrespective of the source of hydrogen) integrated with CO<sub>2</sub> capture for combustion exhaust gases from pyrolysis unit.**

<i>Wet biomass input</i>	<i>kg/hr</i>	116.60
<i>Biomass input</i>	<i>kg/hr</i>	83.40
<i>Biomass moisture (after drying process)</i>	<i>kg/hr</i>	1.70
<i>Dry biomass entering gasification plant</i>	<i>kg/hr</i>	81.70
<i>Amount of Hydrogen used in HDO</i>	<i>kg/hr</i>	13.43
<i>PSA feed pressure</i>	<i>bar</i>	8.1568
<i>PSA off gas pressure</i>	<i>bar</i>	2.3460
<i>Calculated % of H<sub>2</sub> recovery</i>	<i>%</i>	53.42
<i>Pure H<sub>2</sub> recovered from PSA</i>	<i>kg/hr</i>	4.5832
<i>Bio-oil with water</i>	<i>kg/hr</i>	72.4668
<i>Bio-oil without water</i>	<i>kg/hr</i>	13.9221
<i>Char to combustor</i>	<i>kg/hr</i>	2.5201 (from HDO process) + 10.6797 (pyrolysis solids)
<i>SYNGAS mass flow</i>	<i>kg/hr</i>	37.0174 (non-condensable gases)
<i>Electrical Input</i>	<i>kW</i>	14.1311
<i>Electrical Output</i>	<i>kW</i>	33.6050
<i>Net electricity</i>	<i>kW</i>	19.4739
<i>Biogenic CO<sub>2</sub> present in flue gas</i>	<i>kg/hr</i>	57.7673
<i>Biogenic CO<sub>2</sub> emitted to atmosphere</i>	<i>kg/hr</i>	5.7767

The results for the second case are the same compared to the first case, with the exception of the inclusion of a MEA unit with a carbon capture rate of 90% for the flue gas. This attachment will have an effect mainly in the amount of carbon dioxide in the flue gas that is released to the atmosphere and the net electricity balance of the plant. Hence, as well as the first case, a total amount of 13.43 kg/hr of hydrogen was used in the hydrodeoxygenation process, and the resulting products from the process were 37.01 kg/hr of non-condensable gases, 2.52 kg/hr of char, and 72.46 kg/hr of bio-oil mixed with water. The resulting bio-oil separated from water was 13.92 kg/hr and a total amount of 4.58 kg/hr of hydrogen was recovered at the PSA unit. A part of the off-gas stream generated from the process was as well used to fluidize the fast pyrolysis reactor and the other part was sent to the combustor for thermal disposal.

Regarding the steam generated with the high temperature flue gas stream coming from the combustor, since a MEA capture unit with a carbon capture rate of 90% is considered for this case, part of the steam generated is sent to the reboiler of the stripper unit to regenerate the amine loaded with CO<sub>2</sub> from the flue gas before being released to the atmosphere, and the other part of the steam generated is sent to the turbine section to generate electricity and supply the different electrical requirements of the different equipment's at the plant. For that reason, in terms of the electrical input and the electrical output, the total amount of electrical input for the fast pyrolysis plant was in total 14.13 kW, while the electrical output generated was in total 33.60 kW. Resulting in this manner in a net electricity balance of 19.47 kW, and a reduction of 44.93% compared to the first case.

### EFFECT OF HYDROGEN FLOW TO HDO STEP ON BIO-OIL PRODUCTION

Table 15 shows the effect of increase in bio-oil production while increasing the total flow of hydrogen to the HDO step.

**Table 15. Effect of Hydrogen flow to HDO step on bio-oil production.**

<i>Case with increase of hydrogen mass flow in HDO process</i>		
H <sub>2</sub> Entry to HDO [kg/hr]	Bio-oil [kg/hr]	Ratio Bio-oil / dry Biomass (%)
11	13,6978	16,42
12,8	13,9215	16,69
15	14,1950	17,02
17	14,4436	17,32
19	14,6922	17,62
21	14,9408	17,91
23	15,1894	18,21
25	15,4380	18,51

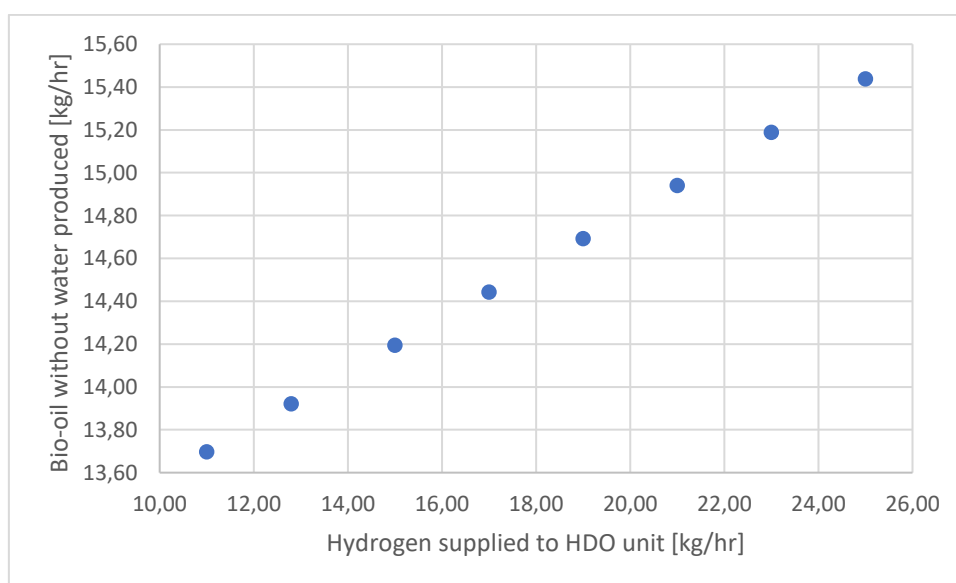


**Figure 18. Bio-oil produced vs Supplied Hydrogen.**

From the main results shown in the table above and the representation of the data in Figure 18, we can appreciate that there is a linear increase in the total amount of bio-oil produced in each case by increasing the amount of hydrogen supplied to the hydrodeoxygenation process. However, the change in the amount of bio-oil produced is not significant compared to the amount of hydrogen that has to be supplied in each increase. For that reason, since the differences are not significant enough to justify an increase in the amount of hydrogen supplied is that hydrogen supplied was kept to the value previously calculated, namely only 10% of hydrogen consumed per kilogram of dry biomass for the rest of the cases.

## EFFECT OF DIFFERENT BIOMASS SPECIES ON BIO-OIL PRODUCTION

The main results obtained for assuming different biomass species are presented in Table 16. The pyrolysis and HDO step conditions are similar to reference case, without being specific about the hydrogen generation process. The composition of different species of Spruce and Pine in presented in Table 24 and Table 25. Four different species of spruce (S1-4) and pine (P1-4) are assumed.

**Table 16. Results of the fast pyrolysis process for different biomass species.**

		Reference	S1	S2	S3	S4	P1	P2	P3	P4
Electrical Input	kW	13,72	13,59	13,07	13,71	13,62	11,48	13,68	13,75	13,67
Electrical Output	kW	49,61	48,56	44,96	49,32	48,34	33,95	50,52	50,13	48,58
Net Electricity	kW	35,88	34,96	31,88	35,60	34,71	22,47	36,83	36,37	34,90
Biogenic CO <sub>2</sub> present in flue gas	kg/hr	57,76	55,01	54,96	58,11	57,32	44,00	61,71	59,89	56,37
Bio-oil	kg/hr	13,92	13,90	13,50	13,92	13,90	12,54	13,73	13,87	13,96

From the results we can appreciate that the amount of bio-oil produced is similar in all the cases except for the case P1. The reason why the amount was lower in the P1 case was due to the amount of ash content in the sample. Therefore, other changes noticeable in the results obtained from using different samples of biomass was the amount of biogenic CO<sub>2</sub> released to the atmosphere, even though in most of the case the difference is not significant enough, we can see that as well in the P1 case the amount of CO<sub>2</sub> released through the flue gas was lower compared to the rest of cases, while in the P2 case the amount of CO<sub>2</sub> released was the highest compared to the other cases. Finally, in terms of the net electricity at the plant, we can appreciate that the electrical input and electrical output is similar in all the cases, except for the P1 case. Hence, from the results obtained we can deduct that these samples of biomass, belonging to the “Softwood” biomass type, yield similar results in terms of bio-oil produced, net electrical balance, and biogenic CO<sub>2</sub> released to the atmosphere. For that reason, with more cases with samples of softwood containing more content of ash we could arrive to a conclusion that the content of ash results in a variance of the amount of bio-oil that we can produce.

## MODELLING OF BIOMASS GASIFICATION PROCESS IN ASPEN PLUS

### Simulation environment setup

The biomass gasification process was modeled following the approach taken in the work of Doherty et al. [31] “*Aspen Plus Simulation of Biomass Gasification in a Steam Blown Dual Fluidized Bed*”, which is based on Gibbs free energy minimization and the use of a restricted equilibrium method for the correct calibration with published experimental data. This restricted equilibrium method can be achieved through the specification of a temperature approach for a specific number of gasification reactions.

As mentioned previously, the gasification process is the thermochemical conversion of the carbon contained within the structure of biomass into combustible gas, which is primarily composed by H<sub>2</sub>, CO, CO<sub>2</sub>, water vapor, higher hydrocarbons, N<sub>2</sub>, and other minor components such as NH<sub>3</sub>, tar, H<sub>2</sub>S, and HCL. Doherty et al. [31] mentions that the biomass gasification can be represented with the following set of reactions.

**Table 17. Biomass Gasification reactions specified in the model – Source: Doherty et al. [31].**

<i>Heterogeneous reactions</i>	
1)	$C + 2H_2 \leftrightarrow CH_4$
2)	$C + H_2O \leftrightarrow CO + H_2$
3)	$C + CO_2 \leftrightarrow 2CO$
<i>Homogeneous reactions</i>	
4)	$CH_4 + H_2O \leftrightarrow CO + 3H_2$
5)	$CO + H_2O \leftrightarrow CO_2 + H_2$
<i>NH<sub>3</sub>, H<sub>2</sub>S, and HCL formation reactions</i>	
6)	$0.5N_2 + 1.5H_2 \leftrightarrow NH_3$
7)	$H_2 + S \leftrightarrow H_2S$
8)	$Cl_2 + H_2 \leftrightarrow 2HCL$

In addition to the gasification reactions shown in Table 17, the combustion reactions are also considered for the model and are automatically generated by Aspen plus. The gasification reactions shown in the table above are endothermic, and for that reason, the required amount of heat required by these reactions is supplied from the combustion of the products generated after the gasification process, char, H<sub>2</sub>, CO, CO<sub>2</sub>, CH<sub>4</sub>, and water.

The overall flowsheet of the FICFB gasification process is depicted in Figure 19, and the assumptions taken for the modeling of the gasification process were the following: the Peng-Robinson equation of state with Boston-Mathias modifications was selected as the property method in Aspen Plus, an operating pressure slightly higher than atmospheric pressure, isothermal and steady state operation, ideal gases, pressure drop of 1% of the inlet stream pressures, char is considered to be 100% carbon, all the N<sub>2</sub> generated from the decomposition of biomass is converted to NH<sub>3</sub>, all the sulfur (S) generated from the decomposition of biomass is converted to SO<sub>2</sub>, all the chlorine (Cl<sub>2</sub>) generated from the decomposition of biomass is converted to HCl, the drying and pyrolysis are instantaneous, tar formation is not considered, the heat loss from the gasification process is neglected, and the heat transferred through the circulation of the bed material from the combustion zone (CZ) to the gasification zone (GZ) is simulated by the use of a heat stream.

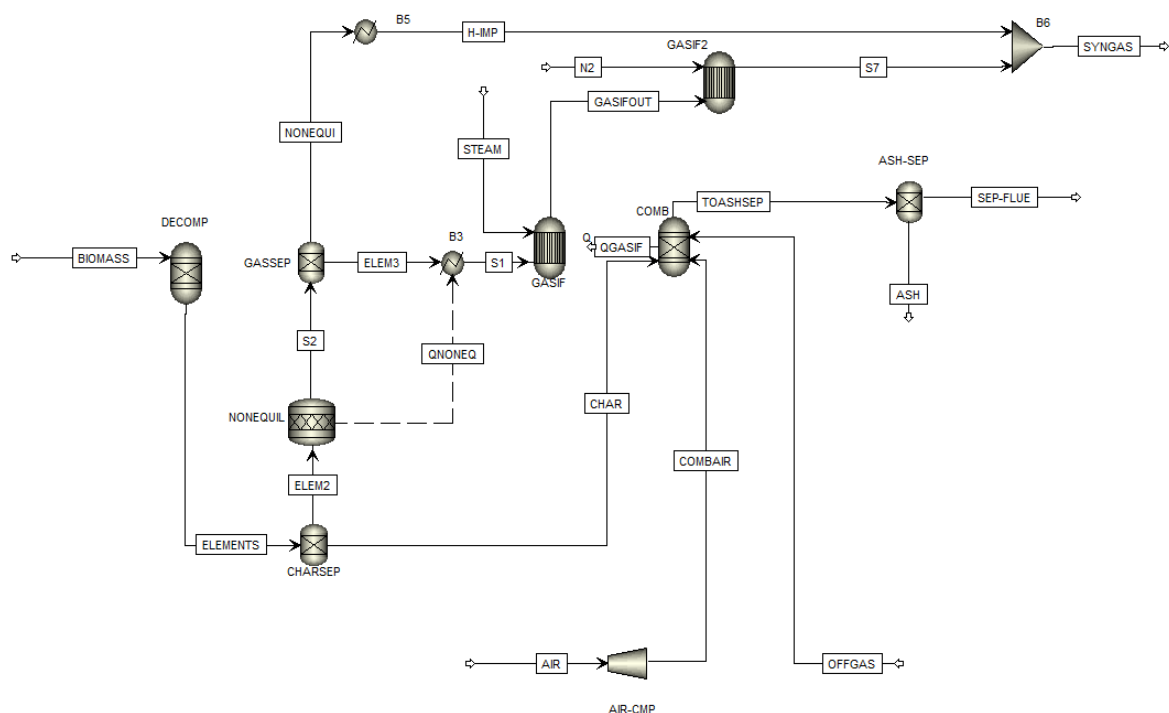


**Figure 19. Overall flowsheet of the biomass gasification process in Aspen Plus.**

From the diagram flow shown in Figure 19, the modeling of the gasification process begins with the specification of the biomass feedstock as a non-conventional stream and providing the ultimate and proximate analyses values in Aspen Plus. The values used for these parameters can be seen in Table 18. The composition for biomass considered here is similar to Douglas fir wood. The composition anyhow is kept same as in the study of Doherty et al. [31].

**Table 18. Biomass composition.**

<i>Ultimate Analysis (Dry Basis)</i>		
Carbon	wt. %	51.19
Hydrogen	wt. %	6.08
Oxygen	wt. %	41.3
Nitrogen	wt. %	0.2
Sulphur	wt. %	0.02
Chlorine	wt. %	0.05
Ash	wt. %	1.16
<i>Proximate Analysis (Dry basis)</i>		
Volatile matter	wt. %	80
Fixed Carbon	wt. %	18.84
Ash	wt. %	1.16
Moisture	wt. %	2.0383
LHV (dry basis)	MJ/kg	19.09
Mass flow rate	Kg/hr	83.4

The biomass enthalpy of formation, specific heat capacity and density were estimated based on the ultimate and proximate analyses and specifying the biomass lower heating value (LHV) with the HCOALGEN and DCOALIGT property models. Then, the specification of the biomass streams finalizes with the input of its conditions of pressure, temperature, and mass flow rate.

The biomass stream then enters the RYIELD reactor named as “*DECOMP*”, where the mass yields were as well calculated based on the ultimate and proximate analyses of the biomass stream. The following table depicts the formulas used for the yield distribution as mass yield of each component per total mass of feed, calculated from the biomass ultimate analysis data.

**Table 19. Yield Distribution of each component based on the biomass ultimate analysis data.**

<i>Yield Distribution</i>		
Yield H <sub>2</sub>	m H <sub>2</sub>	$m_{H_2} = (1 - X_{moisture}) * X_H * m_{feed}$
Yield O <sub>2</sub>	m O <sub>2</sub>	$m_{O_2} = (1 - X_{moisture}) * X_O * m_{feed}$
Yield N <sub>2</sub>	m N <sub>2</sub>	$m_{N_2} = (1 - X_{moisture}) * X_{N_2} * m_{feed}$
Yield H <sub>2</sub> O	m H <sub>2</sub> O	$m_{H_2O} = X_{moisture} * m_{feed}$
Yield S	m S	$m_S = (1 - X_{moisture}) * X_S * m_{feed}$
Yield C	m C	$m_C = (1 - X_{moisture}) * X_C * m_{feed}$
Yield Ash	m Ash	$m_{Ash} = (1 - X_{moisture}) * X_{ASH} * m_{feed}$

When entering the different yield results for each component it is also necessary to specify in the component attribute that the Ash component is: 100% ash in the proximate analysis (moisture, FC, VM were left blank), 100% ash in the ultimate analysis (carbon, hydrogen, nitrogen, chlorine, sulfur, and oxygen were set to 0), and 0% sulfur in the sulphate analysis (pyritic and organic values were set to 0).

Once the yield distribution is set, the “DECOMP” reactor converts the non-conventional components of biomass into conventional components. The outlet product stream “ELEMENTS” is then fed to a separator block “CHARSEP”, which separates a specific amount of the total produced char and all of the ash present in the stream. The amount of char separated is calculated in order to provide a gasification temperature at 950°C. Hence, the separated amount of char and ash are sent to the combustion zone of the gasifier (CZ), which was simulated using an RSTOIC reactor titled “COMB”.

At the combustion reactor, a compressed stream of air “COMBAIR” is supplied. The molar fraction specified for the air stream was 0.79 for N<sub>2</sub> and 0.21, and the mass flow was calculated in a manner that after the combustion, the content of carbon monoxide in the flue gas was almost zero, and the outlet temperature reached up to 1050°C. Thus, since the stream of air is initially at ambient temperature and ambient pressure, 15°C and 1 bar respectively, it is compressed up to 1.16 bar and sent to the combustion zone, where it reacts with char to produce the necessary amount of heat required for the gasification process. As mentioned previously no further specification of additional chemical reactions was required in the combustor reactor, only the option to automatically generate the combustion reactions was activated. Thus, the heat produced from the combustion process is represented with a heat stream “QGASIF” that connects the blocks “COMB” to “GASIF”.

After char is combusted, the resulting flue gas stream contains primarily CO<sub>2</sub>, O<sub>2</sub>, N<sub>2</sub> and ash. For that reason, before releasing any amount of flue gas to the environment, a separator block named “ASH-SEP” is implemented in order to remove the ash content or any amount of unreacted char from the flue gas stream. In a real FICFB gasifier, the material separated would also be separated from the flue gas stream and then recycled back to the combustion zone, but this step was not considered for our model. The flue gas stream is then the final product from the gasifier and used to recover heat through the use of heat exchangers.

Then, the other material stream “ELEM2” separated after the “CHARSEP” block is sent to the non-equilibrium reactor named “NONEQUIL” where all of the biomass bound N<sub>2</sub>, S, and Cl<sub>2</sub> are converted into NH<sub>3</sub>, H<sub>2</sub>S and HCl respectively through the set of reactions shown in Table 17. Furthermore, the enthalpy change in this process is accounted by connecting an additional heat stream “QNONEQ” from the non-equilibrium reactor to a downstream heat exchanger. After the mentioned components are converted into NH<sub>3</sub>, H<sub>2</sub>S and HCl, they have to be removed from the main stream using another separator block “GASSEP”. Thus, after the separation process, the principal fuel stream “ELEM3” is sent to the gasification reactor “GASIF”, which was modeled as a RGIBBS reactor. Then, the steam stream is attached to the block to gasify the biomass and at the same time fluidize the bed. The conditions of the steam sent to the gasification block were the following: a temperature of 120 C and pressure of 1.5 bar. The mass flow rate of steam is defined according the steam to biomass ratio (STBR) parameter, which is defined as the mass flow of biomass moisture plus the mass flow of steam injected to the gasification block, and divided by the total mass flow of dry biomass used as feedstock.

$$\begin{aligned} \text{Steam to Biomass ratio (STBR)} \\ = \frac{\text{Biomass moisture [kg/hr]} + \text{steam injected [kg/hr]}}{\text{Dry biomass total mass flow [kg/hr]}} \end{aligned}$$

For our work, a STBR value of 1.5486 was specified for the base case, being the total mass flow of biomass used as feedstock of 83.4 kg/hr, biomass moisture mass flow of 1.7 kg/hr, and a total amount of injected steam of 124,821 kg/hr. The reason for selecting this specific value for the different gasification cases in our work is because according to Doherty et al. [31], STBR is the second most important parameter in respect of the final syngas composition, and according to the STBR sensitivity analysis results obtained in their work, with a higher steam to biomass ratio it was possible to obtain a higher value in the amount of H<sub>2</sub> in the final syngas composition. This amount of hydrogen to be recovered is important for our case as the amount of hydrogen recovered in the biomass pyrolysis plant is not enough for the hydrodeoxygenation process of bio-oil. For that reason, the recovery of more hydrogen in the biomass gasification with the aid of a PSA block can lead to an integrated case, where we can send the recovered hydrogen in the gasification plant to cover the lack of hydrogen in the pyrolysis plant.

Then, in the “GASIF” block, the gasification reactions from (1) to (5) in Table 17 were specified with zero temperature approach for each reaction. This setting would mean that the chemical equilibrium constant for each reaction was calculated at the reactor temperature in a manner that the GASIF block outputs the equilibrium gas composition [31]. The resulting product stream from this block “GASIFOUT” is then sent to another GIBBS reactor block labeled “GASIF2”, which is an additional block that will help us to adjust the syngas composition to experimental data reported in the literature. In this block, the reactions (4) and (5) were entered, and their equilibrium was restricted through the specification of a temperature approach of -265°C and -90°C respectively. According to Doherty et al. [31], the specification of the temperature approach ensures that the model outputs a more realistic syngas composition. Additionally, a stream of N<sub>2</sub> is supplied to the “GASIF2” block in order to match the composition of the syngas produced by in real life FICFB gasifiers, which utilize N<sub>2</sub> as purge gas in the fuel feeding system.

Finally, the final block in the biomass gasification diagram flow is the mixer block “B6” which function is to mix back to the principal stream the NH<sub>3</sub>, H<sub>2</sub>S, and HCl components that were separated in the “GASSEP” block. However, before they can be mixed up with the main syngas stream, it is necessary to increase the temperature of these components to the same temperature as the main syngas stream. For that reason, a heat exchanger is used before the mixing process and the temperature of these components is increased until matching the temperature of the main syngas stream, and the total syngas product leaving the mixer block is considered as the final output from the gasifier and is ready to be sent to the Water Gas Shift section (WGS) for the removal of any trace of carbon monoxide, and to the Pressure swing adsorption unit (PSA) where hydrogen will be recovered for its later use in the hydrodeoxygenation process in the pyrolysis plant. In the following figure we can appreciate a diagram flow in Aspen Hysys of the WGS section and the PSA unit.

#### *Biomass gasification model validation*

For the validation process of the biomass gasification model, considering the different assumptions and operating conditions taken from the work of Doherty et al. [31], we compared the results obtained by our model with the results obtained by the mentioned study. The validation considered the syngas composition based on two fundamental operating conditions, the gasification temperature (T<sub>g</sub>) and the Steam to Biomass Ratio (STBR). Thus, using the same biomass composition the results obtained by the work of Doherty et al. [31] and our model were the following:

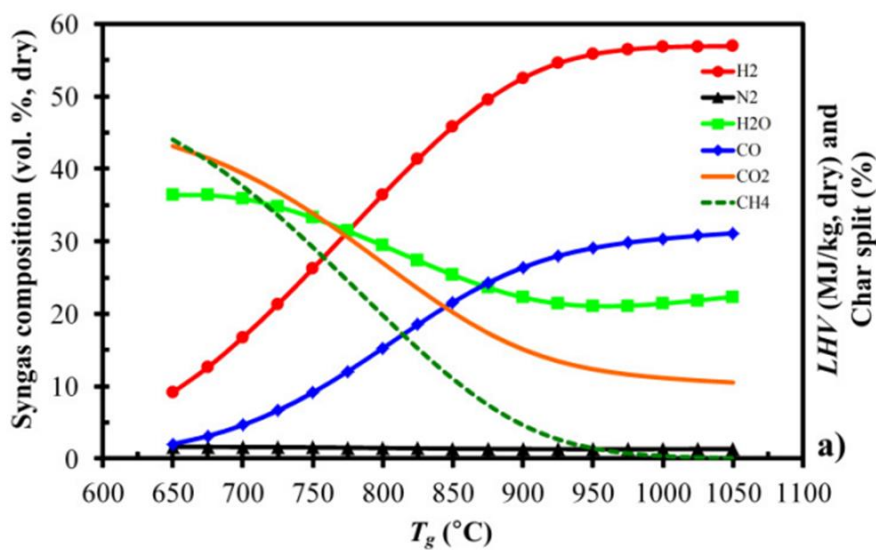


Figure 20. Effect of gasification temperature on the syngas composition by the model of Doherty et al. [31].

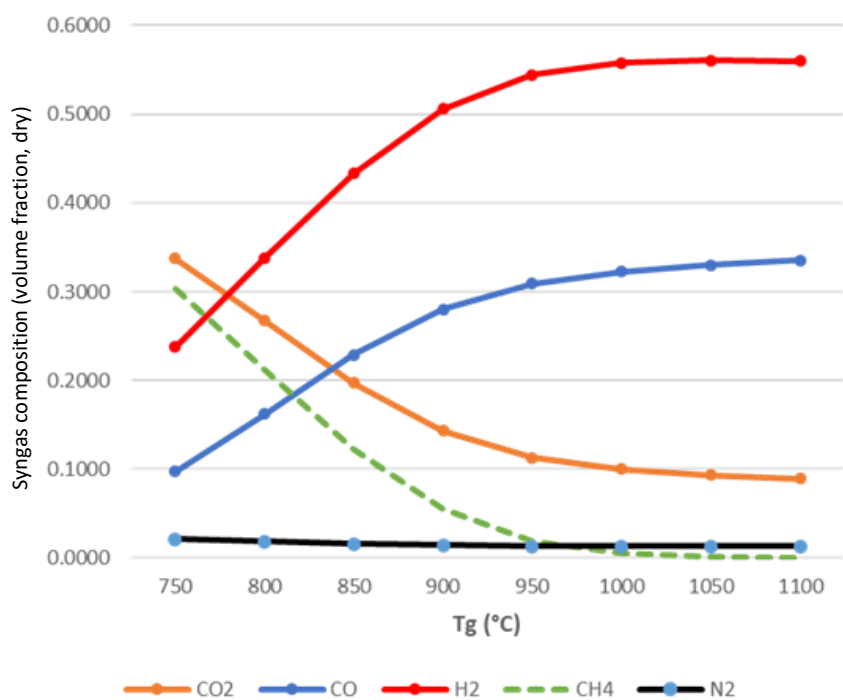


Figure 21. Effect of gasification temperature on the syngas composition by our model.

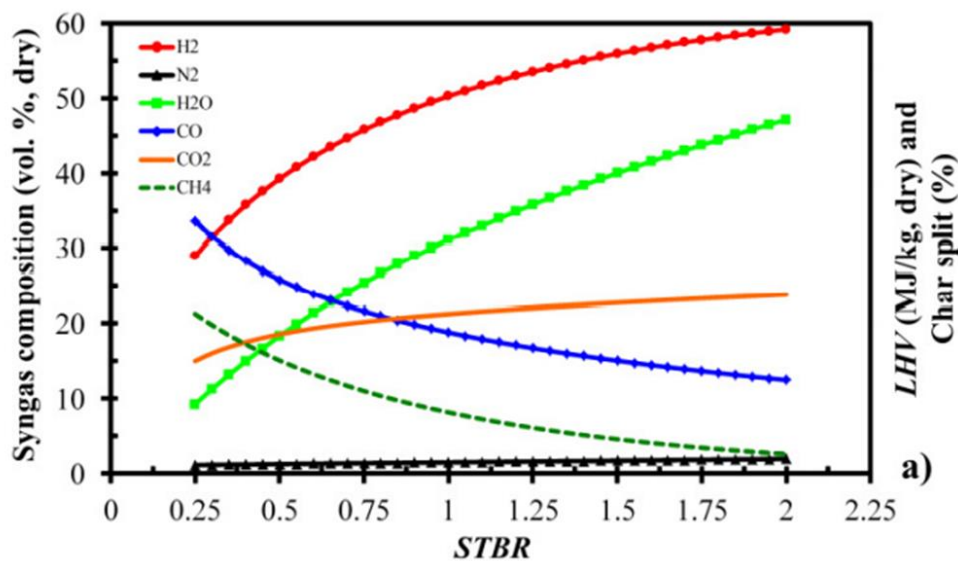


Figure 22. Effect of steam to biomass ratio on the syngas composition by the model of Doherty et al. [31].

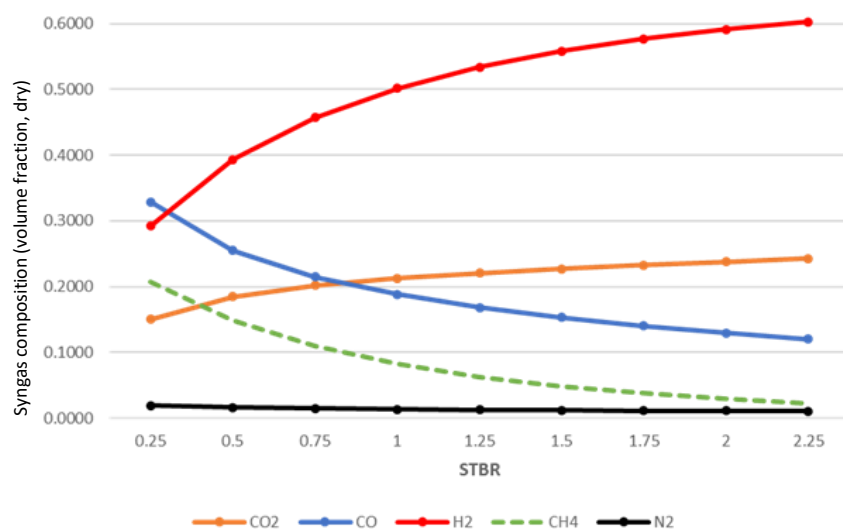


Figure 23. Effect of steam to biomass ratio on the syngas composition by our model.

As seen in Figure 20 and Figure 21, the results obtained of the syngas composition based on different gasification temperatures are in good agreement with the results obtained by Doherty et al [31]. As well in the results shown in Figure 22 and Figure 23, the results obtained of the syngas composition based on different steam to biomass ratios used are in good agreement with the results obtained by the model of Doherty et al [31].

## ANALYSIS OF BIOMASS GASIFICATION PROCESS

For the biomass gasification model, the operating conditions for the gasification reactor were set to a temperature of 950°C, and a pressure of 1.485 bar. Thus, the same biomass mass flow used in the first case of biomass fast pyrolysis was used, and a MEA unit with a carbon capture rate of 90% was considered for the flue gas stream leaving the combustor. Hence, the results obtained for the biomass gasification model are summarized in Table 20.

**Table 20. Results for the biomass gasification process with CO<sub>2</sub> capture.**

Wet biomass input	kg/hr	116.6000
Biomass input	kg/hr	83.4000
Biomass moisture (after drying process)	kg/hr	1.7000
Dry biomass entering gasification plant	kg/hr	81.7000
SYNGAS mass flow	kg/hr	186.2000
PSA feed pressure	bar	25.0000
PSA off gas pressure	bar	1.1800
Calculated % of H <sub>2</sub> recovery	%	84.8753
Pure H <sub>2</sub> recovered from PSA	kg/hr	5.3030
Steam to gasifier	kg/hr	124.8210
Char to combustor	kg/hr	25.0934
STBR (Steam to Biomass Ratio) STBR = (Biomass moisture + Steam) / Dry Biomass flow rate		1.5486
Total Electrical Input	kW	18.9793
Total Electrical Output	kW	3.6180
Net Electrical balance	kW	-15.3613
CO <sub>2</sub> present in flue gas before MEA unit	kg/hr	153.19
CO <sub>2</sub> emitted to atmosphere	kg/hr	15.3191

As seen in the results, the same mass flow of biomass with a specific moisture content was used for the gasification model as the first case of biomass fast pyrolysis. The only difference was the biomass composition specification in the model which was described using the ultimate and proximate analysis, and using the values used in the work of Doherty et al. [31]. Thus, the model was simpler to model compared to the biomass fast pyrolysis model since no additional components or their specific thermophysical properties needed to be described in the simulation environment of Aspen Plus. Hence, for the gasification process, a total mass flow of 124.82 kg/hr was needed to be supplied to the gasifier in order to keep a steam to biomass ratio (STBR) of 1.5486. The reason for keeping this parameter in that specific value was because in the range of STBR of 0–2.25, at 1.5486 is the point in which most hydrogen content is obtained in the syngas composition. Therefore, the syngas was treated through a water gas shift unit and compressed before entering the PSA unit, from where a total amount of 5.30 kg/hr of hydrogen was recovered. The amount of hydrogen recovered then can be used as feedstock for the hydrodeoxygenation process in the biomass fast pyrolysis plant. The off gas generated from the PSA unit was then sent to the combustor unit for thermal disposal and steam was generated from the resulting high temperature flue gas. Thus, since a MEA capture unit with a carbon capture rate of 90% was considered for this case, from the total amount of steam generated from the heat recovery process, part of it was sent to the reboiler of the stripper column of the MEA unit in order to regenerate the amine loaded with CO<sub>2</sub> from the flue gas stream before it is released to the atmosphere. The other part of the steam generated was sent to

the turbine section to generate electricity and supply the different electrical requirements of the different equipment's at the gasification plant. For that reason, in terms of the electrical input and the electrical output, the total amount of electrical input for the gasification plant was in total 18.93 kW, while the electrical output generated was in total 3.61 kW. Resulting in this manner in a net electricity balance of -15.36 kW, namely more electricity from the grid has to be supplied from the grid in order to satisfy the electrical requirements of the gasification plant.

#### PROCESS DESCRIPTION FOR SCENARIOS REF3 AND REF4 AS PROPOSED IN TABLE 7

The results obtained for the integrated cases of both pyrolysis and gasification plants are shown in the following order, first the integration case through char is addressed, and consequently the integration case through steam is addressed. In the first integration case, from the total amount of char produced in the pyrolysis plant, part of it is sent to the gasification plant, along with an increased feedstock mass flow of biomass to generate the necessary amount of hydrogen required by the hydrodeoxygenation process at the pyrolysis plant. Then the results for the second integrated case through steam are addressed, where only the steam produced at the pyrolysis plant is sent to a scaled-up gasification plant, this scaling process was previously done in order to provide the necessary amount of hydrogen required by the hydrodeoxygenation process. Also, as mentioned previously in the proposed study cases section, in both integrated cases plants, a MEA unit with a carbon capture rate of 90% is considered for the flue gas stream leaving the combustor unit of both plants.

*Description of the Ref3 scenario*

**Table 21. Details of Ref 3 scenario.**

		Pyrolysis Plant	Gasification Plant
Wet biomass input	kg/hr	116.6000	194.5194
Biomass input	kg/hr	83.4000	139.1331
Biomass moisture (after drying)	kg/hr	1.7000	2.8360
Dry biomass entering plant	kg/hr	81.7000	136.2971
SYNGAS mass flow	kg/hr	37.0174	310.6306
Amount of Hydrogen used in HDO	kg/hr	13.4300	-
PSA feed pressure	bar	8.1568	41.7065
PSA off gas pressure	bar	2.3460	1.9685
Pure H <sub>2</sub> recovered from PSA	kg/hr	4.5832	8.8468
Net electricity	kW	-9,9890	-25,6267
Steam to gasifier	kg/hr	none	208.2342
Char to combustor	kg/hr	13.1998	41.8623
STBR (Steam to Biomass Ratio) STBR = Biomass moisture + Steam / Dry Biomass flow rate		none	2.5834
Steam to MEA reboiler	kg/hr	116.6000	219.2097
Total Electrical Input	kW	13.4940	31.6624
Total Electrical Output	kW	3.5050	6.0357
Net Electrical Balance	kW	-9.9890	-25.6267
Biogenic CO <sub>2</sub> present in flue gas	kg/hr	57.7673	255.5633
Biogenic CO <sub>2</sub> emitted to atmosphere	kg/hr	5.7767	25.5563

As seen from the results summarized in the table above, for this integrated case of both plants through steam, the process of integration was the following, as compared to the previous integrated case of both plants through char, where part of the total amount of char produced in the pyrolysis plant was sent to the gasification plant, in this case, the base case of the pyrolysis plant remains the same where part of the total char produced is sent to the combustor to generate a high temperature flue gas stream and thus recover the heat by producing steam at 3 bar and 180°C through heat exchangers. In this integrated case however, part of the steam is sent to the stripper reboiler of the MEA unit to regenerate the CO<sub>2</sub> loaded amine, and the rest of the steam generated is sent to a scaled-up gasification plant. The base case gasification plant was scaled up in order to recover the necessary amount of hydrogen in the PSA unit for the hydrodeoxygenation process at the pyrolysis plant. In the previous case the amount of hydrogen was covered by an increased amount of feedstock and part of the char produced at the pyrolysis plant. In this case, the necessary amount of hydrogen required by the hydrodeoxygenation process is covered by the increase of biomass feedstock entering the plant. Hence, without modifying the amount of steam produced in the pyrolysis plant, we can use it to cover the energy requirements by the MEA unit at the plant and send the rest to the scaled-up gasification plant. At the scaled up gasification plant, from the total amount of steam produced through the heat recovery process using the high temperature flue gas stream, part of it is sent to the gasifier to achieve the previously specified steam to biomass ratio (STBR), which as seen previously it was specified to 1.5486, and the rest is sent to the stripper reboiler of the MEA unit in order to regenerate the CO<sub>2</sub> loaded amine from the flue gas stream coming from the combustor. The steam requirement by the stripper reboiler for the scaled-up gasification plant, and for

the 255.56 kg/hr of captured biogenic CO<sub>2</sub> in the amine was a total of 470 kg/hr. This total amount of steam required by the reboiler is supplied by the steam coming from the base case pyrolysis plant and by the steam generated by the scaled-up gasification plant. Thus, thanks to the scaling process of the base gasification plant and the steam coming from the base case pyrolysis plant we were able to supply the total amount of steam required for the regeneration of the amine and thus achieve a carbon capture rate of 90%. Then, the downside of supplying all of these steam to the reboiler only for the regeneration of the loaded amine is that it is not possible to generate the necessary amount of electricity required by both plants in the turbine section, for that reason is that from the results table shown above we can appreciate that the total energy input required by both plants is 13.49 kW for the pyrolysis plant and 31.66 kW for the scaled up gasification plant, thus adding up to 45.15 kW in total in both plants. Regarding the total electrical output in both cases, it was possible to generate 3.50 kW in the base case pyrolysis plant and 6.03 kW in the scaled-up gasification plant. Thus, both plants making a total electrical output of 9.54 kW. Hence, the net electrical balance for this integrated case of both plants resulted in a requirement of 35.61 kW as electrical input. Finally, regarding the total amount of CO<sub>2</sub> present in the fluegas in both plants, we can see from the results that the amount of biogenic CO<sub>2</sub> in the pyrolysis plant remains the same as the base case for the pyrolysis plant as no other additional changes were made except for sending steam to the gasification plant, in the scaled up gasification plant however we can see a significant increase in the amount of biogenic CO<sub>2</sub> content in the flue gas stream leaving the combustor, with a total amount of 255.56 kg/hr compared to the base case gasification plant of 153.19 kg/hr, as well as the previous integrated case, the reason for this significant increase is due to the increased amount of biomass feedstock entering the scaled up gasification plant, which results in more char being separated from the decomposed stream of biomass that is sent to the combustor. Hence, as well as the previous integrated case, a MEA capture unit was attached for the flue gas stream leaving the combustor, and 90% of the CO<sub>2</sub> content in the flue gas stream was captured, and the rest was emitted to the atmosphere. For that reason, regarding the biogenic CO<sub>2</sub> emissions, thanks to the attachment of a MEA capture unit for the flue gas stream in both units is that it was possible to capture 90% of the CO<sub>2</sub> present in the flue gas stream in both plants. Resulting in this manner in total biogenic CO<sub>2</sub> emissions to the environment in the pyrolysis plant and the scaled-up gasification plant of 5.77 kg/hr and 25.55 kg/hr respectively.

Description of the Ref4 scenario

**Table 22. Details of the Ref4 scenario.**

"CASES WITH CCS" SHEET			
		Pyrolysis Plant	Gasification Plant
Wet biomass input	kg/hr	116.6000	160.94
Biomass input	kg/hr	83.4000	115.00
Biomass moisture (after drying process)	kg/hr	1.7000	2.34
Dry biomass entering plant	kg/hr	81.7000	124.21
SYNGAS mass flow	kg/hr	37.0174	278.90
Amount of Hydrogen used in HDO	kg/hr	13.4300	-
PSA feed pressure	bar	8.1568	25.00
PSA off gas pressure	bar	2.3460	1.18
Calculated % of H <sub>2</sub> recovery	%	53.4200	84.88
Pure H <sub>2</sub> recovered from PSA	kg/hr	4.5832	8.9078
Steam to gasifier	kg/hr	none	190.00
Char to combustor	kg/hr	1.6500	40.37
Char to gasification plant	kg/hr	11.5498	11.55
STBR (Steam to Biomass Ratio) STBR = Biomass moisture + Steam / Dry Biomass flow rate		None	1.5486
Total Electrical Input	kW	13.8534	31.0805
Total Electrical Output	kW	0.0000	5.5080
Net Electrical balance	kW	-13.8534	-25.5725
Biogenic CO <sub>2</sub> present in flue gas	kg/hr	20.3894	253.56
Biogenic CO <sub>2</sub> emitted to atmosphere	kg/hr	2.0389	25.3560

As seen from the results summarized in the table above, the mass flow of biomass in the gasification plant was increased and part of the total char produced in the biomass fast pyrolysis plant was as well sent to the biomass gasification plant. This was done in order to produce more syngas and consequently increase the amount of hydrogen recovered from the respective PSA unit. Thus, the amount of hydrogen recovered with the additional char in the gasification plant resulted in 8.9078 kg/hr along with the 4.5832 kg/hr from the PSA unit of the pyrolysis plant. Hence, resulting in a total amount of 13.491 kg/hr of Hydrogen available for the hydrodeoxygenation process at the pyrolysis plant. Due to the increased amount of biomass entering to the gasification plant, more steam has to be provided to the gasifier in order to keep the steam to biomass ratio (STBR) to 1.5486. As discussed previously, this STBR value was kept constant in all the biomass gasification cases due to the resulting higher content of hydrogen in the produced syngas. Thus, this increased amount of steam requires more input from the steam generated at both plants, affecting in this manner the total amount of electricity that can be produced in both plants, first the pyrolysis plant because of the deviation of char that was meant for the combustor at the plant and was sent to the gasification plant, which resulted in a lower temperature flue gas stream and consequently a lower heat recovery rate, our results from the gas stream coming from the combustor of the pyrolysis plant shown that it was not possible to produce steam in situ but still the heat recovery rate was enough to cover other requirements at the plant such as pre heating streams and drying the biomass. The amount of char that is sent to the gasification plant results in a higher temperature flue gas stream coming from the combustor at the plant, which consequently is sued to recover heat through the use of heat

exchanger and thus produce more steam in situ. These changes in the steam produced through the different heat recovery systems at both plants is reflected in the results, where the net electrical balance at the pyrolysis plant and gasification plant resulted in -13.85 kW and -25.57 kW respectively. As well, these values of net electrical balance were affected due to the amount of steam that had to be sent to the stripper reboiler of the MEA units at each plant, as seen before each MEA unit had a carbon capture rate of 90% which resulted in the pyrolysis and gasification plants in biogenic CO<sub>2</sub> emissions of 2.03 kg/hr and 25.35 kg/hr respectively. From the total amount of biogenic CO<sub>2</sub> present in the flue gas stream of each combustor unit at both plants we can appreciate as well the effects of deviating char from the pyrolysis plant to the gasification plant, at the pyrolysis plant the total amount of biogenic CO<sub>2</sub> before the MEA unit was 20.38 kg/hr, less than half of the original value in the base case of 57.76 kg/hr. In the case of the gasification plant we can appreciate that the amount of biogenic CO<sub>2</sub> present in the flue gas stream before the MEA capture unit increased significantly compared to the base case, a total amount of 253.56 kg/hr compared to the 153.19 kg/hr of the base case. This significant increase is as well due to the increased amount of biomass feedstock entering to the gasification plant, which resulted in more char deviated to the combustor, and the amount of char coming from the pyrolysis plant.

#### ANALYSIS OF REF1 SCENARIO

The results for the biomass fast pyrolysis with hydrogen coming from the natural gas reforming are summarized in Table 23.

**Table 23. Details of Ref1 scenario.**

<b>Biomass input</b>	kg/hr	116,6
<b>Biochar</b>	kg/hr	0,0
<b>NG input</b>	kg/hr	29,3
<b>Biogenic CO<sub>2</sub> emitted</b>	kg/hr	57,8
<b>Fossil CO<sub>2</sub> emitted</b>	kg/hr	7,9
<b>Bio-oil produced</b>	kg/hr	13,92
<b>Air flow to the system</b>	kg/hr	775,6
<b>Net electricity generated from the system</b>	kW	7,5
<b>Fresh water</b>	kg/hr	44,8
<b>H<sub>2</sub> from NG plant</b>	kg/hr	8,85
<b>CO<sub>2</sub> for storage (fossil CO<sub>2</sub>)</b>	kg/hr	69,4
		<i>CO<sub>2</sub> is compressed until 110 bar for storage</i>

## BIOMASS SPECIES AND THEIR COMPOSITION

Table 24. Composition of the Douglas fir wood sample and Spruce samples from the work of Caudle et al. [21] and Debiagi et al. [24].

		Composition used in Ref1-4 and CCS1-5 cases in the report	S1	S2	S3	S4
<b>Wood</b>		Douglas fir wood	Spruce	Spruce	Spruce	Spruce
<b>Type</b>		Softwood	Softwood	Softwood	Softwood	Softwood
<b>Physical form</b>		Not specified	Chips wood	Chips wood	Saw shavings	Chips
<b>Ash</b>	wt%	0,0048	0,0145	0,0410	0,0029	0,0047
<b>Cellulose</b>	wt%	0,4293	0,4194	0,4250	0,4461	0,4572
<b>Hemicellulose</b>	wt%	0,2146	0,2378	0,1873	0,1930	0,1735
<b>Lignin – H</b>	wt%	0,1175	0,1929	0,0577	0,0516	0,0154
<b>Lignin – O</b>	wt%	0,1067	0,0347	0,1517	0,1680	0,2118
<b>Lignin – C</b>	wt%	0,0456	0,0162	0,0498	0,0464	0,0300
<b>Triglyceride</b>	wt%	0,0492	0,0642	0,0309	0,0298	0,0113
<b>Tannin</b>	wt%	0,0120	0,0000	0,0362	0,0419	0,0758
<b>Moisture</b>	wt%	0,0204	0,0204	0,0204	0,0204	0,0204
<b>Total cellulose</b>	%	<b>64,39</b>	<b>65,72</b>	<b>61,23</b>	<b>63,90</b>	<b>63,07</b>
<b>Total Lignin</b>	%	<b>26,98</b>	<b>24,38</b>	<b>25,91</b>	<b>26,61</b>	<b>25,71</b>

Table 25. Composition of the Pine samples from the work of Debiagi et al. [24].

		P1	P2	P3	P4
<b>Wood</b>		Pine	Pine	Pine	Pine
<b>Type</b>		Softwood	Softwood	Softwood	Softwood
<b>Physical form</b>		Chips wood	Chips	-	Sawdust
<b>Ash</b>	wt%	0,1424	0,0041	0,0000	0,0059
<b>Cellulose</b>	wt%	0,3350	0,4042	0,4344	0,4546
<b>Hemicellulose</b>	wt%	0,2606	0,2012	0,1951	0,1952
<b>Lignin – H</b>	wt%	0,0164	0,1494	0,0730	0,0450
<b>Lignin – O</b>	wt%	0,1155	0,0596	0,1351	0,1839
<b>Lignin – C</b>	wt%	0,0240	0,1034	0,0727	0,0255
<b>Triglyceride</b>	wt%	0,0788	0,0448	0,0348	0,0281
<b>Tannin</b>	wt%	0,0070	0,0128	0,0345	0,0415
<b>Moisture</b>	wt%	0,0204	0,0204	0,0204	0,0204
<b>Total cellulose</b>	%	<b>59,56</b>	<b>60,55</b>	<b>62,95</b>	<b>64,98</b>
<b>Total Lignin</b>	%	<b>15,59</b>	<b>31,24</b>	<b>28,08</b>	<b>25,44</b>

## COMPONENTS OF BIOMASS CONSIDERED IN MODELLING OF FAST PYROLYSIS IN ASPEN PLUS

Table 26. Biomass components, intermediate species and end products involved in the fast pyrolysis process, reproduced from the work of Gorenssek et al. [25].

<i>Component</i>	<i>Component ID</i>	<i>Type</i>	<i>Formula</i>	<i>Present in Aspen plus databank?</i>
<b><i>Biomass Components</i></b>				
Cellulose	CELL	Solid	C <sub>6</sub> H <sub>10</sub> O <sub>5</sub>	No
Glucomannan	GMSW	Solid	C <sub>5</sub> H <sub>8</sub> O <sub>4</sub>	No
Xylan	XYHW	Solid	C <sub>5</sub> H <sub>8</sub> O <sub>4</sub>	No
C - rich lignin	LIGC	Solid	C <sub>15</sub> H <sub>14</sub> O <sub>4</sub>	No
O - rich lignin	LIGO	Solid	C <sub>20</sub> H <sub>22</sub> O <sub>10</sub>	No
H - rich lignin	LIGH	Solid	C <sub>22</sub> H <sub>28</sub> O <sub>9</sub>	No
Tannin	TANN	Solid	C <sub>15</sub> H <sub>12</sub> O <sub>7</sub>	No
Triglyceride	TGL	Conventional	C <sub>57</sub> H <sub>100</sub> O <sub>7</sub>	No
Moisture	H2OL	Conventional	H <sub>2</sub> O	Yes
Ash	ASH	Solid	CaO	Yes
<b><i>Biomass Pyrolysis intermediate Species</i></b>				
Secondary lignin intermediate	LIG	Solid	C <sub>11</sub> H <sub>12</sub> O <sub>4</sub>	No
C - rich lignin intermediate	LIGCC	Solid	C <sub>15</sub> H <sub>14</sub> O <sub>4</sub>	No
H/O - rich lignin intermediate	LIGOH	Solid	C <sub>19</sub> H <sub>22</sub> O <sub>8</sub>	No
Activated hemicellulose 1	HCE1	Solid	C <sub>5</sub> H <sub>8</sub> O <sub>4</sub>	No
Activated hemicellulose 2	HCE2	Solid	C <sub>5</sub> H <sub>8</sub> O <sub>4</sub>	No
Activated cellulose	CELLA	Solid	C <sub>6</sub> H <sub>10</sub> O <sub>5</sub>	No
Tannin intermediate	ITANN	Solid	C <sub>8</sub> H <sub>4</sub> O <sub>4</sub>	No
<b><i>Biomass pyrolysis end products</i></b>				
Char	CHAR	Solid	C	Yes
Sinapyl aldehyde	FE2MACR	Conventional	C <sub>11</sub> H <sub>12</sub> O <sub>4</sub>	No
Free fatty acid	FFA	Conventional	C <sub>18</sub> H <sub>32</sub> O <sub>2</sub>	Yes
high-molecular-weight lignin	HMWL	Solid	C <sub>24</sub> H <sub>28</sub> O <sub>4</sub>	No
Glyoxal	GLYOX	Conventional	C <sub>2</sub> H <sub>2</sub> O <sub>2</sub>	Yes
Ethylene	C2H4	Conventional	C <sub>2</sub> H <sub>4</sub>	Yes
Acetaldehyde	CH3CHO	Conventional	C <sub>2</sub> H <sub>4</sub> O	Yes
Acetic acid	ACAC	Conventional	C <sub>2</sub> H <sub>4</sub> O <sub>2</sub>	Yes
Glycolaldehyde	HAA	Conventional	C <sub>2</sub> H <sub>4</sub> O <sub>2</sub>	Yes
Ethanol	C2H5OH	Conventional	C <sub>2</sub> H <sub>6</sub> O	Yes
Acrolein	ACROL	Conventional	C <sub>3</sub> H <sub>4</sub> O	Yes
n-propionaldehyde	ALD3	Conventional	C <sub>3</sub> H <sub>6</sub> O	Yes
3-hydroxypropanal	C3H6O2	Conventional	C <sub>3</sub> H <sub>6</sub> O <sub>2</sub>	No
Furfural	FURF	Conventional	C <sub>5</sub> H <sub>4</sub> O <sub>2</sub>	Yes
Xylosan	XYLAN	Conventional	C <sub>5</sub> H <sub>8</sub> O <sub>4</sub>	No
Levogluconan	LVG	Conventional	C <sub>6</sub> H <sub>10</sub> O <sub>5</sub>	Yes
Phenol	PHENOL	Conventional	C <sub>6</sub> H <sub>6</sub> O	Yes
5-hydroxymethyl-furfural	HMFU	Conventional	C <sub>6</sub> H <sub>6</sub> O <sub>3</sub>	Yes

Anisole	ANISOLE	Conventional	C <sub>7</sub> H <sub>8</sub> O	Yes
p-coumaryl alcohol	COUMARYL	Conventional	C <sub>9</sub> H <sub>10</sub> O <sub>2</sub>	No
Formaldehyde	CH <sub>2</sub> O	Conventional	CH <sub>2</sub> O	Yes
Formic acid	HCOOH	Conventional	CH <sub>2</sub> O <sub>2</sub>	Yes
Methane	CH <sub>4</sub>	Conventional	CH <sub>4</sub>	Yes
Methanol	CH <sub>3</sub> OH	Conventional	CH <sub>4</sub> O	Yes
Carbon monoxide	CO	Conventional	CO	Yes
Carbon dioxide	CO <sub>2</sub>	Conventional	CO <sub>2</sub>	Yes
Hydrogen	H <sub>2</sub>	Conventional	H <sub>2</sub>	Yes
Water	H <sub>2</sub> O	Conventional	H <sub>2</sub> O	Yes
<i>Non biomass components also included in the simulation environment</i>				
Argon	AR	Conventional	Ar	Yes
Nitrogen	N <sub>2</sub>	Conventional	N <sub>2</sub>	Yes
Oxygen	O <sub>2</sub>	Conventional	O <sub>2</sub>	Yes
Sand	SAND	Solid	SiO <sub>2</sub>	Yes

### THERMOPHYSICAL PROPERTIES OF BIOMASS INTRODUCED IN MODELLING OF PROCESS USING ASPEN PLUS

Table 27. Estimated properties for conventional solid components in pyrolysis process model. Table reproduced from the work of Gorensek et al. [25].

Component ID	Molecular weight	Standard solid enthalpy of formation	Heat capacity model coefficients		Solid density
	kg/kmol	kJ/gmol	C <sub>1</sub> J/gmol*K	C <sub>2</sub> J/gmol*K <sup>2</sup>	kmol/m <sup>3</sup>
<i>Lignins and Tannins</i>					
LIG	208.21388	-729.31	13.2251	0.82834	7.3002
LIGC	258.27376	-759.39	16.4048	1.02749	5.8852
LIGCC	258.27376	-759.39	16.4048	1.02749	5.8852
LIGH	436.45892	-1722.7	27.7226	1.73636	3.4826
LIGO	422.38868	-1847.5	26.8289	1.68039	3.5986
LIGOH	378.37888	-1429.2	24.0335	1.50530	4.0171
HMWL	380.48392	-958.26	24.1672	1.51368	3.9949
ITANN	164.11736	-616.98	10.4242	0.65291	9.2617
TANN	304.25608	-1079.7	19.3254	1.21042	4.9958
<i>Cellulose Species</i>					
CELL	162.1424	-1019.0	-1.5328	0.67527	9.3745
CELLA	162.1424	-1019.0	-1.5328	0.67527	9.3745
<i>Hemicellulose Species</i>					
XYHW	132.11612	-759.2	-1.2489	0.55022	11.5050
GMSW	132.11612	-759.2	-1.2489	0.55022	11.5050
HCE1	132.11612	-759.2	-1.2489	0.55022	11.5050
HCE2	132.11612	-759.2	-1.2489	0.55022	11.5050

**Table 28. Estimated properties for conventional fluid components in pyrolysis process model. Table reproduced from the work of Gorensek et al. [25].**

	<i>3-hydroxy propanal</i>	<i>Triglyceride</i>	<i>P-coumaryl alcohol</i>	<i>Sinapyl aldehyde</i>	<i>Xylosan</i>
<b>Molecular weight, kg/kmol</b>	74.07944	897.4168	150.1772	208.21388	132.11612
<b>Ideal gas enthalpy of formation, kJ/gmol</b>	-345.3	-1546.3	-193.5	-483.8	-642.3
<b>Critical temperature, K</b>	605.0	934.6	791.4	837.9	744.3
<b>Critical pressure, bar</b>	56.36	2.027	56.90	29.25	2.134
<b>Acentric factor</b>	1.133	2.08419	1.198	0.981	0.292
<b>Ideal Gas Heat Capacity Estimates [J/gmol-k]</b>					
<b>Cp<sup>*,ig</sup> (298 K)</b>	91.46	1304.35	177.30	240.85	142.76
<b>Cp<sup>*,ig</sup> (400 K)</b>	109.33	1648.81	225.11	302.37	179.06
<b>Cp<sup>*,ig</sup> (500 K)</b>	126.37	1950.68	264.73	357.37	215.39
<b>Cp<sup>*,ig</sup> (600 K)</b>	141.02	2194.89	296.16	402.54	240.55
<b>Cp<sup>*,ig</sup> (800 K)</b>	164.75	2564.01	342.81	471.36	281.03
<b>Cp<sup>*,ig</sup> (1000 K)</b>	182.00	2840.98	374.75	520.31	307.48
<b>Aly-Lee Cp<sup>*,ig</sup> Equation Coefficients</b>					
<b>C<sub>cp,1</sub> J/ (kmol K)</b>	77793.84	1008344	128972.6	190226.6	115298.4
<b>C<sub>cp,2</sub> J/ (kmol K)</b>	106997.7	1979396	342667.4	491979.1	224458.5
<b>C<sub>cp,3</sub> K</b>	814.165	777.2196	1575.222	1728.691	824.2086
<b>C<sub>cp,4</sub> J/ (kmol K)</b>	66750.56	1165050	266861.9	371592.6	59411.96
<b>C<sub>cp,5</sub> K</b>	2048.402	2438.886	728.2816	797.2112	2302.592
<b>C<sub>cp,6</sub> K</b>	298	298.15	298	298	298
<b>C<sub>cp,7</sub> K</b>	1000	1500	1000	1000	1000
<b>Extended Antoine Equation Coefficients [K/Pa]</b>					
<b>C<sub>pl,1</sub></b>	136.9781	234.71	286.7075	286.6149	135.2637
<b>C<sub>pl,2</sub></b>	-13924.84	-34699	-25124.63	-25391.53	-14336.53
<b>C<sub>pl,3</sub></b>	-15.46495	-27.25	-37.26739	-37.28766	-15.74501
<b>C<sub>pl,4</sub></b>	1.303768x10 <sup>-17</sup>	1.5475x10 <sup>-18</sup>	1.48627x10 <sup>-5</sup>	1.36118x10 <sup>-5</sup>	2.245921x10 <sup>-18</sup>
<b>C<sub>pl,5</sub></b>	6	6	2	2	6
<b>C<sub>pl,6</sub></b>	261.15	262.15	406.15	406.15	455.4
<b>C<sub>pl,7</sub></b>	605	934.6	791.4	837.9	744.3

## KINETIC SCHEMES FOR BIOMASS FAST PYROLYSIS PROCESS REPORTED IN LITERATURE

**Table 29. Original Multistep kinetic scheme of the biomass fast pyrolysis process. Table reproduced from the work of Ranzi et al. [22].**

Reaction		$A_n$ ( $K^{-x_n} \cdot s^{-1}$ )	$x_n$	$E_a$ [kcal/kmol]
<i>Cellulose</i>				
1)	CELL → CELLA	$1.5 \times 10^{14}$	0	47000
2)	CELLA → 0.4 HAA + 0.05 GLYOX + 0.15 CH <sub>3</sub> CHO + 0.25 HMFU + 0.35 ALD3 + 0.15 CH <sub>3</sub> OH + 0.3 CH <sub>2</sub> O + 0.61 CO + 0.36 CO <sub>2</sub> + 0.05 H <sub>2</sub> + 0.93 H <sub>2</sub> O + 0.02 HCOOH + 0.05 C <sub>3</sub> H <sub>6</sub> O <sub>2</sub> + 0.05 G[CH <sub>4</sub> ]	$2.5 \times 10^6$	0	19100
3)	CELLA → LVG	3.3	1	10000
4)	CELL → 5 H <sub>2</sub> O + 6 CHAR	$6 \times 10^7$	0	31000
<i>Hemicellulose</i>				
5)	GMSW → 0.7 HCE1 + 0.3 HCE2	$1 \times 10^{10}$	0	31000
6)	XYHW → 0.35 HCE1 + 0.65 HCE2	$1 \times 10^{10}$	0	28500
7)	HCE1 → 0.6 XYLAN + 0.2 C <sub>3</sub> H <sub>6</sub> O <sub>2</sub> + 0.12 GLYOX + 0.2 FURF + 0.4 H <sub>2</sub> O + 0.08 G[H <sub>2</sub> ] + 0.16 CO	3	1	11000
8)	HCE1 → 0.4 H <sub>2</sub> O + 0.79 CO <sub>2</sub> + 0.05 HCOOH + 0.69 CO + 0.01 G[CO] + 0.01 G[CO <sub>2</sub> ] + 0.35 G[H <sub>2</sub> ] + 0.3 CH <sub>2</sub> O + 0.9 G[COH <sub>2</sub> ] + 0.625 G[CH <sub>4</sub> ] + 0.375 G[C <sub>2</sub> H <sub>4</sub> ] + 0.875 CHAR	$1.8 \times 10^{-3}$	1	3000
9)	HCE2 → 0.2 H <sub>2</sub> O + 0.275 CO + 0.275 CO <sub>2</sub> + 0.4 CH <sub>2</sub> O + 0.1 C <sub>2</sub> H <sub>5</sub> OH + 0.05 HAA + 0.35ACAC + 0.025 HCOOH + 0.25 G[CH <sub>4</sub> ] + 0.3 G[CH <sub>3</sub> OH] + 0.225 G[C <sub>2</sub> H <sub>4</sub> ] + 0.4 G[CO <sub>2</sub> ] + 0.725 G[COH <sub>2</sub> ]	$5 \times 10^9$	0	31500
<i>Lignins</i>				
10)	LIGC → 0.35 LIGCC + 0.1 COUMARYL + 0.08 PHENOL + 0.41 C <sub>2</sub> H <sub>4</sub> + 1.0 H <sub>2</sub> O + 0.7 G[COH <sub>2</sub> ] + 0.3 CH <sub>2</sub> O + 0.32 CO + 0.495 G[CH <sub>4</sub> ]	$1 \times 10^{11}$	0	37200
11)	LIGH → LIGOH + 0.5 ALD3 + 0.5 C <sub>2</sub> H <sub>4</sub> + 0.2 HAA + 0.1 CO + 0.1 G[H <sub>2</sub> ]	$6.7 \times 10^{12}$	0	37500
12)	LIGO → LIGOH + CO <sub>2</sub>	$3.3 \times 10^8$	0	25500
13)	LIGCC → 0.3 COUMARYL + 0.2 PHENOL + 0.35 HAA + 0.7 H <sub>2</sub> O + 0.65 CH <sub>4</sub> + 0.6 C <sub>2</sub> H <sub>4</sub> + H <sub>2</sub> + 1.4 CO + 0.4 G[CO] + 6.75 CHAR	$1 \times 10^4$	0	24800
14)	LIGOH → 0.9 LIG + H <sub>2</sub> O + 0.1 CH <sub>4</sub> + 0.6 CH <sub>3</sub> OH + 0.05 G[H <sub>2</sub> ] + 0.3 G[CH <sub>3</sub> OH] + 0.05 CO <sub>2</sub> + 0.65 CO + 0.6 G[CO] + 0.05 HCOOH + 0.85 G[COH <sub>2</sub> ] + 0.35 G[CH <sub>4</sub> ] + 0.2 G[C <sub>2</sub> H <sub>4</sub> ] + 4.25 CHAR	$1 \times 10^8$	0	30000
15)	LIG → 0.7 FE2MACR + 0.3 ANISOLE + 0.3 CO + 0.3 G[CO] + 0.3 CH <sub>3</sub> CHO	4	1	12000
16)	LIG → 0.6 H <sub>2</sub> O + 0.4 CO + 0.2 CH <sub>4</sub> + 0.4 CH <sub>2</sub> O + 0.2 G[CO] + 0.4 G[CH <sub>4</sub> ] + 0.5 G[C <sub>2</sub> H <sub>4</sub> ] + 0.4 G[CH <sub>3</sub> OH] + 2 G[COH <sub>2</sub> ] + 6 CHAR	$8.3 \times 10^{-2}$	1	8000

17)	LIG	→	$0.6 \text{ H}_2\text{O} + 2.6 \text{ CO} + 1.1 \text{ CH}_4 + 0.4 \text{ CH}_2\text{O} + \text{C}_2\text{H}_4 + 0.4 \text{ CH}_3\text{OH}$	$1 \times 10^7$	0	24300
<i>Extractives</i>						
18)	TGL	→	ACROL + 3 FFA	$7 \times 10^{12}$	0	45700
19)	TANN	→	$0.85 \text{ FENOL} + 0.15 \text{ G[PHENOL]} + \text{G[CO]} + \text{H}_2\text{O} + \text{ITANN}$	20	0	10000
20)	ITANN	→	$5 \text{ CHAR} + 2 \text{ CO} + \text{H}_2\text{O} + \text{G[COH}_2\text{]}$	$1 \times 10^3$	0	25000
<i>Metaplastic</i>						
21)	G[CO <sub>2</sub> ]	→	CO <sub>2</sub>	$1 \times 10^6$	0	24000
22)	G[CO]	→	CO	$5 \times 10^{12}$	0	50000
23)	G[COH <sub>2</sub> ]	→	CO + H <sub>2</sub>	$1.5 \times 10^{12}$	0	71000
24)	G[H <sub>2</sub> ]	→	H <sub>2</sub>	$5 \times 10^{11}$	0	75000
25)	G[CH <sub>4</sub> ]	→	CH <sub>4</sub>	$5 \times 10^{12}$	0	71500
26)	G[CH <sub>3</sub> OH]	→	CH <sub>3</sub> OH	$2 \times 10^{12}$	0	50000
27)	G[C <sub>2</sub> H <sub>4</sub> ]	→	C <sub>2</sub> H <sub>4</sub>	$5 \times 10^{12}$	0	71500
28)	G[PHENOL]	→	PHENOL	$1.5 \times 10^{12}$	0	71000
<i>H<sub>2</sub>O Evaporation</i>						
29)	H <sub>2</sub> O	→	H <sub>2</sub> OL	1	1	8000

**Table 30. Simplified multistep kinetic scheme for biomass fast pyrolysis process, table reproduced from the work of Caudle et al. [21].**

Reaction		$An$ ( $K^{-xn} * s^{-1}$ )	$xn$	$Ea$ [kcal/kmol]
<b>Cellulose</b>				
1)	CELL → CELLA	$1.5 \times 10^{14}$	0	47000
2)	CELLA → 0.4 HAA + 0.05 GLYOX + 0.15 CH <sub>3</sub> CHO + 0.25 HMFU + 0.35 ALD3 + 0.15 CH <sub>3</sub> OH + 0.3 CH <sub>2</sub> O + 0.61 CO + 0.36 CO <sub>2</sub> + 0.25 H <sub>2</sub> + 0.93 H <sub>2</sub> O + 0.02 HCOOH + 0.05 C <sub>3</sub> H <sub>6</sub> O <sub>2</sub> + 0.05 CH <sub>4</sub> + 0.61 CHAR	$2.5 \times 10^6$	0	19100
3)	CELLA → LVG	3.3	1	10000
4)	CELL → 5 H <sub>2</sub> O + 6 CHAR	$6 \times 10^7$	0	31000
<b>Hemicellulose</b>				
5)	GMSW → 0.7 HCE1 + 0.3 HCE2	$1 \times 10^{10}$	0	31000
6)	XYHW → 0.35 HCE1 + 0.65 HCE2	$1 \times 10^{10}$	0	28500
7)	HCE1 → 0.6 XYLAN + 0.2 C <sub>3</sub> H <sub>6</sub> O <sub>2</sub> + 0.12 GLYOX + 0.2 FURF + 0.4 H <sub>2</sub> O + 0.08 H <sub>2</sub> + 0.16 CO	3	1	11000
8)	HCE1 → 0.4 H <sub>2</sub> O + 0.8 CO <sub>2</sub> + 0.05 HCOOH + 1.6 CO + 1.25 H <sub>2</sub> + 0.3 CH <sub>2</sub> O + 0.625 CH <sub>4</sub> + 0.375 C <sub>2</sub> H <sub>4</sub> + 0.875 CHAR	$1.8 \times 10^{-3}$	1	3000
9)	HCE2 → 0.2 H <sub>2</sub> O + CO + 0.575 CO <sub>2</sub> + 0.4 CH <sub>2</sub> O + 0.1 C <sub>2</sub> H <sub>5</sub> OH + 0.05 HAA + 0.35 ACAC + 0.025 HCOOH + 0.25 CH <sub>4</sub> + 0.3 CH <sub>3</sub> OH + 0.225 C <sub>2</sub> H <sub>4</sub> + 0.725 H <sub>2</sub> + CHAR	$5 \times 10^9$	0	31500
<b>Lignins</b>				
10)	LIGC → 0.35 LIGCC + 0.1 COUMARYL + 0.08 PHENOL + 0.41 C <sub>2</sub> H <sub>4</sub> + H <sub>2</sub> O + 1.02 CO + 0.7 H <sub>2</sub> + 0.3 CH <sub>2</sub> O + 0.495 CH <sub>4</sub> + 5.735 CHAR	$1 \times 10^{11}$	0	37200
11)	LIGH → LIGOH + 0.5 ALD3 + 0.5 C <sub>2</sub> H <sub>4</sub> + 0.2 HAA + 0.1 CO + 0.1 H <sub>2</sub>	$6.7 \times 10^{12}$	0	37500
12)	LIGO → LIGOH + CO <sub>2</sub>	$3.3 \times 10^8$	0	25500
13)	LIGCC → 0.3 COUMARYL + 0.2 PHENOL + 0.35 HAA + 0.7 H <sub>2</sub> O + 0.65 CH <sub>4</sub> + 0.6 C <sub>2</sub> H <sub>4</sub> + H <sub>2</sub> + 1.8 CO + 6.75 CHAR	$1 \times 10^4$	0	24800
14)	LIGOH → 0.9 LIG + H <sub>2</sub> O + 0.45 CH <sub>4</sub> + 0.9 CH <sub>3</sub> OH + 0.9 H <sub>2</sub> + 0.05 CO <sub>2</sub> + 2.1 CO + 0.05 HCOOH + 0.2 C <sub>2</sub> H <sub>4</sub> + 0.025 HMWL + 0.1 ACROL + 4.25 CHAR	$0.4 \times 10^6$	0	30000
15)	LIG → 0.7 FE2MACR + 0.3 ANISOLE + 0.6 CO + 0.3 CH <sub>3</sub> CHO	4	1	12000
16)	LIG → 0.6 H <sub>2</sub> O + 2.6 CO + 0.6 CH <sub>4</sub> + 0.4 CH <sub>2</sub> O + 0.5 C <sub>2</sub> H <sub>4</sub> + 0.4 CH <sub>3</sub> OH + 2 H <sub>2</sub> + 6 CHAR	$8.3 \times 10^{-2}$	1	8000
17)	LIG → 0.6 H <sub>2</sub> O + 2.6 CO + 1.1 CH <sub>4</sub> + 0.4 CH <sub>2</sub> O + C <sub>2</sub> H <sub>4</sub> + 0.4 CH <sub>3</sub> OH + 4.5 CHAR	$1 \times 10^7$	0	24300
<b>Extractives</b>				
18)	TGL → ACROL + 3 FFA	$7 \times 10^{12}$	0	45700
19)	TANN → PHENOL + CO + H <sub>2</sub> O + ITANN	20	0	10000
20)	ITANN → 5 CHAR + 3 CO + H <sub>2</sub> O + H <sub>2</sub>	$1 \times 10^3$	0	25000
<b>H<sub>2</sub>O Evaporation</b>				
21)	H <sub>2</sub> O → H <sub>2</sub> OL	1	1	8000

## SUMMARY OF REVIEW FOR VAPOR PHASE HDO PROCESS

Table 31. Summary of review on vapor phase hydrodeoxygenation.

<i>n</i>	<i>HDO Process</i>	<i>Catalyst used</i>	<i>Temperature</i>	<i>Pressure</i>	<i>Remarks</i>
1	HDO of Guaiacol [48]	Fe/SiO <sub>2</sub>	400°C	1 atm	Good selectivity for Benzene toluene formation The char, oligomers, pyrolysis loss account for 77.7% of carbon atoms from lignin, while the yield of benzene + toluene (mono-aromatic compounds) is very low , only 7.5% C
2	HDO of Guaiacol [49]	Pd-Fe/C	450°C	1 atm	83.2% yield to benzene / toluene / TMB (oxygen free basis) at 100 mg catalyst, P <sub>guaiacol</sub> = 0.4 kPa, P <sub>H2</sub> = 40 kPa, W/F = 0.15 s.g.STP mL <sup>-1</sup>
3	HDO of Anisole [50]	Ru/ Ni over mesoporous aluminosilicate (Al-SBA-15 )	400°C	1 atm	High product selectivity for benzene, and a trace amount of toluene H <sub>2</sub> flow rate = 50 mL/min.
4	HDO of phenolic compound mixtures [51]	Mo <sub>2</sub> C	260-280°C	1 atm	High conversion (95%), and high selectivity to benzene and toluene,high hydrogen efficiency No indication of <u>catalyst deactivation</u> Inhibition of the aromatic hydrogenation function on Mo <sub>2</sub> C during HDO reactions due to in situ modification of the catalyst surface by oxygenates
5	HDO of oak and switchgrass pyrolysis oil [52]	Ru/TiO <sub>2</sub>	400°C	1 atm	Hydrogen partial pressure of 0.58 atm 16-25 wt% organic phase yield
6	HDO Biomass pyrolysis vapor [53]	MoO <sub>3</sub>	450°C	1 atm	The wood pyrolysis vapor was more active toward cracking instead of HDO 93 vol % H <sub>2</sub> concentration
7	HDO of pine pyrolysis vapor [54]	Pt/HBEA	500°C	1 atm	High selectivity towards 1-ring aromatics A gas flow rate of 300 cm <sup>3</sup> /min (33% H <sub>2</sub> , 10% Ar, balance He) flowed through the inner tube in which pyrolysis and vapor phase HDO upgrading occurred
8	HDO of wheat straw pyrolysis vapor [55]	MoO <sub>3</sub> /TiO <sub>2</sub> and Pt/TiO <sub>2</sub>	450°C	1 atm	MoO <sub>3</sub> /TiO <sub>2</sub> had lower efficiency in conversion of acids Pt/TiO <sub>2</sub> showed the highest selectivity to aliphatics and the lowest coke yields 50-90 vol% H <sub>2</sub> considered 19 wt% oil phase yield
9	HDO of cellulose and poplar pyrolysis vapor [56]	5 wt% Pt 2.5 wt% Mo/MWCNT	300-350°C	27 bar	The total C <sub>1</sub> -C <sub>8</sub> + hydrocarbon yield with cellulose is 73% and poplar is 54% of the carbon fed The hydrocarbon yield in the liquid fuel range (C <sub>4</sub> +) is ~55% for cellulose and 32% for poplar Synergistic process integrations of fast-hydrolysis and HDO along with gasification, combustion and reforming
10	Ex situ hydrodeoxygenation of Corn Stover [17]	MoO <sub>3</sub>	500°C	1.8 bar	The yield of larger hydrocarbon products (C <sub>4</sub> +) was 15–26 C%.

**Table 32. Carbon, oxygen and hydrogen wt% for hydro-deoxygenated bio-oil as reported in literature.**

<i>Source</i>	<i>Operation Conditions</i>	<i>Feedstock</i>	<i>C%</i>	<i>O%</i>	<i>H%</i>
<b>Nolte et al., 2016 [17]</b>	<ul style="list-style-type: none"> <li>• Pyrolysis Vapor upgrading</li> <li>• MoO<sub>3</sub> catalyst</li> <li>• Low-pressure H<sub>2</sub> (1.8 bar P total)</li> <li>• 0.1kg H<sub>2</sub> per kg dry biomass</li> </ul>	Corn Stover	87.77	0.00	12.23
<b>Wang et al., 2016 [57]</b>	<ul style="list-style-type: none"> <li>• Bio-oil 2 stage hydrotreating</li> <li>• Ru/C stage 1 catalyst</li> <li>• CoMo/Al<sub>2</sub>O<sub>3</sub> stage 2 catalyst</li> <li>• Hydrogen flow 152 ml/min</li> <li>• Biomass 100g/hr</li> </ul>	Switchgrass	85.6	2.1	12.3
<b>Wang et al., 2012 [58]</b>	<ul style="list-style-type: none"> <li>• Catalytic pyrolysis oil HDO over Pt/MZ-5</li> <li>• 473 K and 4 Mpa total pressure</li> <li>• Constant H<sub>2</sub>/oil volume ratio at 600</li> </ul>	Dibenzofuran model compound	83.8	5	11.2
<b>Auersvald et al., 2018 [59]</b>	<ul style="list-style-type: none"> <li>• Bio-oil HDO</li> <li>• NiMo/Al<sub>2</sub>O<sub>3</sub> catalyst</li> <li>• 320°C and 8 Mpa</li> <li>• hydrogen flow rate 90 NI-h-1</li> </ul>	Straw barley/wheat 1/1 (w/w)	81.69	6.62	10.84
<b>Elliott et al., 1989 [60] Ahmad et al., 2010 [61] Huber et al., 2006 [62]</b>	<ul style="list-style-type: none"> <li>• Two-step hydrotreating process</li> <li>• 270°C, 136 atm</li> <li>• 400°C, 136 atm</li> <li>• Co-Mo</li> <li>• Al<sub>2</sub>O<sub>3</sub> or sulfided Ni-Mo/Al<sub>2</sub>O<sub>3</sub></li> </ul>	Not specified	85.3 - 89.2	0.0 - 0.7	10.5 - 14.1
<b>Roberts et al., 2015 [63]</b>	<ul style="list-style-type: none"> <li>• IH<sub>2</sub> process for drop-in hydrocarbon fuels</li> <li>• 350-460°C</li> <li>• 20-35 barg</li> <li>• 5 wt % H<sub>2</sub> added</li> </ul>	Corn Stover  Wood	86.10  88.62	1.18  < 0.4	12.48  11.69

ASSUMPTIONS FOR YIELD IN MODELLING HDO STEP

Table 33. Yield used in the HDO process model.

<i>Substance</i>	<i>Weight fraction for RYield Reactor</i>	<i>Carbon weight fraction</i>	<i>Hydrogen weight fraction</i>	<i>Oxygen weight fraction</i>	<i>Others</i>	<i>Carbon recovery in weight fraction</i>
Corn Stover	1	0.4392	0.0601	0.4044	0.0963	1
Biochar	0.32965	0.18886	0.00943	0.01797		0.43
Raw bio-oil vapors	0.67035	0.25034	0.05067	0.38643		0.556
						0.986
Hydrogen	0.10000					
Total entering HDO	0.77035	0.25034	0.15067	0.38643		
NC gas	0.25827	0.14142	0.09342			0.322
Methane	0.04333	0.03250	0.01083	0.00000	0	0.074
Ethane	0.04776	0.03821	0.00955			0.087
Ethylene	0.00154	0.00132	0.00022			0.003
Propane	0.03811	0.03118	0.00693			0.071
Propylene	0.00102	0.00088	0.00015			0.002
n-butane	0.00425	0.00351	0.00073			0.008
i-butane	0.02972	0.02460	0.00512			0.056
CO <sub>2</sub>	0.03060	0.00834	0.00000	0.02225		0.019
CO	0.00205	0.00088	0.00000	0.00117		0.002
Excess H <sub>2</sub>	0.05988		0.05988			
Bio-oil	0.09708	0.08520	0.01187			0.194
i-pentane	0.01581	0.01318	0.00264			0.03
n-pentane	0.02424	0.02020	0.00404			0.046
n-hexane	0.00262	0.00220	0.00043			0.005
Benzene	0.01427	0.01318	0.00110			0.03
Toluene	0.01876	0.01713	0.00163			0.039
Ethyl benzene	0.00921	0.00834	0.00087			0.019
Xylene	0.00823	0.00747	0.00076			0.017
C9+ Benzene	0.00392	0.00351	0.00041			0.008
Naphthalene	0.00000	0.00000	0.00000			0
Coke	0.01757	0.01757				0.04
Water	0.40839		0.04538	0.36301		
Total leaving HDO	0.78130	0.24420	0.15067	0.38643		

PROCESS DETAILS FOR DIFFERENT BIOMASS SPECIES

Table 34. Analysis for Ref1 case when using different biomass types

		<i>Ref1</i>	<i>S1</i>	<i>S2</i>	<i>S3</i>	<i>S4</i>	<i>P1</i>	<i>P2</i>	<i>P3</i>	<i>P4</i>
<b>Biomass input</b>	kg/hr	116.6	116.6	116.6	116.6	116.6	116.6	116.6	116.6	116.6
<b>Biochar</b>	kg/hr	0.0	0.0	0.0	0.0	0.0	0.0	0.0	0.0	0.0
<b>NG input</b>	kg/hr	29.3	29.3	29.0	29.3	29.4	28.2	29.1	29.2	29.5
<b>Biogenic CO<sub>2</sub> emitted</b>	kg/hr	57.8	55.0	55.0	58.1	57.3	44.0	61.7	59.9	56.4
<b>Fossil CO<sub>2</sub> emitted</b>	kg/hr	77.4	77.4	76.5	77.5	77.6	74.5	76.8	77.2	77.8
<b>Bio-oil produced</b>	kg/hr	13.92	13.91	13.51	13.93	13.90	12.54	13.74	13.88	13.97
<b>Air flow to the system</b>	kg/hr	775.6	750.7	690.9	774.0	758.1	476.5	794.3	788.3	759.7
<b>Net electricity generated from the system</b>	kW	44.3	43.4	40.2	44.0	43.1	30.6	45.2	44.8	43.4
<b>Fresh water</b>	kg/hr	44.8	44.8	44.3	44.9	45.0	43.2	44.5	44.7	45.1
<b>H<sub>2</sub> from NG plant</b>	kg/hr	8.85	8.85	8.75	8.87	8.87	8.52	8.78	8.83	8.90

Table 35. Analysis for Ref2 case when using different biomass types

		<i>Ref2</i>	<i>S1</i>	<i>S2</i>	<i>S3</i>	<i>S4</i>	<i>P1</i>	<i>P2</i>	<i>P3</i>	<i>P4</i>
<b>Biomass input</b>	kg/hr	116.6	116.6	116.6	116.6	116.6	116.6	116.6	116.6	116.6
<b>Biochar</b>	kg/hr	0.0	0.0	0.0	0.0	0.0	0.0	0.0	0.0	0.0
<b>Biogenic CO<sub>2</sub> emitted</b>	kg/hr	57.8	55.0	55.0	58.1	57.3	44.0	61.7	59.9	56.4
<b>Fossil CO<sub>2</sub> emitted</b>	kg/hr	0.0	0.0	0.0	0.0	0.0	0.0	0.0	0.0	0.0
<b>Bio-oil produced</b>	kg/hr	13.92	13.91	13.51	13.93	13.90	12.54	13.74	13.88	13.97
<b>Air flow to the system</b>	kg/hr	610.0	585.0	527.0	608.0	592.0	317.0	630.0	623.0	593.0
<b>Net electricity generated from the system</b>	kW	-335.7	-336.8	-335.7	-336.7	-338.0	-335.4	-331.8	-334.6	-339.0
<b>Fresh water</b>	kg/hr	79.6	79.7	78.8	79.8	79.9	76.7	79.0	79.5	80.1
<b>H<sub>2</sub> from electrolysis</b>	kg/hr	8.85	8.85	8.75	8.87	8.87	8.52	8.78	8.83	8.90
<b>Biomass input</b>	kg/hr	116.6	116.6	116.6	116.6	116.6	116.6	116.6	116.6	116.6

**Table 36. Analysis for Ref3 cases for different biomass types**

		<i>Ref3</i>	S1	S2	S3	S4	P1	P2	P3	P4
<b>Biomass input</b>	kg/hr	311.12	311.21	309.06	311.53	311.71	303.94	309.60	310.79	312.33
<b>Biochar</b>	kg/hr	0.00	0.00	0.00	0.00	0.00	0.00	0.00	0.00	0.00
<b>Biogenic CO<sub>2</sub> emitted</b>	kg/hr	313.33	310.70	307.82	314.22	313.66	290.13	315.28	315.02	313.53
<b>Fossil CO<sub>2</sub> emitted</b>	kg/hr	0.00	0.00	0.00	0.00	0.00	0.00	0.00	0.00	0.00
<b>Bio-oil produced</b>	kg/hr	13.92	13.91	13.51	13.93	13.90	12.54	13.74	13.88	13.97
<b>Air flow to the system</b>	kg/hr	1202.2	1177.5	1112.9	1201.5	1186.0	887.4	1217.6	1214.2	1188.9
<b>Net electricity generated from the system</b>	kW	45.55	44.63	41.45	45.28	44.40	31.77	46.42	46.02	44.62

PROCESS DETAILS FOR REF4, CCS2, CCS3, CCS4 AND CCS5 CASES

**Table 37. Process details for the Ref4 case**

		Ref4
Biomass input	kg/hr	277.54
Biochar	kg/hr	0
Biogenic CO <sub>2</sub> emitted	kg/hr	273.96
Fossil CO <sub>2</sub> emitted	kg/hr	0
Bio-oil produced	kg/hr	13.92
Air flow to the system	kg/hr	949.00
Net electricity generated from the system	kW	29.78

**Table 38. Process details for the CCS2-5 cases**

		CCS2	CCS3	CCS4	CCS5
Biomass input	kg/hr	311.12	311.12	277.54	311.12
Biochar	kg/hr	0.00	0.00	0.00	0.00
Biogenic CO <sub>2</sub> emitted	kg/hr	261.34	31.33	27.69	83.35
Fossil CO <sub>2</sub> emitted	kg/hr	0.00	0.00	0.00	0.00
Bio-oil produced	kg/hr	13.92	13.92	13.92	13.92
Air flow to the system	kg/hr	1202.23	1202.23	949.00	1202.23
Net electricity generated from the system	kW	23.43	-66.53	-66.43	-47.40
Additional steam from external sources	kg/hr (kW)	0.00	0.00	24.1 (15.2)	0.00
CO <sub>2</sub> for storage (only biogenic)	kg/hr	51.96	282.00	246.27	229.97

